Sigurd Aurvåg Sørum

Feasibility Study of the "Launch and Forget" Installation Method for Deep Water Marine Operations

Masteroppgave i MTMART
Veileder: Kjell Larsen
Januar 2019

Masteroppgave

NTNU
Norges teknisk-naturvitenskapelige universitet
Fakultet for ingeniørvitenskap
Institutt for marin teknikk

NTNU
Kunnskap for en bedre verden

Sigurd Aurvåg Sørum

Feasibility Study of the "Launch and Forget" Installation Method for Deep Water Marine Operations

Masteroppgave i MTMART
Veileder: Kjell Larsen
Januar 2019

Norges teknisk-naturvitenskapelige universitet
Fakultet for ingeniørvitenskap
Institutt for marin teknikk

NTNU
Kunnskap for en bedre verden

NTNU Trondheim
Norges teknisk-naturvitenskapelige universitet
Institutt for marin teknikk

MASTER THESIS FALL 2018

for

Stud. tech. Sigurd Aurvåg Sørum

Feasibility Study of the "Launch and Forget" Installation Method for Deep Water Marine Operations

Background

To be able to design, fabricate and install large subsea facilities in deep water, a cost-effective and safe installation method is crucial. Present capital expenditure of the marine operations for a subsea production system in 300-3000m water depth is for some cases in the range 30-40% of the total capital invested.

Installation of subsea equipment is a challenge – particularly in deep water. The main challenges are:
- Plan and perform installation operations more cost-effectively while maintaining safety and accuracy. This requires that the operations must be done smarter and faster using new methods, equipment and technology.
- Existing lifting crane systems based on steel wire ropes have limitations wrt water depth and weight capacity. This is partly due to the weight of the lifting wire.
- Increase operational limits to extend the season where installation activities can be performed.
- Understand and manage the risk involved in deep water operations. An important part of this is to reduce the uncertainty of equipment and systems used.

Scope of Work

1) Review relevant literature and describe briefly state-of-art installation methods for subsea hardware in deep water. This activity shall also include:
- A brief description of the technology status of installation systems based on crane and use of synthetic ropes.
- A brief overview of the planning process where the importance of high operational limits, short duration of operation and large weather windows are discussed.

2) The innovative installation method "Launch and Forget" shall be briefly discussed. The discussion shall include description of the main steps, their exposed hazards, uncertainties and main challenges.

3) Plan a small scale experiment campaign in "Lilletanken". The main objective of the experiments shall be to reduce some of the main uncertainties discussed in item 2). As a base case, Equinor will provide a 3D printed model of a subsea template that will be the object to install. Some modifications of this model wrt. right scaling etc. must be accounted for.

4) Perform experiments in "Lilletanken". Initial scope of test programme to be based on plan established in item 3). Additional tests and sensitivities to be performed based on results of on-going tests.
A theoretical hydrodynamic assessment of static and dynamic stability during launch and descend in water shall be included.
The results from the experiments shall be used to indicate if there is an upside in increasing the operational limits and reducing the time consumption of the "launch and forget" method.

5) Conclusions and recommendations for further work.

General information
The work scope may prove to be larger than initially anticipated. Subject to approval from the supervisor, topics may be reduced in extent.

In the project, the candidate shall present his personal contribution to the resolution of problems within the scope of work.

Theories and conclusions should be based on mathematical derivations and/or logic reasoning identifying the various steps in the deduction.

The candidate should utilise the existing possibilities for obtaining relevant literature.

Report/Delivery
The thesis report should be organised in a rational manner to give a clear exposition of results, assessments, and conclusions. The text should be brief and to the point, with a clear language. Telegraphic language should be avoided.

The report shall be written in English and shall contain the following elements: A text defining the scope, preface, list of contents, main body of the project report, conclusions with recommendations for further work, list of symbols and acronyms, reference and (optional) appendices. All figures, tables and equations shall be numerated.

The original contribution of the candidate and material taken from other sources shall be clearly defined. Work from other sources shall be properly referenced using an acknowledged referencing system.

The report shall be:
- Signed by the candidate
- The text defining the scope included
- An electronic copy to be sent to the supervisors

Ownership
NTNU has according to the present rules the ownership of the project results. Any use of the project results has to be approved by NTNU (or external partner when this applies). The department has the right to use the results as if the work was carried out by a NTNU employee, if nothing else has been agreed in advance.

Thesis supervisor**:**
Prof. II Kjell Larsen, NTNU/Equinor
Prof. Trygve Kristiansen, NTNU

Deadline: XXXX, 2018

Trondheim, August 28th, 2018

Kjell Larsen (date and signature):

Trygve Kristiansen (date and signature):

Sigurd Aurvåg Sørum (date and signature):

Table of Contents

List of Tables

List of Figures

Nomenclature

AHC Active Heave Compensation

CAPEX Capital Expenditure

CDF Cumulative distribution function

CoB Centre of Buoyancy

CoG Centre of Gravity

DOF Degrees of Freedom

DP2 Dynamic Positioning Level 2

DVL Doppler Velocity Log

HMPE High Molecular Polyetylen

INS Inertial Navigation Systems

ITS Integrated Template Structure

L&F Launch & Forget

LBL Long Base-Line

LCP Liquid Crystal Polymer

NoB No Added Buoyancy

PIM Pendulous Installation Method

QTM Qualisys Track Manager

ROV Remotely Operated Vehicle

SDS Subsea Deployment System

SDV Submersible Deployment Vehicle

SHS Special Handling System

USBL Ultra-Short Base-Line

WoW Waiting on Weather

Chapter 1

Introduction

1.1 Background and Motivation

The oil industry of today continues exploring into deeper and more inaccessible waters in the search of oil reservoirs. Simultaneously a trend of developing fields subsea is growing, leading to more and larger equipment to be installed in deeper sea and in harsher weather.

Larger modules installed in deeper waters is challenging using conventional installations by crane. For deep-water installation, the self weight of the traditional steel wire may for many vessels become limiting for the payload capacity. In addition, the complexity of lowering and landing of structures increases with depth, leading to an increase in the length of the operation and subsequently required weather window. Synthetic fiber-rope is an up and coming alternative hoist-line material promising solution to the self-weight problems of wire-rope, but as conventional crane installation is used the time-related issues remain mostly unchanged.

There is a limited amount of vessels capable of breaking the so-called *300Te to 3000m* limit. The ones that are, such as DVC Balder, DCV Aegir, Deep Blue and Sapiem 7000 are expensive and in high demand [31]. Installation of equipment for subsea production constitutes a large percentage of the total CAPEX of the project, often up to 33% [2]. Improving the time-use and cost of installation may significantly affect the expected CAPEX for a project. Recent variations in oil-price forces the industry to consider and explore new methods and technologies in

order to bring break-even price of projects down.

A new method for installing subsea equipment without the use of crane is suggested in this thesis. The method can be explained briefly as normal transport to site, unorthodox overboarding by sliding launch without crane or rope, subsequent autonomous descent and landing, and goes under the name *Launch & Forget*.

With recent advancements in robotics and autonomous control, it is believed possible for a subsea structure outfitted with actuators to guide itself to the planned installation site while descending the water-column. By initiating the descent by sliding the structure of an installation vessel in the same manner as a jacket-launch, crane lifts can be omitted. This may severely reduce operation time and required vessel capacity. The CAPEX of the project may be greatly reduced, while at the same time having less environmental impact.

Severe risk is however connected to allowing a subsea template structure fall free of any connected lines or topside control. The risk during launch, descent and landing must be assessed, understood and managed down to acceptable levels before the method can be a viable alternative to methods used today.

Tofteng (2018) assessed the controllability of a subsea structure during descent, assuming passive stability of the structure. This thesis aims to contribute to the Launch & Forget (L&F) method by assessing the stability of a subsea structure during descent [28]. Model-scale experiments has been performed to explore how added buoyancy affect the stability during descent of a subsea template, and a theoretical model of the dynamics have been made.

1.2 Research Questions and Objectives of the Thesis

This thesis aims to be a contribution towards more efficient methods for safe installation of large subsea structures at ultra-deep waters. The area of study is complex and require much research into different aspects, from launch to safe landing. The goal of this thesis is reduce uncertainty around the feasibility of the L&F method. To fulfil this, the following objectives have been set:

- Perform model-scale tests to gain insight into the dynamic behaviour of a falling a subsea structure, and how buoyancy affects this.
- Improve the understanding of the dynamics of a falling subsea structure by

building a simplified simulation model and assessing sensitivity of parameters.

- Assess challenges connected to landing velocity based on model-scale tests.

1.3 Previous Work

In this section, relevant literature directly connected to L&F method is presented. Literature works used in this thesis regarding marine operations, offshore lifting operations and various installation methods is presented in Chapter 2- Background material.

The master's thesis of Tofteng (2018) presents the L&F method as an autonomous solution to some of the challenges connected to subsea installation in ultra-deep waters. Tofteng outlines the L&F method, presenting the main steps, uncertainties and challenges, with focus on the descent phase of the method. The thesis of Tofteng presents a 6 DOF simulation model of the descent phase with control elements, and discusses feasibility of the method based on the results of several simulated cases connected to the behaviour of a 260 Te Integrated Template Structure (ITS) during descent. He suggests actuation hardware design, controller software design and outlines external sensor requirements. Tofteng use the notations Drop & Forget for the method referenced to as Launch & Forget in this thesis.

The thesis concludes that autonomous controlled descent is feasible based on the simulations performed, with a minimum of 200kN actuator capacity needed for surge/sway control and 500kN for yaw control of the ITS in question. The necessary sensor equipment is readily available, but the need for passive methods to reduce landing velocity is underlined, in addition to necessity of buoyancy devices to achieve passive stability in roll and pitch as these are unfeasible to control.

The method is outlined and discussed in Section 3.

1.4 Structure of the Thesis

This thesis have been arranged into nine parts.

Chapter 2 - Background material
Relevant background for understanding the fields of marine operations and subsea installation are presented in Chapter 2, in order to understand the limitations and challenges of the current state-of-art and how the L&F method may improve aspects of this.

Chapter 3 - Experimental Setup
The method used for the experiments is explained in Chapter 3. Here the test facilities, instruments, model-scale and overview of experiments performed is presented.

Chapter 4 - The Launch & Forget Installation Method
Here the L&F method will be introduced and discussed. Each phase will be outlined, and a short case study will be presented, assessing the potential of the method with regards to statistical operability.

Chapter 5 - Theoretical model
Here a simplified theoretical model of the structures descent is suggested, using experimental results for estimations of the drag force and induced moment. The equations of motion and the calculation of the inherent terms are presented.

Chapter 6 - Results
In chapter 6 the observations and results from the experiments and simulation is presented, with a sensitivity analysis of the theoretical model and short discussions/elaborations directly related to the specific results.

Chapter 7 - Discussion
A general discussion of errors and uncertainties and an assessment of the validity of the theoretical model is presented in Chapter 7.

Chapter 8 - Conclusion
In Chapter 8, the concluding remarks regarding the thesis is found, summarising the findings of this thesis.

Chapter 9 - Further Work
Recommendations for further work is presented in the final chapter of this thesis.

Chapter 2

Fundamental Concepts of Subsea Installation Operations

In this chapter relevant concepts regarding subsea installation operations are presented. This includes an overview of the terminology connected to marine operations, an outline of the different phases of offshore lifting operations and presentation of different state-of-art installation methods. The chapter begins with previous work on these topics, before presenting the topics themselves.

2.1 Marine Operations

In this section, marine operations and connected terms for planning and performing such operations will be introduced. The definitions are taken from the VMO standard [3].

The VMO standard defines a marine operation as a non-routine activity at sea were an object is transported from one safe condition to another. In this context, safe condition is defined as a condition where the risk of damage or loss to the object is less or equal to the perceived risk connected to normal operational conditions[3, 15].

Marine operations are carefully planned to reduce risk on equipment and crew, with defined restrictions to characteristic environmental conditions. Characteristic

conditions are defined as environmental conditions with a set probability of being exceeded within a known period of time [3]. The environmental condition limiting for the operation is usually taken as either waves or wind, depending on which the operation is most sensitive for. In addition, current, tide and special conditions like ice concentration or thickness can also be dimensioning.

The two main parameters involved with planning and performing marine operations are time and weather conditions. Based on the estimated time of operation, a marine operation can be defined as either weather restricted or unrestricted. The differing factor between these being how the limiting environmental conditions are set.

2.1.1 Unrestricted and Restricted Operations

Weather unrestricted operations use and dimension equipment and operation for weather criteria based on statistical extremes for the location. Based on the duration and seasonality of the operation, the weather criteria can be between 1 to 100 year return period. Dimensioning the operation for statistical extremes increases the operability of the operation, as the operation can commence almost regardless of weather, but is connected to higher cost in seafastening and required vessel size and capabilities. Design criteria for unrestricted operation are closer to that of permanent or semi-permanent structures like platforms or semi-submersibles [21].

If the estimated operational reference time (T_R) is less than 96 hours, with a planned operation time (T_{pop}) of less than 72 hours, the operation can be planned and performed as a *weather-restricted* operation. This entails that the operation is planned to be performed within the period for a reliable weather forecast, and can thus avoid using statistical extremes to decide the operational design criterion, OP_{lim}. Intead, OP_{lim} can be calculated from load effects on the vessel or equipment and should be taken as the lowest of any restrictions such that safe conditions for crew, equipment, position keeping system or vessel is assured. This leads most often to significant reduction in the design criterion compared to unrestricted operations, as the operation can be designed based on available equipment and vessels, and then launched when a favourable and reliable forecast occurs.

The reliability of forecasts are divided into three levels, where the highest level A is what applies to offshore installation operations. This level requires a dedicated meteorologist, two independent forecast sources and a maximum forecast interval of 12 hours [5].

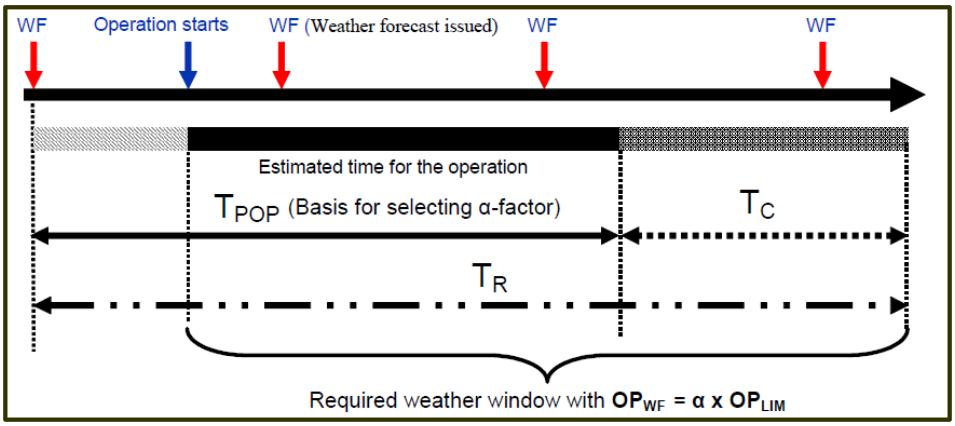

Figure 2.1: Figure showing the relation between the different periods of an operation and the α-factor. From [4]

In addition, the α – factor is introduced to express the uncertainty of the weather forecast. The value of this uncertainty factor is based on the values of OP_{lim} and T_{pop}, with lower OP_{lim} and longer T_{pop} yielding larger uncertainty. The α-factor influences the planning and performance of the operation through correcting the design criterion OP_{lim}, resulting in the operational criterion OP_{wf}, See Figure 2.1. This criterion is used, in combination with the weather forecast, when considering if the operation can be initiated.

The operation is divided into sub-operations or phases, each with a calculated design criterion. The total planned time of operation is the sum of the planned time of operation for each phase. T_{pop} should be based on a detailed schedule and should include time for expected or often occuring delays. In addition, contingency time, which covers uncertainty and contingency events, is added to the planned operation time. T_c is usually taken to be equal to the planned operation time, and seldom/only in special circumstances less than 6 hours. The operation reference period T_R is the sum of the total planned operation time and the contingency time, see Eq. 2.1.

$$T_R = T_{pop,tot} + T_{c.tot} \tag{2.1}$$

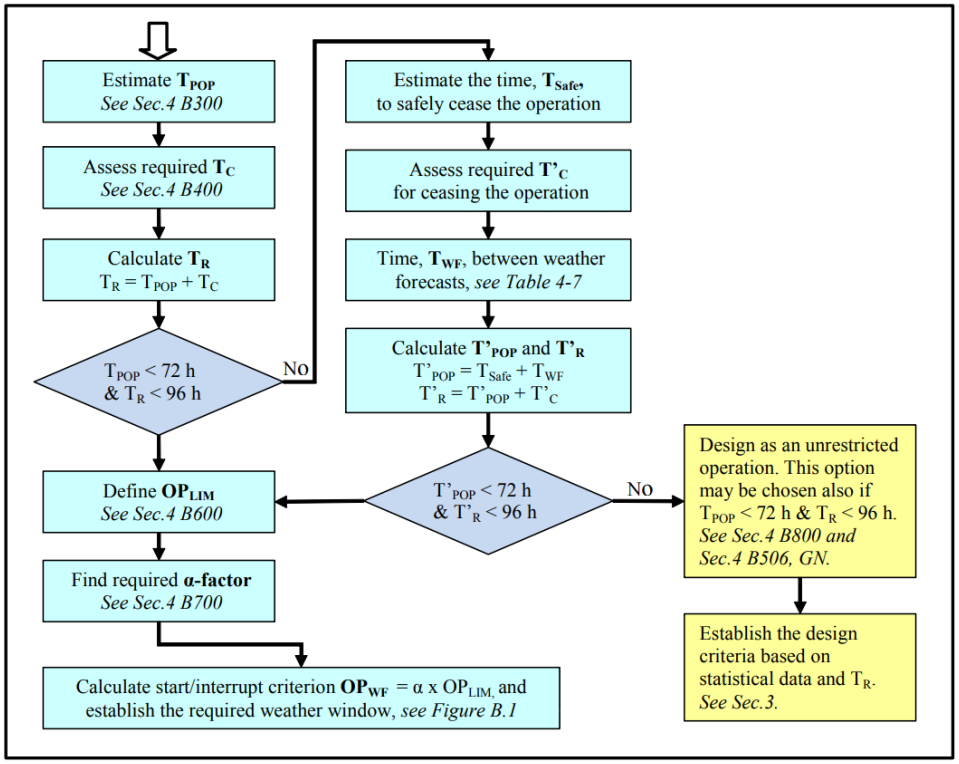

Figure 2.2: Summary of the process defining T_R, T_{POP} and T_C, as well as OP_{WF}. Courtesy of [5]

2.1.2 Point of No Return

Point of no return is usually denoted as the point where it will take more time or involve more risk to revert the operation back to the previous safe condition. In offshore lifting, this is often around when the seafastenings are cut and the object is lifted. At this point, landing the object back on deck and fastening it is often deemed more risky and time-consuming than completing the operation [15].

If the operation can be safely halted, a longer operation can still be viewed as weather restricted if the total time of safely ceasing the operation is within the previously stated limit of 96 hours. The total time of halting must include contingency time and maximum allowed interval between weather forecasts, see Figure 2.2.

2.2 Conventional Offshore Installation

In this section, the different phases of a conventional offshore lifting operation is presented, then a short introduction to hoist-line materials, and finally an overview of state-of-art installation methods still relying on crane operations.

Conventional lifting is here used to denote the offshore lifting operations performed by ordinary crane systems. Installation by crane systems are usually divided into four or five phases, where each phase have different challenges and risks included. In this thesis, the four phase definition for subsea lift from [4] is used. These four phases span the operation from the cutting of seafastenings to landing on the seabed. When considering installation as part of a larger operation, transport to site is usually considered the first phase, but in this thesis transport to site and the relevant seafastening is not assessed in detail.

All phases of offshore lifting are weather dependent. Wave induced motions on the ship are transferred to movement of the crane tip, both horizontally and vertically. Installation vessels are usually positioned to reduce roll as much as possible. Roll motions induce more vertical motion on the crane tip than vessel pitch motions, because crane is located closer to the vessels axis of pitch. The motion of the crane tip is a function of the vessel motion, the cranes position and its geometry.

Phase 1 - Lift off and air manoeuvring

The first phase entails everything from when installation vessel reaches site to when the object to be installed is hanging ready to be lowered through the wave zone. This is a complex phase where crew is needed on deck to rig lifting equipment, connect tugger-lines and cut the seafastenings. There are many dangers to vessel, crew, equipment and structure in this phase. Wave excitation during lift-off may cause snap loads in the hoisting line, lurching motions of the structure or slamming with the deck. As the structure is hanging in air, wind or waves may induce pendulum motions and resonance, leading to risk of damage to vessel, equipment or crew. Advanced cranes with active heave compensation (AHC) are used for smooth lift-off and control of structure in air and tugger-lines are used to give horizontal tension in the system, reducing pendulum possibilities.

Limiting weather criteria in this phase is most often connected to wave induced motions and its effect on the work environment for crew or motions induced on object. If the object is lifted from a barge, relative motion between barge and installation vessel, as well as transfer of personnel to and from the barge can reduce

operational window significantly. Wind gusts might also be a design factor, which can produce pendulum motions or hinder transfer of personnel to and from barge.

Phase 2 - Transversing the wave zone

The second phase considers the lifting operations transition from air to water. Waves, wind and current will affect the transition, leading to the largest variation of forces in the whole operation. In addition to wave-induced motions on from the crane tip, the structure will also be directly affected by the waves. Slamming, direct wave excitation forces, varying weight, added mass and buoyancy may lead to snap loads in the hoisting line and damage to the structure.

Especially structures with suction anchors can provide challenges through the wave zone. Little to no added mass is experienced from the suction anchors prior to the perforated lid on top is lowered through the free surface. When submerged however, added mass from the entrapped water within the suction anchor is fully developed, and thus a large increase in added mass will be experienced by the lifting system over a very short span of vertical movement [23].

It is also important to assess the stability of the installation vessel, as this might be affected by the load variations in the lifting system.

Phase 3 - Deployment through the water-column

While lowering the structure through the water column, less load variation is expected. As the structure is deployed however, the stiffness of the lifting system decreases and the natural period increases. Thus, resonance with the wave-induced motions of the crane tip will occur if the depth is sufficiently deep and AHC or passive dampeners to be utilized to minimize the possibility of slack sling and snap loads on the hoisting line.

Phase 4- Landing the structure

The final positioning and landing of the structure is done by aid of a Remotely Operated Vehicle (ROV). The ROV is only capable of correcting the orientation of the structure, not the possibly considerable horizontal offset the current has had time to introduce on the structure during the descent. The current is hard to measure, time dependent and vary in both magnitude and direction with depth. This leads to high uncertainty regarding predictions [15]. Figure 2.3 illustrates how a 0.8 m/s current will give 160 m offset of a 30 Te module in 1000 m water depth. Considering this for deep-water installations is an important part of Phase 4.

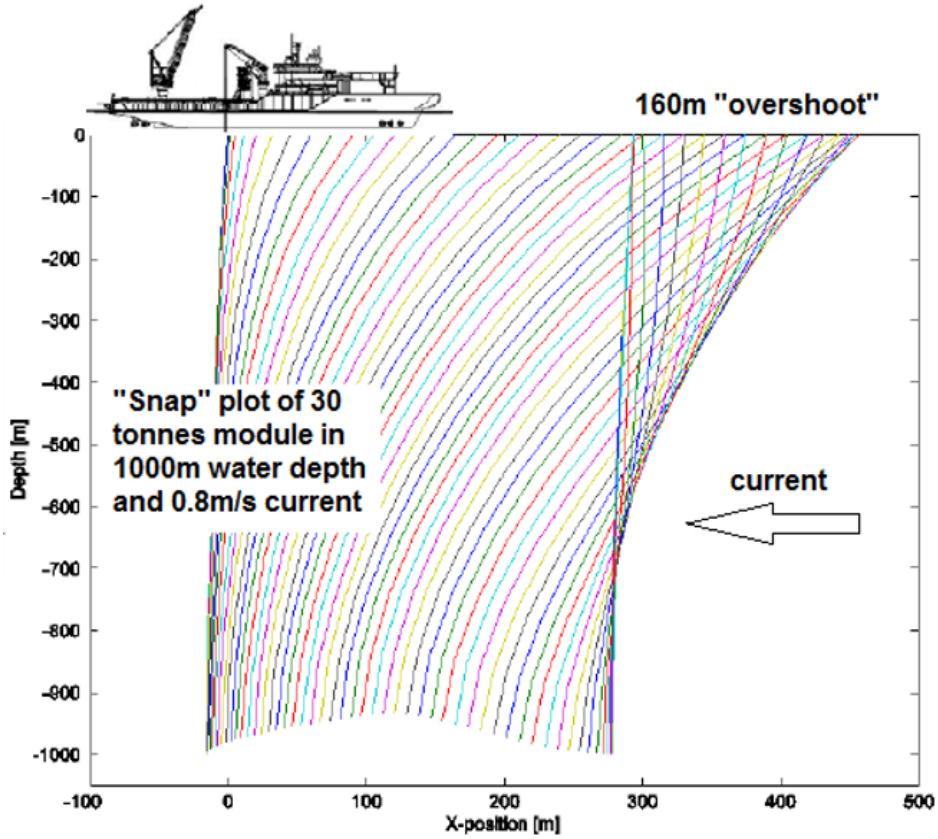

Figure 2.3: Figure showing how depth and current affects the landing process. Moving the object 300 m results in 160 m overshoot for installation vessel.

To counteract this the topside vessel re-positions, but as the length between the structure and vessel is large, the motions of the structure is severely delayed and hard to control. It may take several hours to deploy the structure to the correct position on the sea bottom, thus straining the operation time. Wave induced motions is also an issue, and most often AHC must be utilized to ensure that the impact velocity is low enough to not risk damage to the structure.

2.2.1 Wire and Fiber Ropes

Wire rope is one type of standard rigging equipment for offshore installation. It is strong, abrasion resistant, cheap, mechanically well understood with a long and reliable record. It has however downfalls, especially when considering deep-water installation.

Wire ropes have considerable weight, adding complexity and cost when used for deep-water installation. Crane and wire must be designed for both the weight of the structure to be installed and weight of the length of wire used. Capacity of storage on the vessel must also be considered. Additionally, torsion in the wire may be affected by the large depth, causing problems such as reduced capacity [34].

Synthetic fiber rope is an up and coming alternative to the traditional wire rope. Being much lighter, close to neutrally buoyant in water and torque free, it conquers many of the challenges of wire rope. However, the reduced weight introduces more offset by current, increasing the difficulties connected with the landing phase. Another challenge introduced is the pronounced visco-elastic propertie of fiber rope. Mechanically it is less understood than the ideal elastic-plastic response of steel, and thus exposed to some uncertainty from the industry [34]. Challenges connected to fiber rope include creep, abrasion, core crushing and heat induced degradation. Additionally it is more costly than conventional wire rope.

The industry will likely turn towards fiber rope for deep-water installation as the amount of successful cases and confidence grows along with a better understanding of mechanical properties [33].

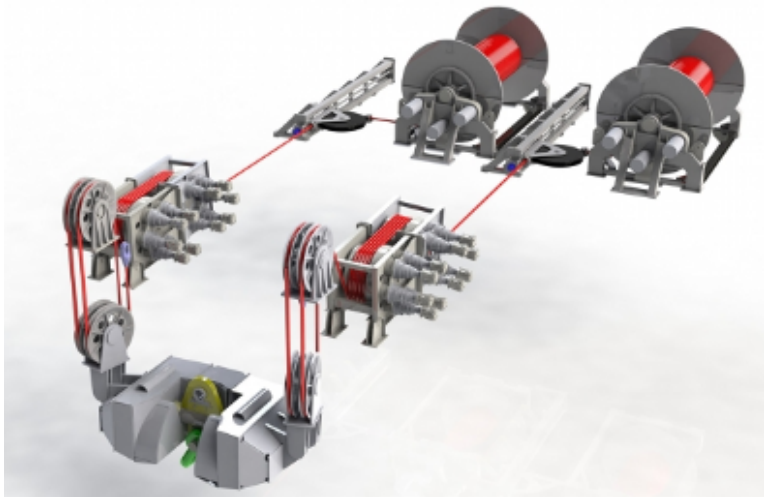

Figure 2.4: Figure showing Multi-Fall installation system with lifting block [27].

2.2.2 Wet Handshake and Multi-Fall Lifting Systems.

Many vessels have a dedicated system for deep-water installations, reducing the needed capacity of the vessel crane. This system is often placed inside the ship side, reducing the motions induced on the installation object as the lifting point is closer to ship center, see Figure 2.5. These systems rely on what is called a *wet handshake* to get the installation object connected to the deep-water installation system. When performing a wet handshake the structure to be installed is over-boarded by the vessel crane as normal, but once it has cleared the wave zone, the load is transferred to the dedicated deep-water installation system and the vessel crane is disconnected. There are however challenges connected to this method. ROV is used for connecting and disconnecting the different lifting equipment of the systems, a job difficult to preform with strong current or large ship movements. This must also be performed twice, as the rigging equipment must be transferred back to the crane and brought aboard.

These systems often utilize two winches and multi-fall technique to reduce the needed capacity of each winch. With the load distributed between winches, the needed diameter or capacity of the hoist line is reduced, but more storage space is needed as the length of line is doubled. Synchronization is paramount for the stability during descent, as the line from each winch runs through the lifting block of the module.

With multi-fall techniques and wire ropes, comes challenges related to rope rotation and twist of the lifting block pulleys. To avoid twist of the pulleys or twist of the whole lifting block during multi-fall wire lifting, oppositely spun wires must be used to reduce the resultant torque to zero. This is however vulnerable for deviations in lowering speed, as the lack of equilibrium of opposing torque between the ropes eventually may cause the beam to rotate [34].

2.2.3 Special Handling System

The Special Handling System (SHS) is a method which to some degree reduce the risk involved in the lift-off and overboarding phase. Relatively new and installed on the *North Sea Giant*, this system for heavy module launch and recovery uses rail-system on the vessel side and a specially built crane to safely lower the modules through the wave zone. This reduces much of the on-deck risk as there is no suspended load for wave-induced ship motions to affect. Well through the wave-zone, the object is lowered by wire as usual.

The system is capable of lifting up to 420Te in significant wave heights up to 4.5m, which greatly reduces waiting on weather and opens for operation outside the established season. By utilizing its specially designed docking technique for the module, the need for manual rigging and crew on deck can be removed, which facilitates safe operation at higher sea states compared to conventional lifting [1].

2.3 Alternative Installation Methods

This section presents and shortly discusses alternative installation methods such as the Pencil-Buoy method, Subsea Deployment System and Pendulous Installation Method. These methods are all meant to solve different problematic aspects of conventional lifting, thus they are an important point of study to understand the challenges of offshore installation.

2.3.1 Pencil-Buoy Method

An often limiting phase of an installation operation is the offshore overboarding phase, with challenges such as snap loads, pendulum motions in air and slamming when lowering through the splash-zone. Several methods have been developed to

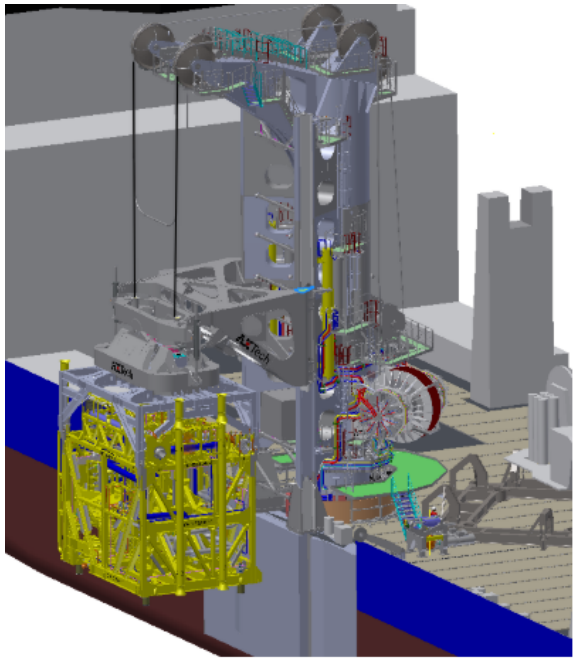

Figure 2.5: Special Handling System, taken from [18].

surmount these challenges and two will be presented; the Pencil-Buoy method and Subsea Deployment System method. For both methods, the lifting is done inshore before the structures are towed sub-surface to site.

The inshore lifting reduces the hire-time and the needed capacity of the lifting vessel, as the structure only needs to be overboarded and not lowered to the seabed. Performing the overboarding inshore makes the operation possible for a larger part of the year, due to inshore weather conditions. Additionally, smaller and simpler equipped ships can be used for the tow and installation, since deck space and crane capacity is not a limiting factor. However, these methods facilitate only a single structure per trip, leaving the them unpractical for smaller multiple installations.

The Pencil-Buoy method is an installation method utilizing sub-surface transportation and inshore lifting to avoid the challenges connected to offshore overboarding. The module is transported on barge to an inshore site, where it is overboarded by a crane vessel and connected to an installation vessel. The module is suspended below a pencil shaped buoy, launched from the installation vessel, and the system is towed to site. At site, the module load is transferred from the buoy to the installation vessel. After retrieving the buoy, the module is lowered and installed.

During landing, a wire with clump weights is used to guide the structure, see Figure 2.6. This limits the operational criteria somewhat, as the vessel may need to rotate away from beam sea to guide the structure.

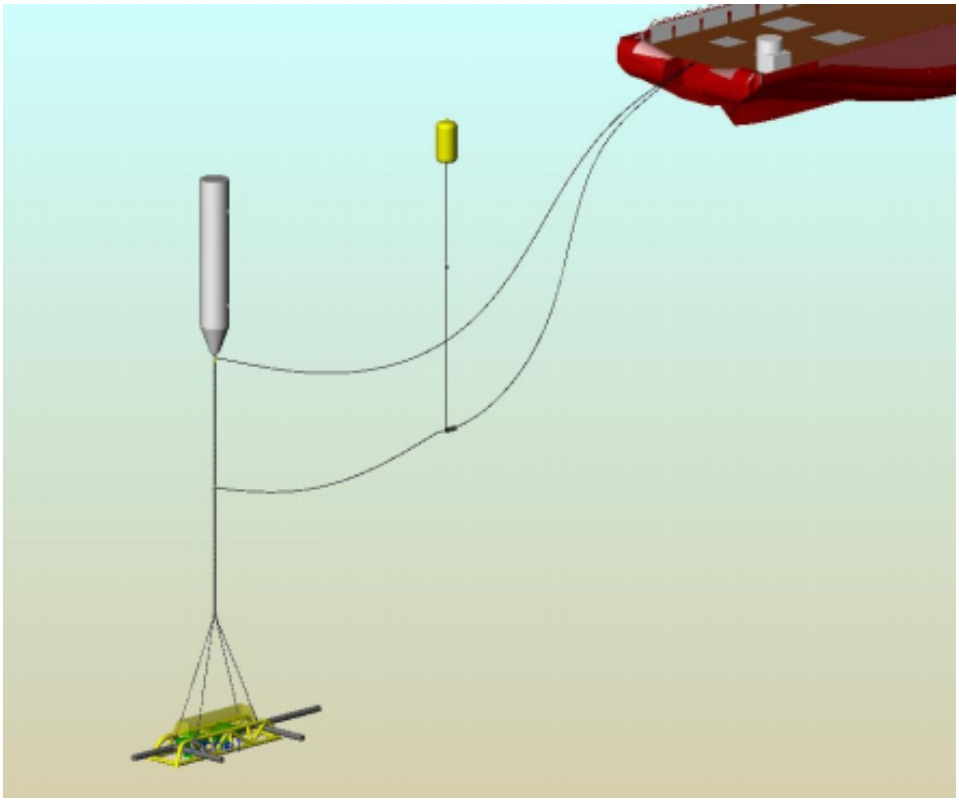

Figure 2.6: Figure showing Pencil-Buoy Installation method, taken from [19].

The method is developed by Aker Marine Contractors, and has been tested on several occasions. The method is reported to have better or similar operational limitations as a heavy lift vessel [19]. The method has also seen use in recovery of suction anchor in 2006.

2.3.2 Subsea Deployment System

Subsea Deployment System is another variation of this method. Here a submersible deployment vehicle (SDV) is connected to the structure prior to the subsurface tow and installation. The SDV is a steel frame with buoyancy modules,

rendering the structure and SDV system slightly buoyant during tow. The depth of tow is controlled by clump weigths on the towing line and the speed of the vessel. The merging of SDV and structure is done inshore by lifting or float over of SDV.

During installation, the heave motion of the system is only controlled by chains lowered into the SDV, ballasting the system to descend or ascend. When landed, the SDV is ballasted with weights til the buoyancy elements are equalized. The structure, now resting by its own weight on the seabed, is disconnected from the SDV. The SDV is then floated off by manipulating the weight of chains on the SDV and returned to shore by subsurface tow. The method is illustrated in Figure 2.7.

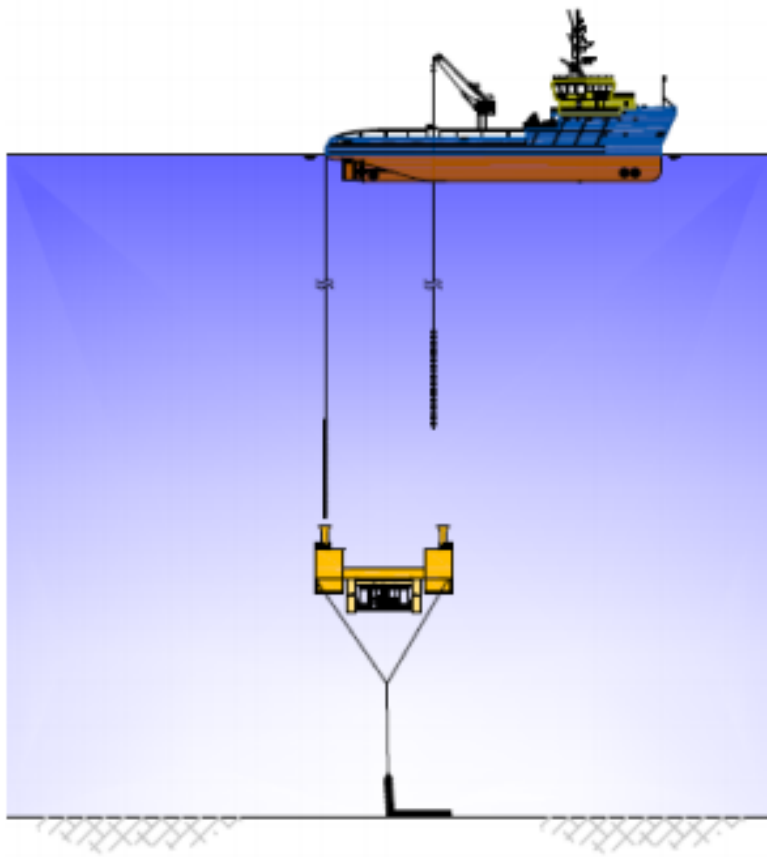

Figure 2.7: Figure installation phase of SDS method, taken from [13].

Most notable about this method is the reduced dynamic response as the structure is not directly suspended beneath the installation vessel. Additionally, no snap loads

are experienced during landing, so the structure can be re-landed if orientation or position is found to be wrong. Another possibility of the method is avoiding any point-of-no-return, as the clump weights on the towing line can be used to "anchor" the structure at seabed if needed. This method has not been tested fullscale, and its disadvantages has not fully been mapped.

2.3.3 Pendulous Installation Method

This method is of special interest for this thesis as this is the closes anyone has been intentionally free-falling a subsea structure.

The Pendulous Installation Method (PIM)) was created by Petrobras in 2005 to circumvent some of the challenges connected to the established way of deep-water installation. The method is mainly concerned with reducing the need for specialized installation vessels or rigs, which are both scarce and costly, driving up total operation cost and limiting operational periods to when the scarce vessels are available.

PIM only needs two conventional DP2 class vessels, one of which must have the capability of overboarding the structure to be installed, and the other must have a winch-system capable of safely landing the structure at seabed.

The method is initiated with a link-up between the vessel transporting the structure and the vessel installing the structure, where the deployment line from the installation vessel is connected to the structure lifting arrangement. The deployment line consists primarily of fiber-rope, with steel wire or chains at the end-connections to the structure and installation winch and is pre-loaded with buoyancy elements to minimize the winch requirements of the installation vessel.

After the installation vessel is moved to the predetermined position while paying out the planned length of deployment line, the transportation vessel overboards the structure. Well beneath the splash zone, given time for water ingress, the structure is lowered beneath the installation vessel in a pendulous motion. Once there, positioned some 50m above the seabed and fully supported by the installation vessel, the final landing is done with ROV guidance.

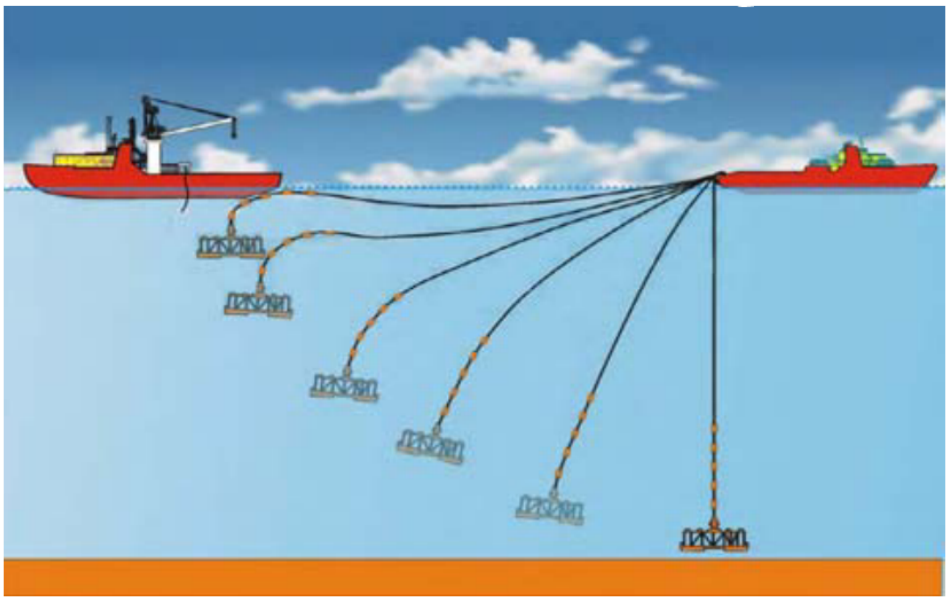

Figure 2.8: Pendulous installation method. Taken from [31]

In Petrobras 2007 campaign, the structure was simply released from the transportation vessel, free falling in a pendulous motion beneath the installation vessel. This first phase of freefall, before the deployment line is sufficiently tensioned to control the structure, is viewed as the most critical, as the complex form of the structure may lead to tumbling or other hydrodynamic instability such as fluttering. Research towards a tumbling-free shape is being conducted, preliminary findings suggest better spacing between centre of gravity and buoyancy and using near vertical panels around equipment. The speed of the descent is however relatively low as the drag forces are immense, leaving the system almost super-critically dampened with no overshoot [32, 25, 7, 24].

Wang (2013) analysed the possibility of using the PIM for installing a 195 Te manifold to 1500m, and proposed an additional line between transportation vessel and the structure [33]. After overboarding, the structure is transferred to a launch line, connected to a winch on the transport vessel. By paying out this launch line, a pendulous motion with gradual tensioning of installation line is still achieved, and the problematic free fall phase is omitted. The operational time is however increased, and the operation becomes somewhat more complex to both plan and implement as two vessels must continuously communicate throughout the lowering phase.

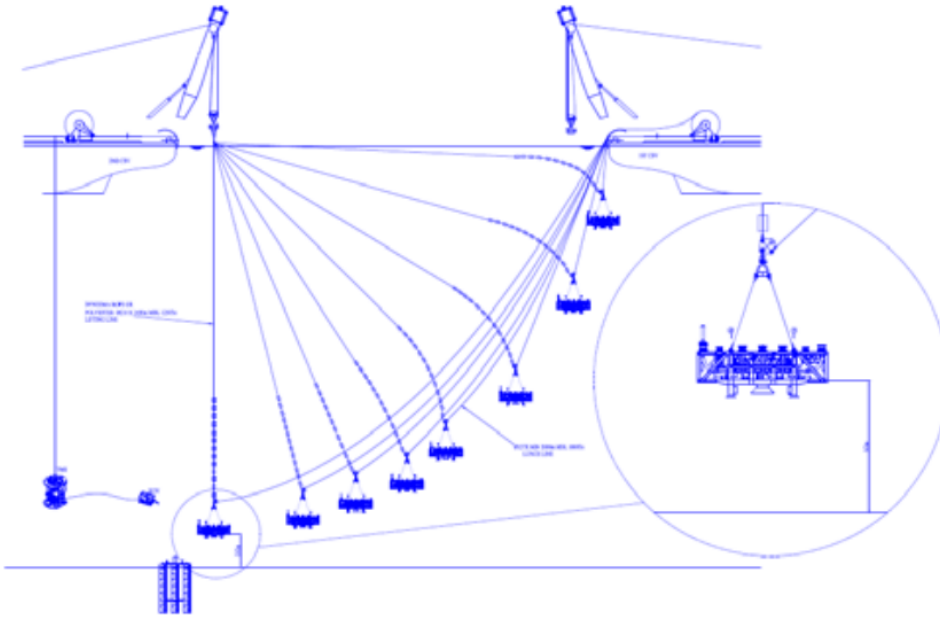

Figure 2.9: PIM with two vessels, avoiding the free-fall phase. Taken from [32].

The method was as mentioned born from a deficit of specialized deep-sea construction vessels and is in this regard a possible solution. Cost might be reduced, but this depends on too many factors to be categorical, like availability and cost of possible vessels, and size and weight of structure to be installed. The method is not widely utilized in today's industry, but as it is largely insensitive to water depth, it might gain popularity in the future.

While using fiber rope to reduce the capacity needed, PIM also circumvents some of the challenges of fibre rope deployment system. With pre-laid line, lowering through the critical depths for axial resonance is avoided and with wire at the topside end of the deployment-line, Active Heave Compensation (AHC) can be used in the landing phase without any added modifications to cater fiber rope. As the fiber rope is not bent over shelves, stern roller of vessel or exposed to the rapid cycling in AHC, damage and fatigue on the rope is minimized. There are however not only positives connected to this method. It involves ship-to-ship transfer of the deployment line, causing risk due to the proximity and complexity due to the vessels moving relative to another. The free-fall phase is also not fully understood and will in most cases demand extensive pre-studies with model and numerical analysis to ensure the safety of the structure.

The carry-over from this method to this thesis are especially connected to the experiences made of the free-fall phase. In the structures Petrobras installed, there was no separation of centre of gravity and centre of buoyancy. The module was a subsea production manifold, complete with mudmat, leading to a more compact structure than the model used in this thesis.

Chapter 3

Launch & Forget Installation Method

The following chapter outlines the proposed alternative installation method, with discussions around exposed hazards, uncertainties and main challenges. The method is still under development and the outline presented here builds on the work of Tofteng (2018) [28].

3.1 Introducing Launch & Forget

The Launch & Forget method suggests an installation method aimed to reduce cost of ultra-deep-water equipment installation by omitting the crane lift, which tends to be an extremely time consuming part of the operation. By reducing operation time, the installation can be performed without costly and scarce high-capacity installation vessels specialized for ultra-deep-water installations. The method is thought possible to perform with vessels like smaller anchor handling vessels, without need of cranes. Instead a launch method similar to jacket-launching is suggested.

Some preparations are however required before the structure is launched. The structure to be installed must be outfitted with means of regulating its position and attitude during descent. For this a robust control-system will be needed, with necessary equipment for accurate positioning. This will include inertial navigation

system (INS), ultra-short base lines (USBL) and Doppler velocity logs (DVLs) for information on position, orientation and current velocity. Means of underwater navigation must be placed at site, and is necessary for accurate positioning during descent and landing. By mapping the current profile prior to dropping the structure, the method is able to predict an optimal decent path for the structure.

Buoyant elements for stability and control of attitude will be needed in addition to some form of actuators capable of moving the structure, which is thought assembled in a *Guidance-rig* connected to the top of the structure. With the structure safely placed on the seabed, the guidance-rig is disconnected and reused.

Overall, the purposed method shares many similarities with an AUV docking operation. Because of the attenuation of seawater, little communication will be possible with the structure after launch, unless umbilical is used.

Making the structure neutrally buoyant would significantly reduce risk and complexity of the installation, but the necessary size of buoyancy elements would likely be so large that it would complicate launch and transport to site. For the ultra-deep-water installations this method is intended for, the buoyancy elements will need internal supporting structure, increasing weight and reducing the effective buoyancy gained.

The Launch & Forget method can be divided into four phases: Transport to site, launch of structure, autonomous decent, and lastly, landing and disconnection of the guidance ring. The four phases will be introduced in the following.

Phase 1 - Transport to site

The first phase is similar to the transport phase of any conventional offshore crane installation. The structure to be installed is transferred from quay to vessel and secured. The only differing aspect to the new method may be placement on deck and the seafastening. To avoid the need for crane operations, the structure should be fastened such that launch can be initiated without moving the structure. For this phase, hazards and weather limiting criteria is assumed to be the same as for transport for conventional installation.

Phase 2 - Launch of structure

At site, the vessel will be orientated to minimize wave induced motions and in a favourable position regarding the estimated or mapped current. When properly positioned, the seafastening of the structure is cut and the structure is slided or launched from the vessel. Likely something similar to the rocker-arm of jacket

launches will be needed ensuring launch without damage to vessel or structure. This phase is critical for the method, and future studies are needed for detailed design for detailed launch methodology. Specific design details regarding the launching mechanism is not a part of the thesis scope, however important issues regarding the launch will be pinpointed and discussed.

It will be very important to avoid damage to vessel or structure during launch. Velocity and angle of launch must be calculated so that proper clearing is ensured between vessel and structure. Some sort of rail-system might be needed to avoid damage to the suction anchor edge during launch. In addition, some sort of rocker-arm system like for jacket-launching will be needed to avoid damage to guide-funnels as the first pair of suction anchor leaves the ramp. For the specific structure of this thesis, broadside launch might be best to avoid the possibility of protruding parts of structure connecting with vessel stern.

The structure subject to launch will rotate and enter the water at an angle. This may cause issues for stability and structural integrity of the structure. Bending loads on suction anchor and guide-funnel connection must be accessed in detail so that slamming loads from water entry does not exceed deformation load limit. Suction anchors will initially act as buoyancy elements until air is expelled, but may destabilize the structure through unequal amount of air entrapped in different suction anchors or trapped air-pockets dependent on placement of ventilation holes.

The optimal water entry angle for the structure is not known and the optimal launch orientation for the structure might not be in the upright position. How the structure is orientated during descent will affect the forces experienced, and any offset from the intended installation orientation will need to be counteracted during descent. If parachutes are to be used, stable and upright descent will also be crucial to ensure correct opening of parachutes.Thus, passive stability of the structure must be ensured to counteract rotations induced by launch.

For jacket-launching operations, the limiting factor is often transfer and work conditions for crew when cutting seafastenings. If the release from seafastenings and launch could be automated or remote-controlled from bridge, crew on deck could be avoided and weather limitations can be set equal to that of the SHS method. This, combined with the shortened total duration of the L&F method, would increase operability and reduce cost.

How sea and wind will affect this phase is not known as the mechanism for launch is not defined yet. Wave-slamming will probably be an issue if any kind of ramp

or plate is extended from the vessel. The relative motion between the structure and vessel during launch can also be an issue. The launch is planned at vessel stern, an area very connected the pitch movement of the vessel. Care must be taken while designing so that the structure is not damaged during launch.

Phase 3 - Autonomous Descent

This phase is covered in detail in the thesis of [28].

After the structure is submerged below the wave-zone, and the air trapped inside has been expelled, the stable autonomous decent phase begins. The control system gathers position data by USBL from vessel and pre-laid LBL network, plans the optimal path towards the target site and orients itself to best utilize or counter-act the current. As the descent progresses, the error in the USBL mesurements will increase, but the error will decrease from to the LBL signals, ensuring adequate position accuracy when landing.

For activation during descent, Toftseng purposes thrusters to control surge, sway and yaw, leaving roll and pitch controlled by the passive stability of the system. This is the safest method utilizing well-proven technology from subsea robotics, but a substantial amount of energy will be needed to move the structure. This will require a rather sizeable battery-pack or umbilical connection with vessel. Batterypack will increase weight and affect the center of gravity of the structure. Umbilical connection will introduce issues connected to additional current drag and may need to be prepayed out to avoid loads as structure is falling.

Parachutes may also be a possible method of utilizing the descent itself for positioning of the stucture. Parachutes can be used both as a pure drag parachute to reduce descent velocity or as controllable paraglider for less energy-demanding control for surge, sway and yaw. However, the dynamics of underwater parachutes are not well known. It might be easier to change the density of the medium to model the effect. Extensive testing is needed to completely map parachute dynamics, such that an accurate model can be utilized by a control system.

The thesis shows that achieving stable descent is highly dependent on the amount of buoyancy outfitted on the structure. In this thesis a singular buoyant element positioned directly above the center of gravity has been considered. Another possibility for buoyancy not assessed in detail is a pre-outlayed buoyant line. This would allow the structure to become neutrally buoyant and ensure smooth landing, but current drag will however be considerable and the structure would need thrusters to counteract this.

Evaluating different decent speeds, we are likely to encounter varying challenges which are a function of that particular speed. A fast descent will reduce the effect of current, but the impact speed with the seabed might be problematic. Reversely, a slow descent will allow more time for current to affect the descent, but will yield a comfortable impact speed. Regardless of what activators used by the guidance-rig, a stable and controlled descent is vital for correct positioning at target-site. A system for finely tuning the attitude of the structure will be needed to avoid structure landing unevenly. Buoyant tanks at structure fringe area could be a possibility, maximizing moment arm minimizes necessary buoyant force generation. This would give control of pitch and roll, but yaw have to be controlled by other means such as smaller lift surfaces, thrusters or a parachute.

There is a high level of risk connected to this phase due to the many variables and tuning parameters. The control system of the guidance-rig must be able to re-calculate and counteract and measured changes current during descent. By position data from USBL and LBL, and additional velocity and current data from a DVL. Systems in place to handle blackout, either in structure or vessel if umbilical is used. Passive stability and method of achieving descent below impact speed limit must be ensured. The advantages are however significant due to the reduced cost of the L&F method.

Phase 4 - Landing and guidance-rig disconnect

Well through the water-column, the structure lands at the planned position. For the landing phase, the impact speed with the seabed and the attitude at impact will be critical for the structure. As the structure which descents through the water column is disconnected from the surface vessel initiating the launch, the only remaining force acting on the structure is gravity. To avoid damage to the structure the descent velocity must be constant below, or reduced below the impact velocity limit before landing. In addition, horizontal velocity should optimally be zero to reduce strain on structure and landing position and attitude of structure should be controlled to ensure correct orientation relative to the seabed and planned pipe-paths to other structures.

A possibility of fast descent, but slow landing comes in the form of additional parachutes deployed by the system before impact. The risk involved is however large, as releasing parachutes may cause unwanted dynamics, twisting or otherwise causing the structure to touchdown out of place or correct attitude. If errors occur and structure land in wrong position, a crane-vessel will be needed for correction. Though the vessel will only be needed for a short time compared to a full conventional offshore lift operation, all challenges connected to ultra-deep-water

landing by crane will be present and greatly increase the length of the operation.

After safe landing, the guidance rig disconnects and returns to the surface. There are several issues with the notion of safe return of guidance-rig for repeated use, snap loads while disconnecting, reeling-in used parachutes, control while ascending, but they have not been assessed in detail in this thesis.

3.2 Case Study: Operability

In this section, a case study regarding the operability of an installation operation is presented, comparing the L&F method to conventional lifting. This is done in order to underscore the potential benefits of the method. The section will finish with an explanation of the term *waiting on weather*, and an assessment of how the operation reference period affects this.

Here, a slightly different notation will be used for the phases of offshore installation. Phase one will include all activities between reaching target site and cutting the sea-fastenings. Phase 2 will be the complete overboarding of the structure, from lift-off to lowered through the wave zone. Phase 3 and 4 will be the lowering and landing as denoted in section 2.2.

H_s is assumed the governing parameter, and all phases are assumed to share the same operational criterion OP_{wf}. Statistical data from the Johan Castberg field in the Barents sea has been used and the considered scenario is heavy module offshore installation of equipment at 3000m of depth. This depth is not applicable for the Barents sea, a rather shallow shelf sea, but is necessary to create a realistic scenario for comparing the two methods.

The proposed T_{pop} for the methods are based based on experience of [16], for offshore lift operations. A generic winch-speed of 0.2 m/s is assumed, giving around 4 hours for T_{pop} for Phase 3. Positioning of installation vessel at site before operation commences is assumed. Thus equal time for phase 1 is taken for both methods. The details are presented in Table 3.1 and 3.2.

OP_{wf} of 4 m is possible for SHS previously described in section 2.2.3. The operational limits of L&F has not been assessed in detail as most of the method is still at the idea stage. As the method omits the problems connected to crane overboarding, mostly problems connected to crew cutting the seafastening remain. If the module could be released by an automatic system from the bridge, operation

can be performed without crew on deck, and an operational limit of 4 m is within reach.

The total T_{pop} for the L&F method may seem low, but there are some arguments to be made why it is beneficial. As the method entails that the structure guides itself to target location, time need not be wasted finely tuning the installation vessels position and heading before launch. It is assumed that the object to be installed is more or less in position on the shipdeck for launch when seafastenings are cut. The closest reference for this phase are jacket-launch operations, where the launch initiates immediately when the seafastening is cut. T_c is simply taken to be equal T_{pop} for both methods.

Phase	Offshore lift	L&F
1	2h	2h
2	3h	1h
3	4h	-
4	3h	-
T_{pop}	12h	3h
T_c	12h	3h
T_R	24h	6h

Table 3.1: Timetable for the different methods

Case	OP_{wf}	T_R
1	2m	24h
2	2m	6h
3	4m	24h
4	4m	6h

Table 3.2: Different cases assessed

Operability or availability of an operation is the percentage of a time period where the given operation can be performed. Operability is dependent on the operational limiting criteria and the operation reference period, as well as the characteristic sea states of the target location.

The probability that an operation can be performed is equal to the probability that the experienced sea state H_S is less than the operational criteria OP_{wf}, and the length of this calm period τ_c being larger than the operation reference period T_R. For a given time period T_{tot}, the available time for performing the operation T_{op} can be expressed as: [15]

$$T_{op} = T_{tot} * P[H_s \leq OP_{wf} \cap \tau_c > T_R] \tag{3.1}$$

$P[H_s \leq OP_{wf}]$ is the probability that the operational criterion is not exceeded, and is called the cumulative distribution function (CDF). By utilizing hind-cast

data of the Barents sea from NORA10 database (from 1985 to 2012, every third hour), and analysing time series of wave height for the region, long term wave statistics of the location can be established. The CDF shown in Figure 3.1 was made using a 3-parameter Weibull distribution with parameters from [6].

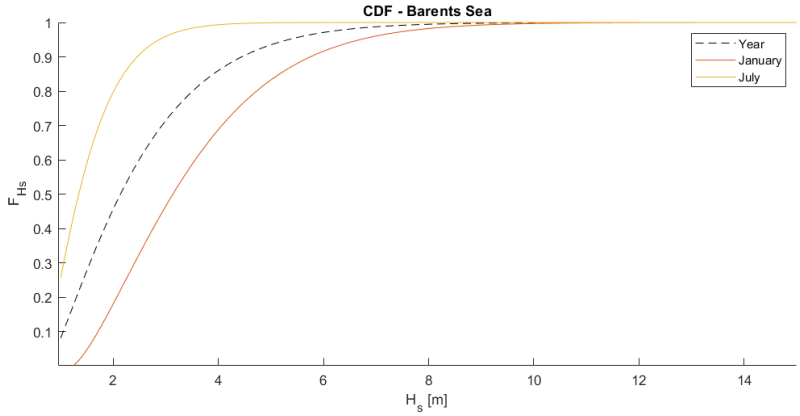

Figure 3.1: Cumulative distribution function for the Barents Sea, based on parameters from [6].

$$P[H_s \leq h] = F_{Hs}(h) = 1 - e^{\frac{h-\lambda}{\rho}^{\beta}} \tag{3.2}$$

Eq. 3.2 show the cumulative density function for the 3-parameter Weibull distribution of H_s, where β is the shape-, ρ is scale- and λ is the location- parameter.

To define the probability of a sea state experiencing a calm period longer than the operational reference period, or $P[\tau_c > T_R]$, the CFD of τ_c must be established.

An expression for the average length of calm, $\overline{\tau}_c$, can be expressed as a function of CDF of wave height [21]:

$$\overline{\tau}_c = A * [-ln(F_{Hs})]^{-\frac{1}{B}} \tag{3.3}$$

Barents sea conditions give $A = 54.838$ and $B = 2.882$, [22].

The expression is found by rank regression of the CDF for wave height and $\overline{\tau}_c$.

With this the cumulative distribution function for length of calms can be found. From [21], the cumulative probability of the length of calm can be expressed as a 2-parameter Weibull distribution:

$$P(\tau_c \leq t) = 1 - e^{-(\frac{t}{t_c})^{\beta}} \tag{3.4}$$

The scale and shape parameters t_c and β vary with location. β is taken from Figure 3.2, which is based on data from the North sea. The sea states here are similar to the Barents sea, and is assumed valid for the Barents sea t_c can be found by setting the rank regressed expression for $\overline{\tau}_c$ in Eq. 3.3 equal to the MTTF or mean of the 2-parameter Weibull distribution for τ_c in Eq.3.4:

$$t_c * \Gamma(1 + \frac{1}{\beta}) = \overline{\tau}_c = A * [-ln(F_{Hs})]^{-\frac{1}{B}} \tag{3.5}$$

By inserting the calculated parameters and the probability for H_s, t_c for different parts of the year can be found. In Table 3.3, t_c for the year-average is shown.

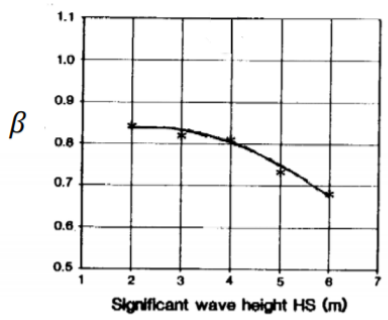

Figure 3.2: β for different H_s, [30]

OP_wf	β	t_c
2m	0.84	61.02
4m	0.81	495.1

Table 3.3: Resulting shape and scale parameters for the 2-parameter Weibull distribution of τ_c, whole year Barents sea.

With t_c and β established, the CDF of τ_c can be plotted. Figure 3.3 show the probability of exceedance for τ_c.

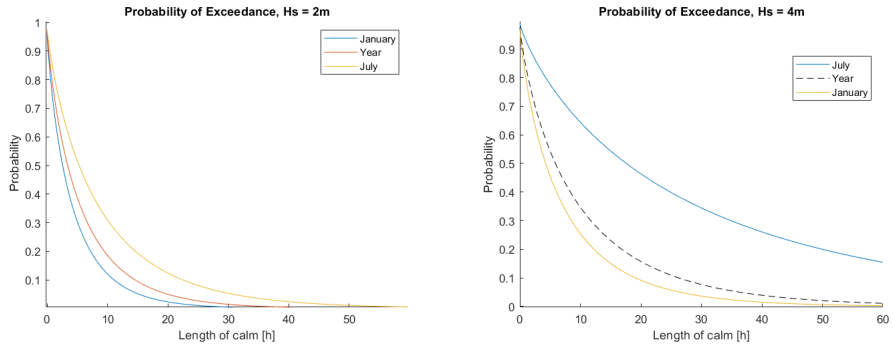

Figure 3.3: Probability of τ_c being longer than a time-period *t*, for H_S of 2 m and 4 m

With the CDF of both wave height and length of calm established, operability can be assessed for the different cases, by Eq. 3.6. Figure 3.4 and 3.5 show a graphical representation of operability, and Table 3.4 show the resulting operability for the stated cases in Table 3.2.

$$P[H_s \leq OP_{wf} \cap \tau_c \geq T_R] = F_{Hs}(OP_{wf}) * (1 - P[\tau_c \leq t]) \tag{3.6}$$

Case	July	Year	January
1	55.7%	27.5%	9.5%
2	71.6%	38.8%	14.8%
3	87.2%	62.4%	45.5%
4	95.3%	77.7%	60.4%

Table 3.4: Operability for the different cases in different seasons

As can be seen in Table 3.4, reducing T_R to 6 hours will, for the cases with OP_{wf} = 2m, increase operability with 5% in the summer and off-season, and around 10% for the yearly average . For OP_{wf} = 4m the operability is lifted around 5-7% in the summer and yearly average, and 15% in the off-season. For January it means an additional 4.5 days available for operation. This is significant when combined with reduced T_R, giving a shorter operation that can be performed in greater parts of the year.

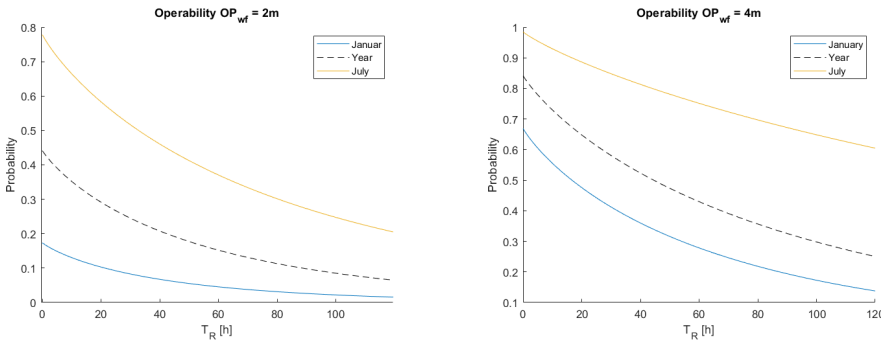

Figure 3.4: Operability for OP_{wf} of 2 and 4 meters in the Barents Sea

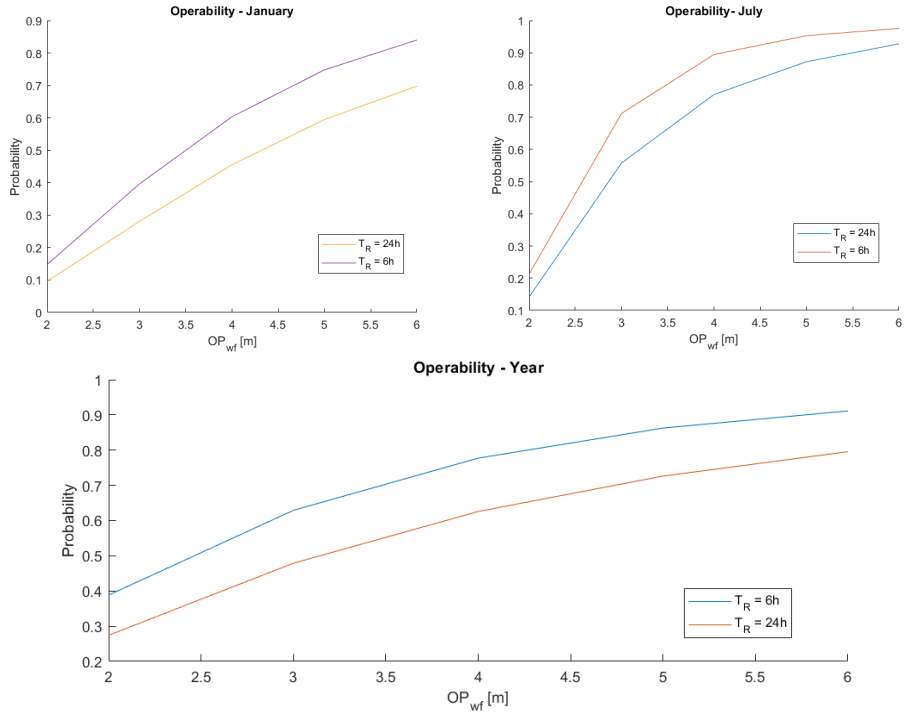

Figure 3.5: Operability as function of the operation criterion

3.2.1 Waiting on Weather

Waiting on weather (WoW) is the term used to describe the period where vessel and crew are ready to proceed with the operation, but the weather is unfavourable. Depending on where, when and with what limiting criterion for the operation, the delay may be days or weeks. The average WoW-period for given location can be calculated from long term statistics, see Figure 3.6.

Another important aspect of offshore operations are weather windows and weather caused delays. Waiting on weather is defined as the amount of time the operation is halted because the forecasted weather does not meet the operational criterion OP_{wf}, or the forecasted calm period is shorter than the operational reference period T_R [15]. Consequently, a weather window is a time period larger than T_R, in which the experienced or predicted weather conditions are lower than the decided OP_{wf}. Waiting for a favourable weather window is a costly and unwanted affair. Vessel and crew must be constantly ready in the case of a favourable weather forecast occur, increasing the cost of the operation, in addition to being unavailable for other operations. Below is shown a statistical analysis of waiting on weather, taken from [6].

Figure 3.6 shows the total duration of an operation, including time spent waiting on weather, assuming the operation is started without regarding any weather forecast. P10, P50 and P90 lines denotes that the indicated duration will not be exceeded respectively 10%, 50% and 90% of the time.

During summer, mean duration of operation with OP_{wf} = 2 m is around 36 hours with a 10% chance of using more than 72 hours, which in most cases is accepted. In the off season however, the expected duration can rise to 12 days, rendering the operation in many cases unfeasible.

Reducing T_R gives on average 4.5 fewer days of operation in the off-season, and 2-3 fewer days in spring and autumn. A similar illustration to Figure 3.7 was found for T_R = 6 hours, but reducing the T_R will likely reduce the delays, as smaller periods of calm can be utilised.

Increasing the OP_{wf} to 4 m greatly reduces the expected delays, more or less allowing for year round operation regardless of T_R, depending on how much delay is accepted.

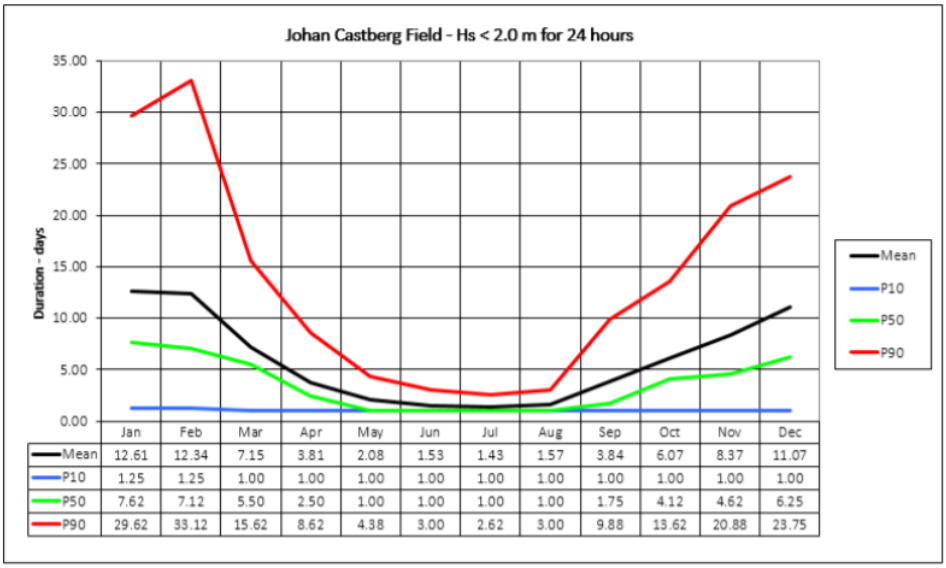

	Jan	Feb	Mar	Apr	May	Jun	Jul	Aug	Sep	Oct	Nov	Dec
Mean	12.61	12.34	7.15	3.81	2.08	1.53	1.43	1.57	3.84	6.07	8.37	11.07
P10	1.25	1.25	1.00	1.00	1.00	1.00	1.00	1.00	1.00	1.00	1.00	1.00
P50	7.62	7.12	5.50	2.50	1.00	1.00	1.00	1.00	1.75	4.12	4.62	6.25
P90	29.62	33.12	15.62	8.62	4.38	3.00	2.62	3.00	9.88	13.62	20.88	23.75

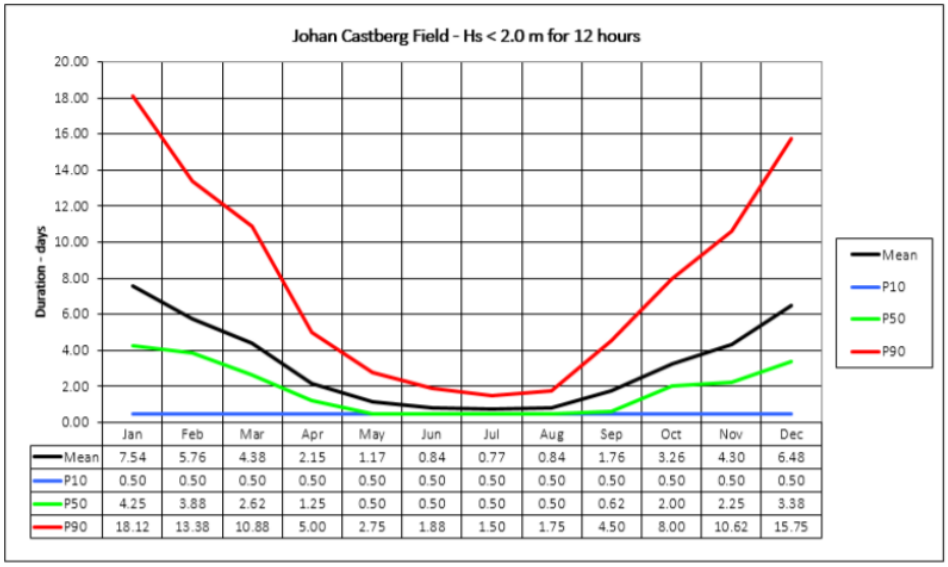

	Jan	Feb	Mar	Apr	May	Jun	Jul	Aug	Sep	Oct	Nov	Dec
Mean	7.54	5.76	4.38	2.15	1.17	0.84	0.77	0.84	1.76	3.26	4.30	6.48
P10	0.50	0.50	0.50	0.50	0.50	0.50	0.50	0.50	0.50	0.50	0.50	0.50
P50	4.25	3.88	2.62	1.25	0.50	0.50	0.50	0.50	0.62	2.00	2.25	3.38
P90	18.12	13.38	10.88	5.00	2.75	1.88	1.50	1.75	4.50	8.00	10.62	15.75

Figure 3.6: Waiting on weather, OP_{wf}= 2m. Figure shows difference in delays between operations of length 12 and 24 hours. Taken from [6].

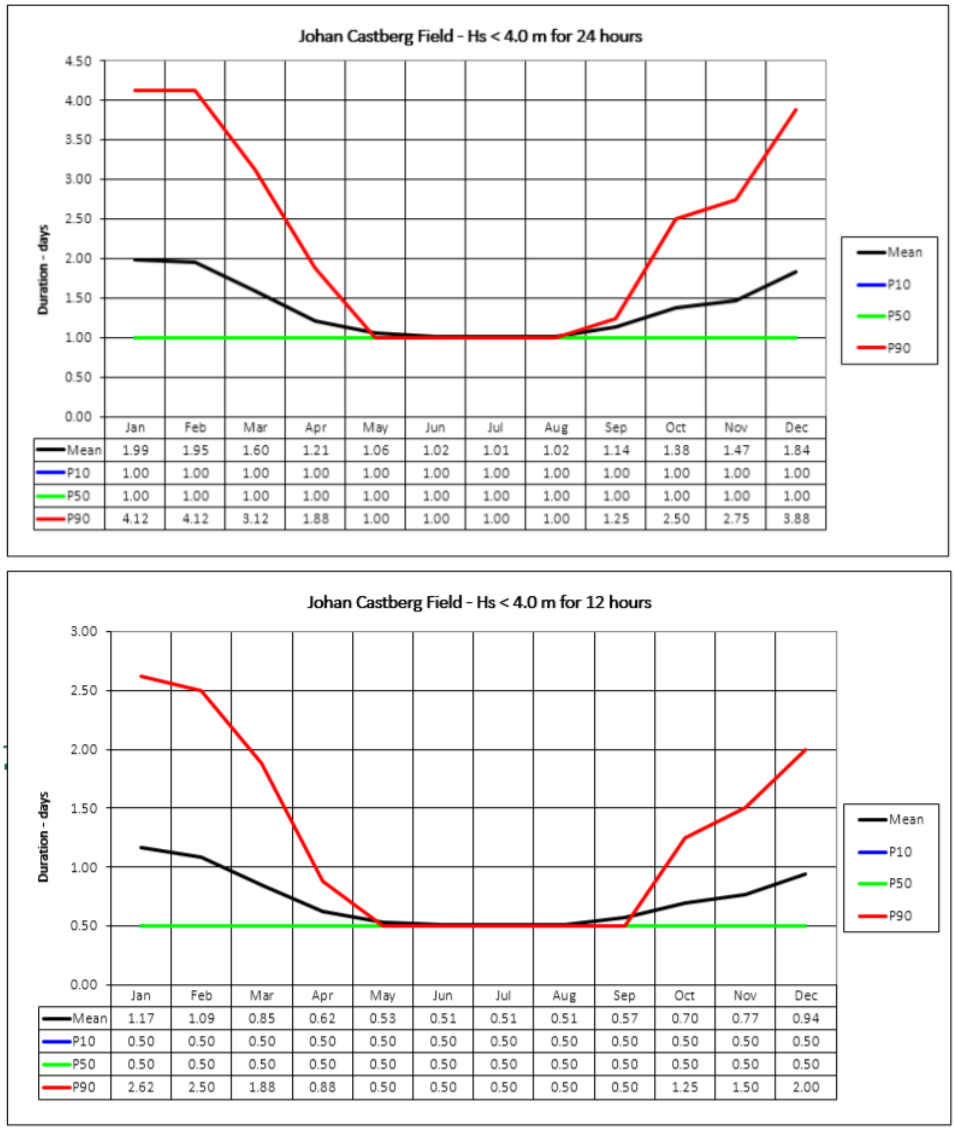

Figure 3.7: Waiting on weather, OP_{wf}= 4m. Figure shows difference in delays between operations of length 12 and 24 hours. Taken from [6]

Chapter 4

Experimental Setup

This section presents what experiments have been done, with what equipment used and how they were performed. Firstly the test facilities and the instruments used to gather data from the experiments are outlined. Then the model-scale is introduced and how it was modified for the experiments. Additionally, a short introduction to scaling is presented, with a short review of possible scale effects. Then the different experiments are described in detail, before the process of data gathering was analysed and processed in different softwares is presented at the end of this section.

4.1 Test Facilities

The experiments have been conducted in calm waters at SINTEF Oceans "Dokka Basin" in Trondheim between 30.11.2018 and 13.12.2018. The basin is a chlorine fresh-water basin of approximately 12m x 6m x 5m, with a pathway in the middle enabling drop-tests without interference from the walls of the basin. See Figure 4.1 and4.2 for visualisation.

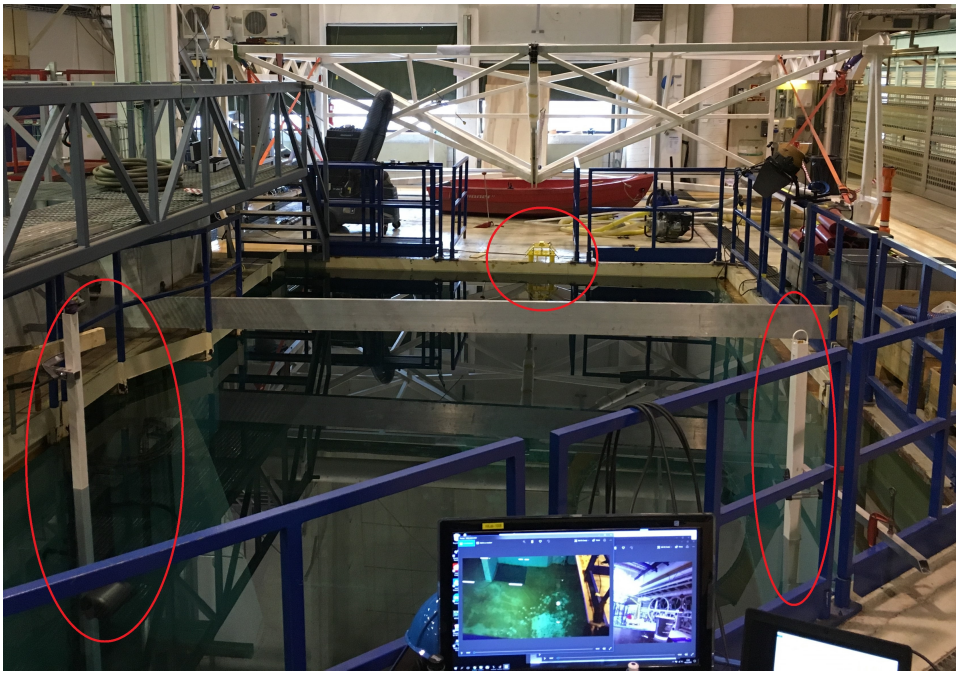

Figure 4.1: Overview picture of the "Dokka" Basin. Notice model and camera support poles encircled red

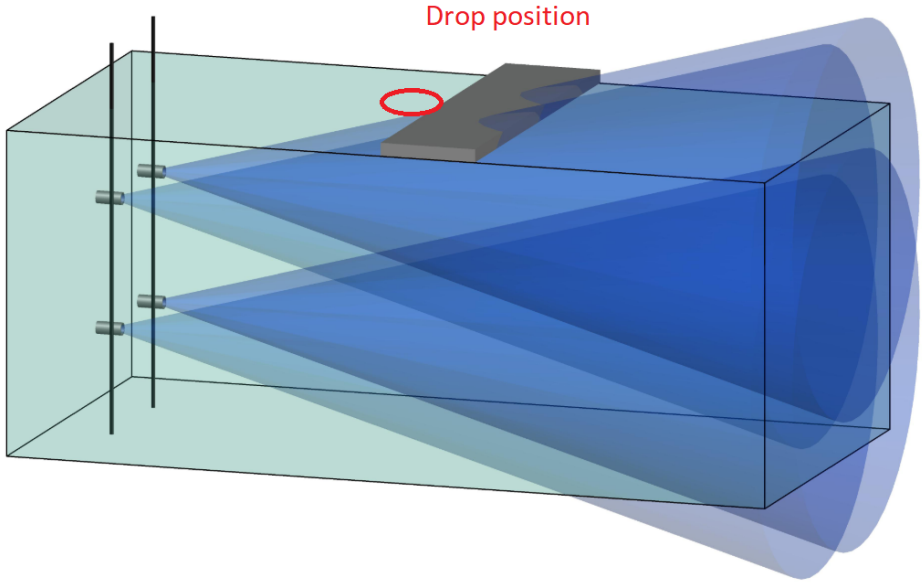

Figure 4.2: Simple sketch of the drop-zone and camera placement. Taken from [10].

4.2 Instruments

4.2.1 Qualisys Motion Capture System

A Qualisys motion capture system consisting of four Oqus Underwater Cameras and the Qualisys Track Manager (QTM), was used to track the position and orientation of the descending structure.The field-of-view for the cameras are 40°, creating a minimum distance necessary from the drop-zone for capturing the whole 5m descent. The cameras were positioned 4.5m away from the drop zone, see Figure 4.2, at depths of 0.5m and 3.5m. This was done to ensure two cameras could view the model at all times, a requirement of the QTM for quality motion tracking. The motion tracking system utilises high-powered cyan LED strobes and reflective markers placed on the models, using the reflected light to position the model by triangulation.

Placement of cameras is a trade-off between high resolution, giving high-quality data and field-of-view. Due to other ongoing experiments in the vicinity of the test basin and the limitations of the basin itself, the cameras could not be placed in an optimal configuration for target tracking. An optimal setting would include more cameras configured in a surround around the drop-zone.

4.3 Model

The 3D printed model used in this thesis was provided by Equinor, and is a replica of a 315Te integrated template structure in scale ratio 1:75. The model can be seen in Figure 4.4, and its specifications are presented in Table 4.1.

4.3.1 Model Modification

3D printed in Nylon, a weight discrepancy between the models self weight and the theoretically correct scaled weight from full-scale model was experienced. The discrepant weight was divided between four weights of formed lead. Corrected for their own buoyancy, each weighed 82 g. The weights were placed at the top of each suction anchor, vertically in-plane with the models CoG, to not offset this. The position can seen in Figure 4.4.

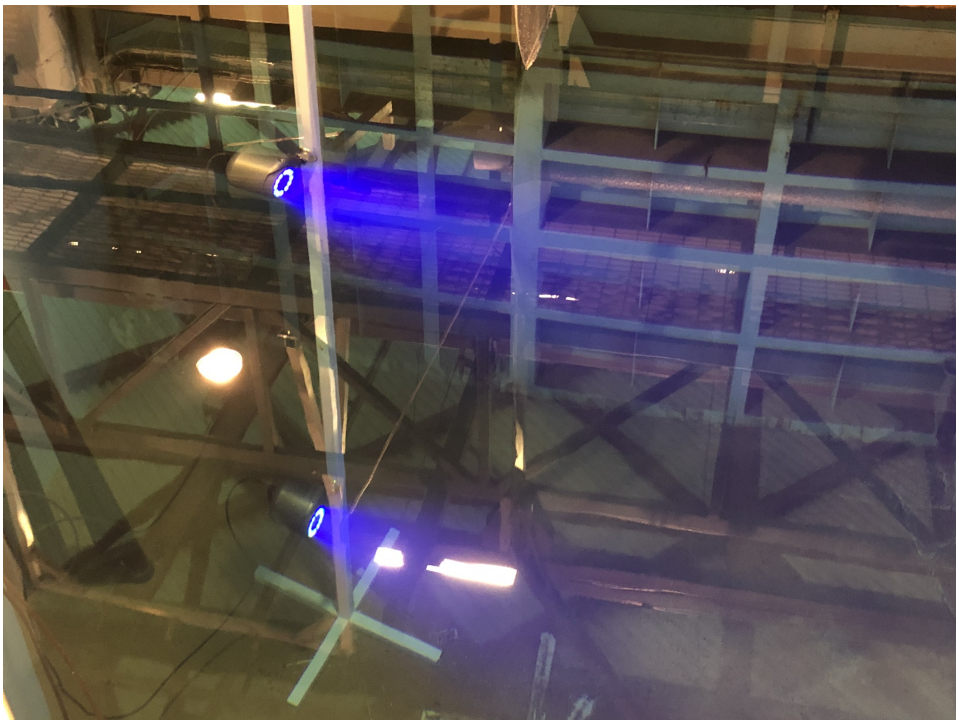

Figure 4.3: Two of the four Ocus Undewater Cameras used to track the descending structure.

Table 4.1: Estimates of properties produced by 3D-printing software, smaller deviations to be expected. CoG from bottom of structure.

Model-scale properties	**Values**
Volume	408.7 cm^3
Original weight	429.2 g
Density	1049.8 kg/m^3
CoG	89.6 mm
LxBxH	38.7x25.0x18.7 cm

Table 4.2: Table showing calculations for mass of added weights.

Type	Weight
Full-scale mass	315 Te
Scaled mass	746.67 g
Model Mass	429.16 g
Discrepancy	317.51 g

The suction anchors came truncated, but not perforated, giving air no exit during submerging unless the model was upside down. To correct this, ventilation holes of diameter 5% of the suction anchor diameter, 3 mm, was drilled in each suction anchor at the correct places corresponding to the full-size structure. It was intended to incrementally increase the size of the ventilation holes throughout the test campaign in order to document the effect, but time was not found for this. This results in a constant perforation rate of 0.025% for the suction anchors of the model.

For the Qualisys motion tracking system, 7 reflective ball-shaped trackers were placed on the model as seen Figure 4.4. Each weighted 3.5g with adhesives but as they were found to be buoyant in water, their effect on the weight of the model were neglected.

4.3.2 Added Buoyancy

A total of 7 different buoyant blocks have been made, used in 12 different configurations to incrementally span 0 to 40% added buoyancy to the model. The blocks are rectangular boxes made from Divinycell with a density of 60 kg/m^3. Some of these "blocks" are different blocks combined to give fitting volumes. For these cases where the buoyant force came from two un-identical blocks placed atop each other.

These blocks were taped on the top of the model, placed so that CoB and CoG of the model remained vertically inline.

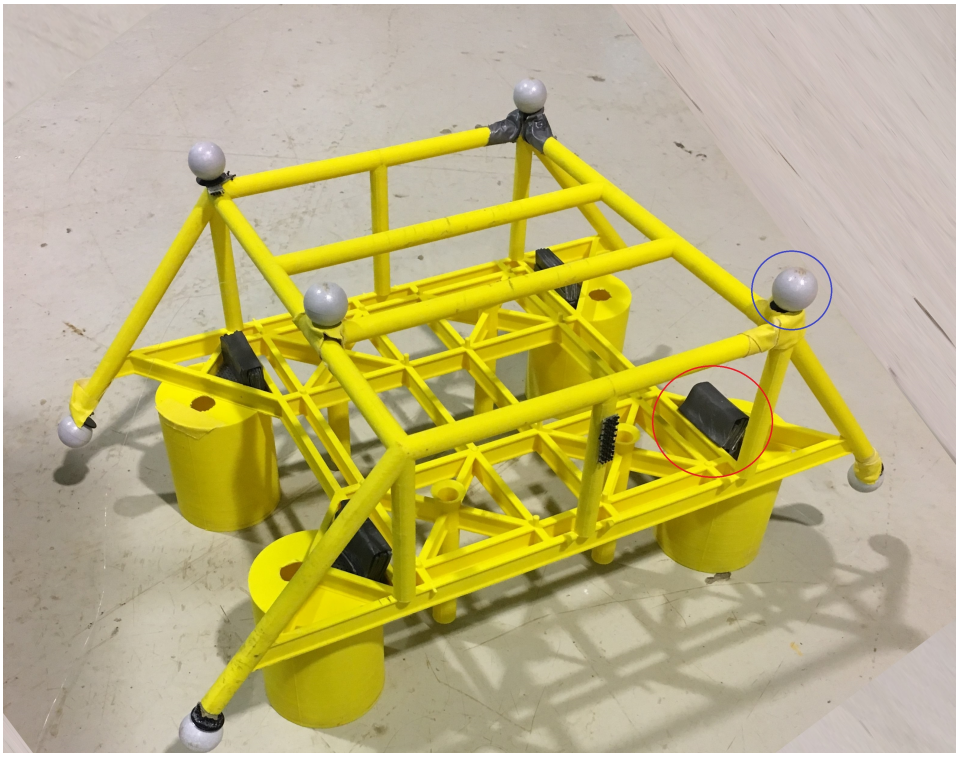

Figure 4.4: Picture of modified model. Notice lead weights ringed red and reflective markers ringed blue. Picture from ongoing experiments by J.B. Andersen, note that the ventilation holes visible were introduced after the experiments of this thesis.

Table 4.3: Overview Buoyancy Blocks used. Added Buoyancy is % compared to original structure buoyancy.

Block	**Dimentions[cm]**	**Volume[cm^3]**	% Added buoyancy
B_1	2x2.5x7	35	8.5%
B_{1-2}	2x3x5.9	41.4	10.1%
B_{1-3}	2x4x6.7	53.6	13.1%
B_{1-4}	1x7x8.5	59	14.4%
B_2	2x6x6	72	17.6%
B_{2-2}	2x5x8.5	85	20.8%
B_{2-3}	B_{1-2}+B_{1-3}	95	23.2%
B_3	B_1+B_2	107	26.1%
B_{3-2}	2x7x8.5	119	29.1%
B_{3-3}	B_{2-2}+B_{1-2}	126.4	30.9%
B_{3-4}	B_{1-3}+B_{2-2}	138.6	33.9%
B_4	3x6.5x8.5	165.75	40.5%

4.4 Description of Experiments

Experiments have been performed where the models have been outfitted with buoyant blocks, drag-parachutes or a combination. These have then been slided of a ramp or released from a completely submerged position.

The initial test-plan was 5 drop-series spanning 0-40% added buoyancy. These series were performed with buoyancy blocks B4, B3, B2, B1 and no added buoyancy(NoB). Based on the observations of drop-series performed with these, it was decided to perform tests with additional variations of buoyancy in order to get more datapoints for specific results.

4.4.1 Drop With Varying Degree of Added Buoyancy

These drop-series were performed by releasing the model with initial orientation as standing. The model was held by hand, completely submerged and air was allowed to escape the suction anchors before release. The model was outfitted with a single fishing line, for retrieval after landing.

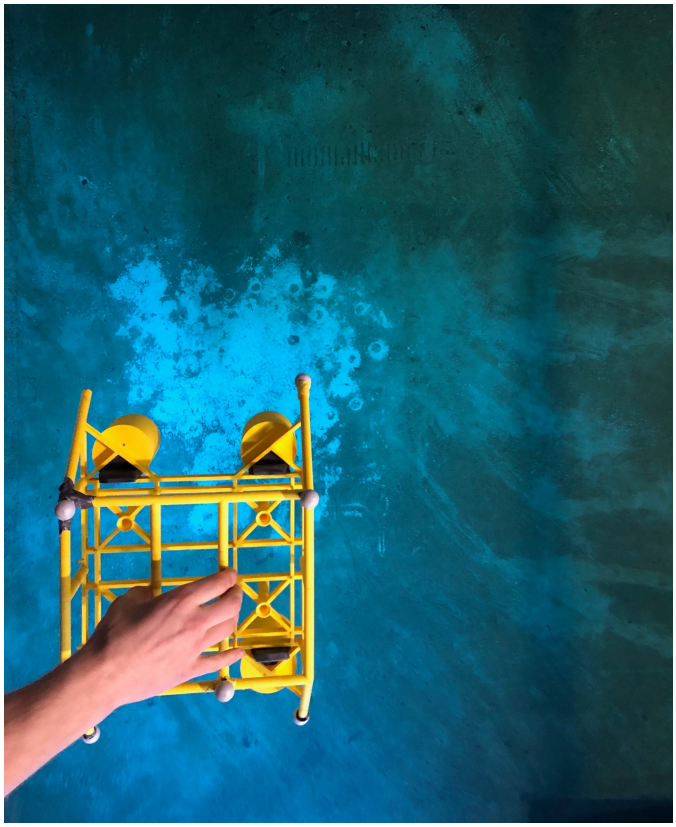

Figure 4.5: Figure showing how single drops were performed.

The first drop-series was done without any additional buoyancy, theoretically giving the structure no self-righting capacity as CoG and CoB is located in the same point. These tests were performed to give insight into the dynamic stability of the model during descent; continuous tumbling or stable descent, and if so, in which orientation.

Subsequent drop-series were performed with increasingly added buoyancy, in order to observe how amount of added buoyancy affected the stability during descent.

4.4.2 Drop with Varied Initial Orientation

Based on the observations of drop-series with the smallest buoyancy-block, *B1*, additional drop-series were planned investigate. In these additional drop-series, release orientation of the model was varied.

The variations were:

- Shortside-down, or rolled 90° from normal standing orientation.
- broadside down, or pitched 90° from normal standing orientation.
- Upside-down, or rolled 180° from normal standing orientation.

Similar series were planned for other buoyancy-blocks, but time was not found. The curious observations of B1 was however not replicated to the same degree in drop-series with larger buoyant blocks.

4.4.3 Sliding Launch

A short investigation into how launch would affect the descent stability was done by sliding the model down a wooden ramp, see Figure 4.6. This drop-series was only performed with the largest buoyancy block *B4*, as this had shown the most promise during tests.

The ramp was made of the smoothest surface readily available, but models still needed help overcoming the static friction. Small variations in launch velocity were experienced because of this initial push. In motion, the models were free to rotate, and were often observed to do so.

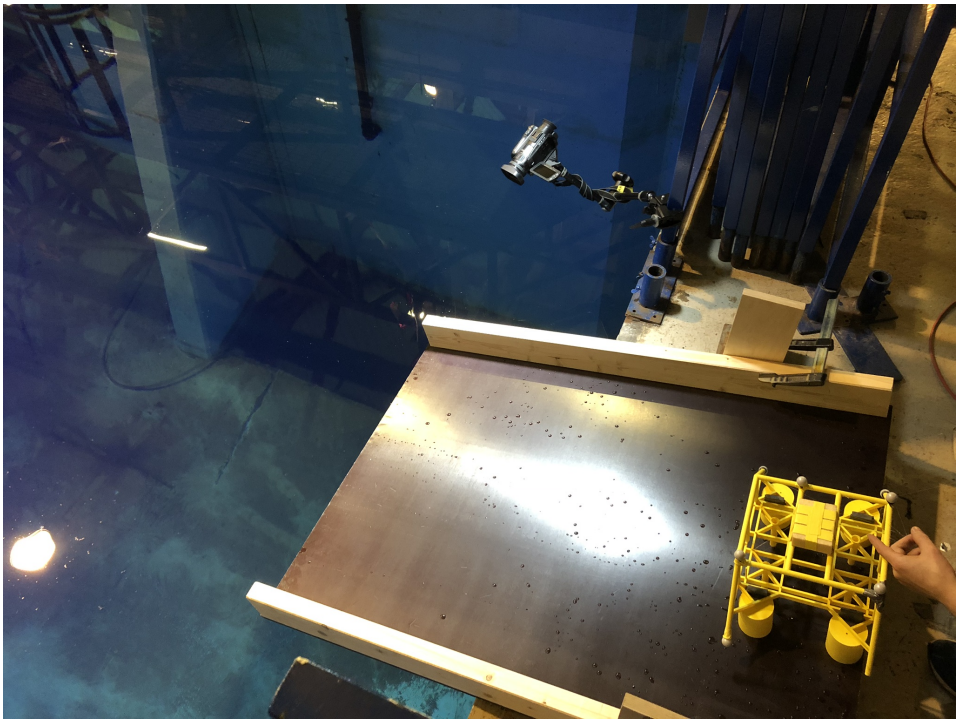

Figure 4.6: Overview of setup for ramp-launched drop-series. Ramp edge is about 2cm above the water, corresponding to 1.5m full-scale height. The ramp was tilted 12.3° and had a smooth wooden surface. Launch velocities were estimated to span 0.8-1.1m/s.

4.4.4 Retardation of Descent Velocity

Based on observations from previous drop-series, additional experiments with parachute from [10] was performed to see if the descent velocity of the system could be reduced to acceptable levels for impact velocity. Three drop-series were preformed, with buoyancy blocks B4, B1 and no added buoyancy (NoB).

(a) Parachute A3 from [10]. The parachute has a diameter of 0.79 of structure length and is not optimized for the dropped structure. Image from [10]

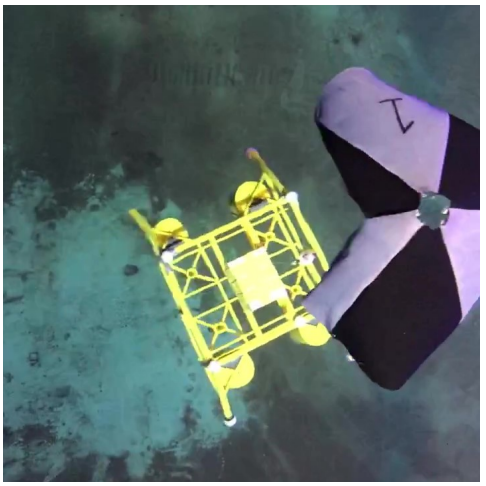

(b) Picture of parachuted drop shortly after release. Parachute is unfolding.

The additional drag force was estimated in Section 5.2.

4.4.5 Supplementary Tests for Estimation of Drag Force and Moment

In addition to the four main buoyancy blocks (B1, B2, B3, B4) used, an additional eight intermediate buoyancy blocks were tested, see Table 4.3. These additional blocks were not tested as intensively as the four main blocks, the intention was to gain more data useful for the later estimations of the drag induced force and moment. This is used to estimate coefficients of drag and moment of the structure in Section 5.1.5.

4.5 Analysis and Processing of Measured Data

4.5.1 Processing in Qualisys Track Manager

Post-processing of the data is done with the Qualisys Track Manager (QTM) software. The software allows visualisation of the reflective markers during the drop,

and supports export of 6DOF of the model data to MATLAB.

Some manual processing in the Qualisys software was necessary as the automatically produced data from the software could be severely fragmented if the system misinterpreted the observed data. Rather than "blindly" interpolating the all gaps in MATLAB, tuning of calculation parameters in QTM was performed to improve the fill-level, the percentage of frames were the system observed enough distinct markers to calculate the virtual body of the model, which was necessary for 6DOF data. The fill-level of any given drop could vary between 3% to 80%, regardless of the fill-level of previous drop. This issue was resolved by manual tuning of the calculation parameters of the software, until a fill level off 80% or better was achieved.

The measurement data from the Oqus cameras give the 3DOF path of each observable marker on the model, often non-continuous where the tracking lost the marker. QTM can then be used to discard phantom markers, interpolate missing parts and arrange the data into continuous trajectories. For the full 6DOF data, the QTM compares the configuration of observable markers to a pre-defined virtual body. This virtual body describes the distances between different markers placed on the model, rendering the system capable of calculating the virtual body if enough markers are identified. To calculate the virtual body, and thus create 6DOF data, a minimum of three markers have to be identified. In order to arrive at the correct orientation of the virtual body, the markers have to be placed non-symmetrical so that only one orientation fit the observed model. This was done for the model, notice in Figure 4.4 how the four reflective markers on top of the body are not placed in a square.

The post-processing done in QTM revolved around tuning parameters and settings connected to the calculation of the 6DOF body. QTM often found and tracked several marker trajectories, but did not calculate the full body because parameters like Bone Length Tolerance, Prediction Error or Maximum Residual were exceeded. Bone Length Tolerance is the maximum acceptable deviation between the measured distance between two markers and the corresponding distance given by the body. Maximum Residual is connected to error between different cameras viewing the same marker, and Prediction Error denotes the allowable deviation between predicted and measured position of marker.

In Figure 4.8 it is shown how the QTM software defined the model. Notice position of green markers correspond to the position of reflective markers shown in Figure 4.4, except for one at the top of the structure. This is a virtual marker only produced by the software when enough markers to identify body is observed.

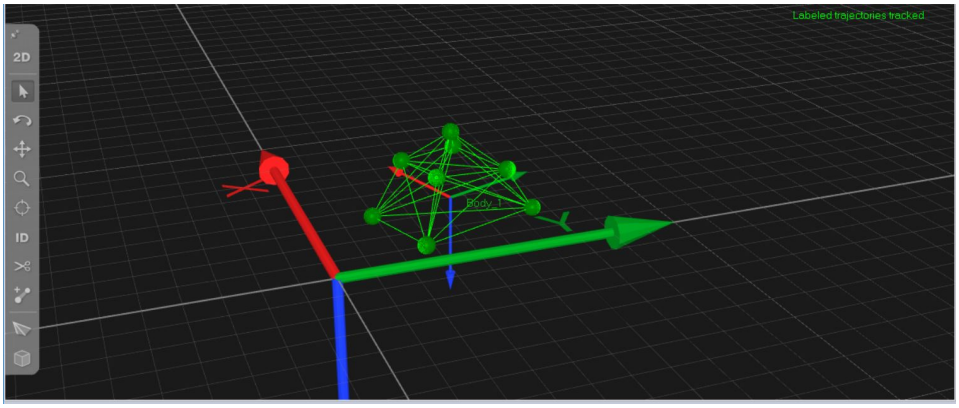

Figure 4.8: How the model body was defined in QTM. Model is landed next to global coordinate system of the software. Notice definition of Body-coordinate system, with y axis in direction traditionally reserved for the x-axis. This affects the definition of roll and pitch of the structure.

The definition of body fixed axes was decided as shown in Figure 4.4 because of Euler-angle singularity issues experienced by the software for pitch rotation outside [-90°,90°]. Implementing unit quaternions is not a feature in QTM and the software was not understood well enough to circumvent this with special software settings. With the definition as shown, the singularity issue only became problematic for the small number of experiments deviating from normal upright orientation at release.

4.5.2 Post-Processing in MATLAB

Refined data from the Qualisys software was exported to MATLAB, which was then used to filter noise, interpolate missing sections and visualise drop-series by plotting graphs. MATLAB functions *fillmissing.m* and *smooth.m* was used.

4.5.3 Simulation of Theoretical Model

The simulation was done using the *ode45* solver in MATLAB, a single-step solver based on an explicit Runge-Kutta formula [17]. This ordinary differential equation solver, solves systems of equations on the form $y' = f(t,y)$. The system of equations used will be presented in Section 5.1, though not in state space form.

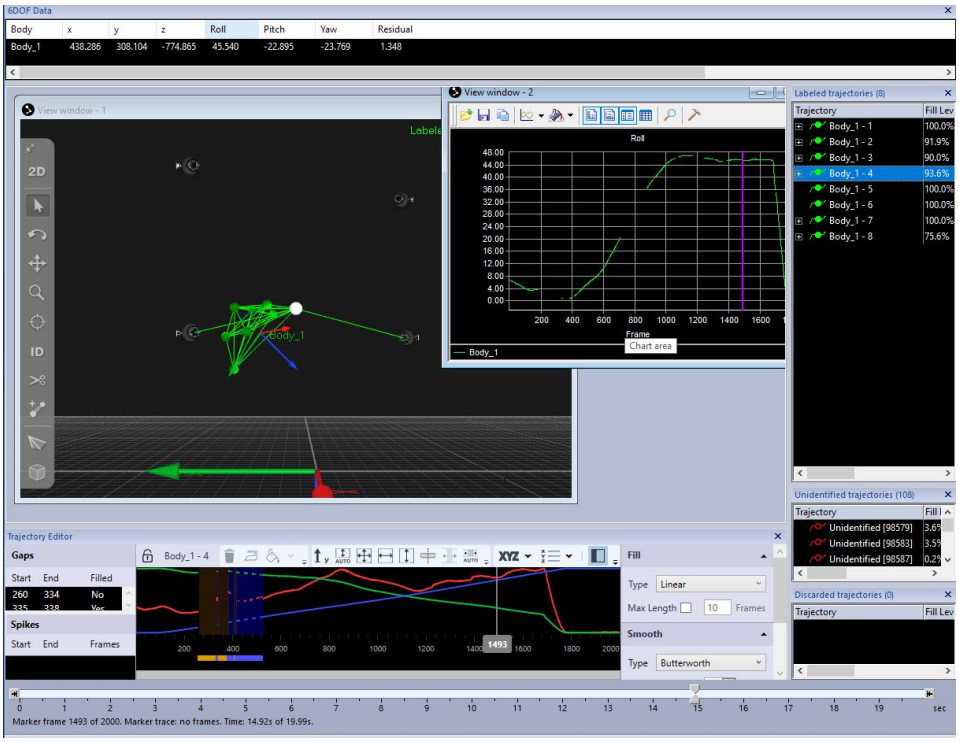

Figure 4.9: Screenshot of Qualisys Track Manager, the software used to map the structure during descent.

Chapter 5

Theory and Theoretical Model

This chapter outlines and describes basic two-dimensional theory of forces affecting an falling object. General equations of motion are presented, along with derivations of the related terms. Basic calculations for estimating the drag force of a parachute is also presented. Last in this section is short review of theory regarding scaling, model-testing and the considerations taken for the scaled model used in this thesis.

5.1 Theoretical Model

In order to better understand the experimental results, simplified theory of the motion was explored and will here be presented. General equations of motions from [8] were used as basis, and simplified to 2D.

Much is unknown regarding the hydrodynamics of a falling template structure. Complex geometry with interaction when flow going through the structure and vortex shedding at trailing edge of suction anchors and any potential buoyancy module. These effects have not been considered in this thesis, which instead considers a simplified scenario where force on the suction anchors dominate.

Water entry has not been considered, only submerged and fully water-filled descent. The model has for the theoretical calculations been reduced to a rectangular box of uniformly distributed mass, with truncated cylinders representing the

suction anchors. The body is assumed rigid throughout the motion and double-symmetric around the centre of gravity. The lift effects on the structure are unknown and difficult to model because of the complex geometry. In the observations of the experiment, lift effects did not seem to dominate and were therefore neglected from the theoretical model. Instead of estimating drag effects based on simplified geometry, measurements from the experiments were used.

Figure 5.1 defines the basis for the equations, showing the global X_G-Z_G coordinate system coinciding with the waterline. The body-fixed coordinate system consists of x' and z', with U_1 and U_3 being the body velocity in x' and z' direction respectively. θ is the roll of the body and thus the angle between the local and global coordinate systems, defined positive counter-clockwise in agreement with the right-hand-rule. The notation "roll" is used for easier comparison with the experimental results.

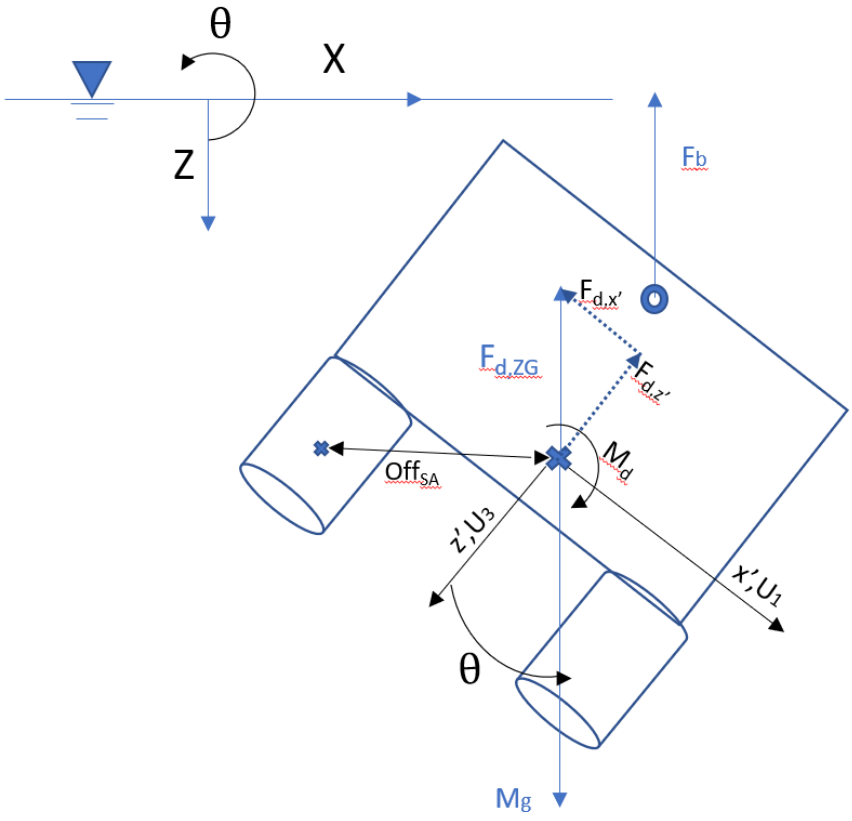

Figure 5.1: Definitions of coordinate systems and forces

M_d is the induced momentum from drag. Any deviation from perfect upright position will lead to non-symmetric flow release on the suction anchor edges, resulting in a tumbling momentum.

5.1.1 Equations of Motion

Based on simplified rigid body equations of motion from [8], the following equations give the equilibrium of force and moment in the body-fixed coordinate system.

$$(M + A_{11})\dot{U}_1 = F_{dx'} - (Mg - F_b)\sin\theta - \underbrace{MU_3\dot{\theta}}_{Coriolis\ force} \tag{5.1}$$

$$(M + A_{33})\dot{U}_3 = F_{dz'} + (Mg - F_b)\cos\theta + \underbrace{MU_1\dot{\theta}}_{Coriolis\ force} \tag{5.2}$$

$$(I_{55} + A_{55})\ddot{\theta} = M_D(\dot{Z}_G,\theta) - M_{F_b} + M_T \tag{5.3}$$

Where $F_{dx'}$ and $F_{dz'}$ are the decomposition of the total drag force Fd. The Coriolis force is taken by right hand rule [29].

Additional equations related to the calculation of the total drag force are shown below:

$$M\ddot{Z}_G = Mg - F_b - F_{d,Z_G}(\dot{Z}_G,\theta) \tag{5.4}$$

$$U_{tot} = \sqrt{U_1^2 + U_3^2} \tag{5.5}$$

$$F_{d,Z_G} = \cos(\beta) * F_{d,tot} \tag{5.6}$$

$$F_{d,X_G} = \cos(\beta) * F_{d,tot} \tag{5.7}$$

$$F_{dx'} = F_{d,Z_G}\sin\theta - F_{d,X_G}\cos\theta \tag{5.8}$$

$$F_{dz'} = F_{d,Z_G}\cos\theta - F_{d,X_G}\sin\theta \tag{5.9}$$

$$\tag{5.10}$$

The motion relative to the global inertial coordinate system can be expressed as:

$$\dot{X_G} = \frac{dX_G}{dt} = U_1 \cos\theta + U_3 \sin\theta \tag{5.11}$$

$$\dot{Z_G} = \frac{dZ_G}{dt} = -U_1 \sin\theta + U_3 \cos\theta \tag{5.12}$$

- M = Total mass of model
- g = Acceleration of gravity
- ρ = Density of water
- M_D = Overturning moment from viscous effects
- F_B = Buoyant force equal to $\rho g \nabla$
- M_{F_b} is the stabilising moment from the buoyant force
- M_v is the velocity dependent moment opposing the rotation.
- F_{DZ_g} is the Drag force in global z-direction [4].
- β is the angle between the total velocity vector U_{tot} and and the velocity vector $\dot{X_G}$.
- h_{SA} is the height of a suction anchor.

5.1.2 Velocity Dependent Moment Opposing the Rotation

As the structure rotates, a moment opposing the rotation will appear. This is a result of drag force from the flow created as the structure rotates, and is thus dependant on the speed of rotation. With definitions shown in Figure 5.2, this moment is derived in Eq. 5.13 below.

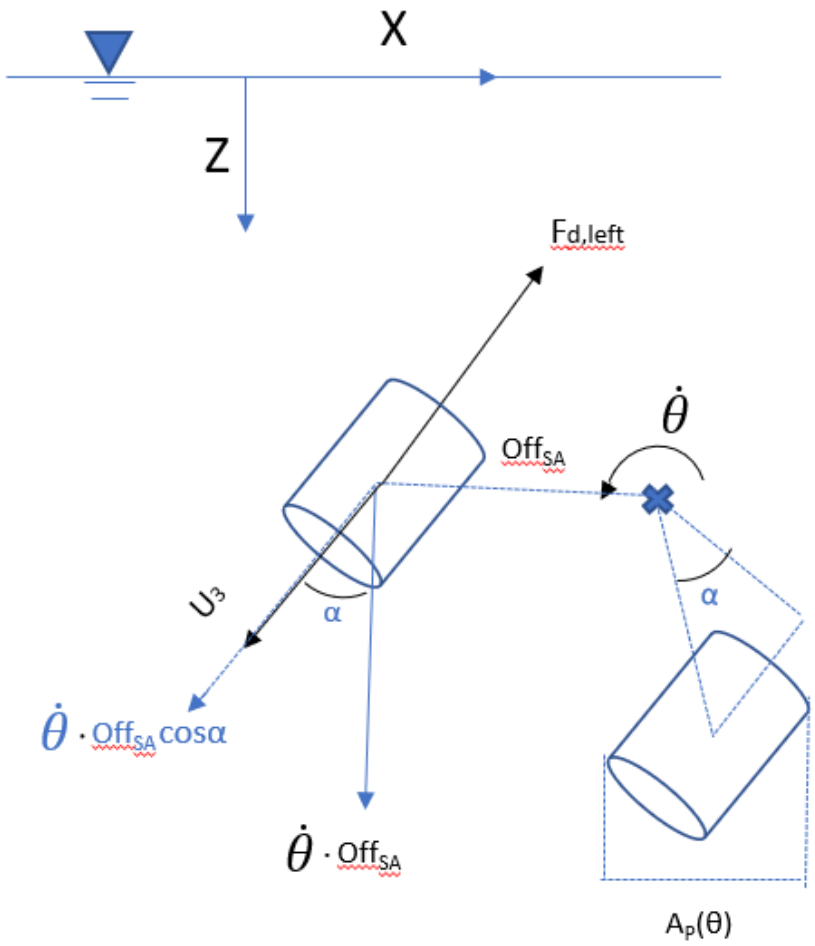

Figure 5.2: Basis for calculation of M_v. α was found to be 22°, and is the angle between the body coordinate system and the offset line between CoG and a suction anchor.

$$M_v = F_{d,left} off_{SA} - F_{d,right} off_{SA} \tag{5.13}$$

$$= 0.5 off_{SA} \rho A_p(\theta) C_D \tag{5.14}$$

$$... * (\dot{z'}_{rel,right}) * |\dot{z'}_{rel,right}| - (\dot{z'}_{rel,left} * |\dot{z'}_{rel,left}|) \tag{5.15}$$

$$\dot{z'}_{rel,right} = U_3 + \dot{\theta} off_{SA} \cos\alpha \tag{5.16}$$

$$\dot{z'}_{rel,left} = U_3 - \dot{\theta} off_{SA} \cos\alpha \tag{5.17}$$

Where $\dot{z'}_{rel}$ is the relative velocity of the left and right suction anchors. $A_p(\theta)$ is the projected area of a suction anchor as a function of θ, see Eq. 5.18. Here the suction anchor is simplified to a box of dimensions D_{SA}xD_{SA}xh_{SA}. This will slightly exaggerate the projected area of a suction anchor, but this is considered positive as the projected area of the rest of the structure has been neglected.

$$A_p(\theta) = D_{SA} * (h_{SA} \sin\theta + D_{SA} \cos\theta) \tag{5.18}$$

5.1.3 Added Mass

Added mass of the model is simplified to regarding the four suction anchor only, which are assumed to dominate. The formulas for calculations A_{33} and A_{11} are taken from [5, 11] which are based on potential theory and corrected for end effects. A_{55} is simplified to the contribution by Steiners theorem for A_{33}. Hydrodynamic interaction is assumed small and neglected in the first approximation. 3D end effects on lower end will be neglected.

The size of the ventilation hole at the top of the suction anchors gives a perforation rate of less than 5% and its effect on A_{33} is therefore neglected, as per [5].

By strip theory, A_{11} can for a cylinder be expressed as

$$A_{11,cylinder} = \rho\pi R_{SA}^2 h_{SA} * 0.63 \tag{5.19}$$

where 0.63 is the correction for end effects[5]. The total added mass in surge is then:

$$A_{11,tot} = A_{11,cylinder} + m_{entrappedwater} \tag{5.20}$$

Added mass in heave, A_{33}, of a suction anchor is taken to be: [5, 11]

$$A_{33} = \rho\pi R_{SA}^2 h_{SA}(1 + \frac{4R_{SA}}{3h_{SA}}) \tag{5.21}$$

where R_{SA} and h_{SA} is the radius and height of the suction anchors.

The A_{55} was then found by applying Steiners Theorem from all four suction anchors

$$A_{55} = 4 * A_{33} off_{SA}^2 \tag{5.22}$$

Where off_{SA} is the in-xz-plane distance between the local center of a suction anchor and the roll axis of the model.

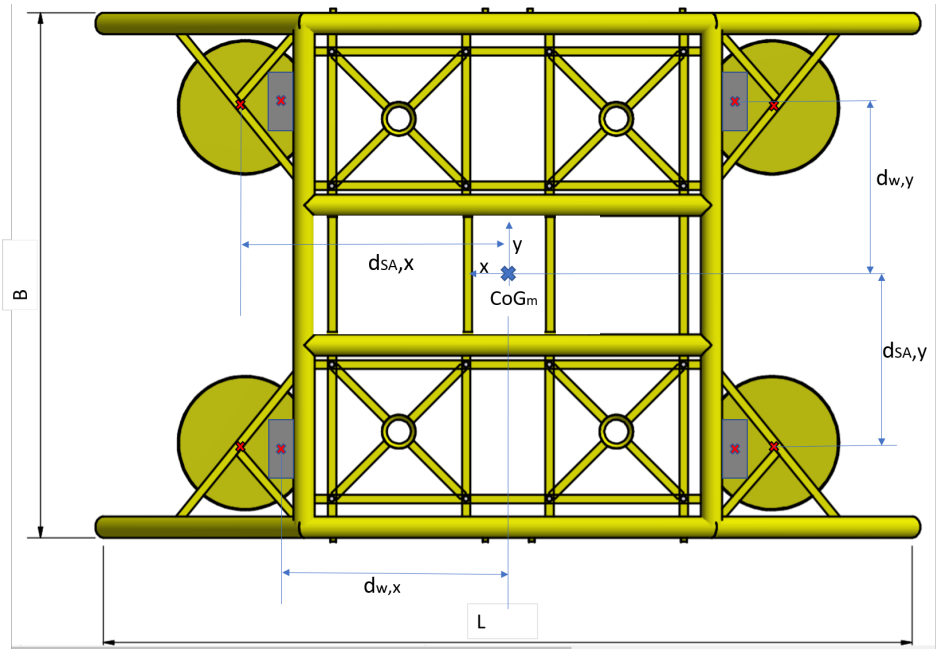

Figure 5.3: Overview of distances used to calculate A_{55} and I_{55}

5.1.4 Moment of Inertia

The moment of inertia of the model was approximated/estimated using Steiners theorem and basic formulas for moment of inertia taken from [12]. In these calculations of I_{55}, the model has been simplified to a rectangular box of evenly distributed mass, and the added weights have been simplified to point masses near the edges of the box, vertically in-plane with the CoG.

$$I_{55,m} = M_m * (L^2 + H^2) \tag{5.23}$$

$$I_{weight} = offset^2_{weight} * M_{weight} \tag{5.24}$$

$$I_{55,tot} = I_{55,m} + 4 * I_{weight} \tag{5.25}$$

where d_{weight} is the distance between the centre of a lead-weight and the model CoG. M_m is the mass of the model without the lead-weights.

5.1.5 Estimation of Drag-induced Moment and Force

‘

As previously mentioned, little is know of the hydrodynamic properties of the modelled structure. As an alternative to calculating the the drag induced effects from a further simplified version of the structure, experimental data was used.

Most of the performed drop-series reached a quasi- steady state during the descent, see Figure 5.4 and 5.5, and this region was used to calculate estimations of M_d and F_b.

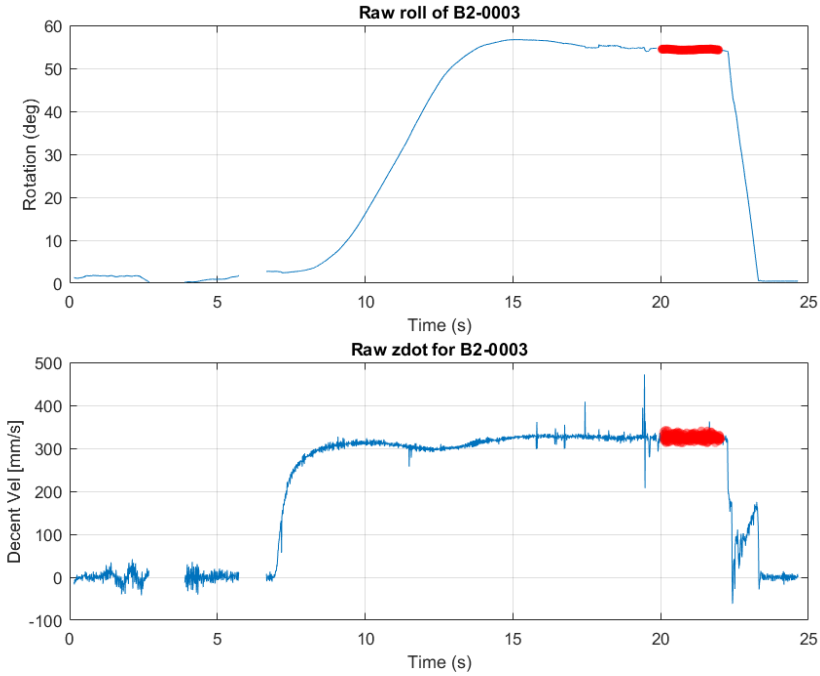

Figure 5.5: Drop with quasi- steady-state marked red, used to estimate C_m and C_d

In steady state, Eq.5.2 and Eq.5.3 will be reduced to

$$M_d = M_{F_b} \tag{5.26}$$

and

$$F_{dZ_G} = Mg - F_b \tag{5.27}$$

So, for each drop, the global descent-velocity $\dot{Z}_G$ and θ of the steady state region was noted, and the corresponding C_d and C_m were calculated from Eq. 5.29 [[14]]. These dataseries were then exported to the curvefitting tool in MATLAB and fitted to a polynomial. The datapoints and fitted polynomial is shown in Figure 6.5 in Section 6.2.

For C_m, a 3rd order polynomial was fitted using least square curvefit methods in MATLAB. The polynomial was constrained in (0,0) and (π,0) as no momentum is expected when the model is perfectly upright or upside down.

$$C_d(\theta) = \frac{F_{d,ZG}}{0.5\rho A_p \dot{Z}_{GSS}(\theta)} \tag{5.28}$$

$$C_m(\theta) = \frac{M_d}{0.5\rho A_p D_{SA} \dot{Z}_{GSS}(\theta)} \tag{5.29}$$

The resulting polynomial for Cm can be shown below, in Eq.5.30. This polynomial is only valid for θ between 0 and π, and was thus in the simulations mirrored around zero to give the correct values for negative θ-values. For Cd, no special trend was found, so the average value of 3.674 was used.

$$Cm = 1.7511\theta^3 - 12.5165\theta^2 + 22.0393\theta \tag{5.30}$$

$$Cd = 3.674 \tag{5.31}$$

Cm is zero for roll angles (0,180°) as the structure is symmetric. In the simulations, a initial roll angle of 0.01° is used to break the equilibrium this definition of Cm causes.

5.2 Calculation of Added Drag Force From Parachute

As parachutes were used in the experiments, a method for estimating of the forces contributed will here be presented.

For the parachuted drop-series, parachute A.3 from [10] was used.

Parachute	D_c [mm]	S_o [mm^2]	D_v [mm]	Cd
A.3	305	97650	40	1.41

Table 5.1: Parachute A.3 characteristics, taken from [10].

Here, D_c is the constructed diameter, S_o is the nominal total surface area of canopy including vent hole and D_v is the vent hole diameter. The parachute is a hand made quarter-sphere parachute with height equivalent to 25% of the sphere diameter. The drag force from the parachute can be estimated by Eq. 5.32 below.

$$F_{d,parachute} = 0.5\rho A_p V_{descent}^2 C_{d,parachute} \tag{5.32}$$

Where the projected area is calculated from the constructed diameter minus the vent hole diameter.

5.3 Model Tests and Scaling

Model tests are often performed to gain understanding in cases where the underlying physics are not fully understood or too complex for an advanced numerical analysis to be viable. Model tests can be used to represent complex geometries, configurations and physics, expose unexpected physical effects and give a visual overview of the processes involved. The drawbacks are connected to time-use, cost and scale effects.

When planning scale model tests, proper scaling is paramount. Misleading results may be produced if done carelessly, leading to wrongly dimensioned and fault-prone full-scale structure. For the results to be applicable in full-scale, similitude between model and full-scale must be met [20].

Achieving similitude consists of achieving three types of similarity; geometric, kinematic and dynamic. Geometric similarity is when all linear dimensions of the model is scaled by a factor λ. Kinematic similarity is connected to similarity of velocity or motion between full-scale and model, such that circular motion in full-scale must be circular motion in model-scale. Dynamic similarity is connected to similarity in forces, such that all relevant force ratios are kept constant [26].

It is unfeasible to maintain all force ratios constant in many scale model test scenarios, especially scenarios regarding the combination or interface between two fluids. In these cases, a specific force ratio is assessed as dominating or deemed most important to uphold. The remaining force ratios which cannot be maintained are denoted as scale effects and estimated as well as possible [9].

In the case of this model test, it is impossible to maintain both the Froude number and Reynolds number. Froude scaling will be used as the velocities involved are

expected to be low, and forces of gravity and buoyancy are assumed governing or most vital to preserve. The scaling laws used are given in 5.6.

Physical Parameter	Unit	Multiplication factor
Length	[m]	λ
Structural mass:	[kg]	$\lambda^3 \cdot \rho_F / \rho_M$
Force:	[N]	$\lambda^3 \cdot \rho_F / \rho_M$
Moment:	[Nm]	$\lambda^4 \cdot \rho_F / \rho_M$
Acceleration:	[m/s^2]	$a_F = a_M$
Time:	[s]	$\sqrt{\lambda}$
Pressure:	[Pa=N/m^2]	$\lambda \cdot \rho_F / \rho_M$

Figure 5.6: Table showing Froude scaling, taken from [26].

Difficulties in scaling often related to viscous flow effects like turbulence, flow separation and vortex shedding. Model consists of four suction anchors connected together by a a mixture of square and circular members. The suction anchors are assumed dominating the hydrodynamic force experiences.

Scale effects are not focused on in this thesis, as this is an initial feasibility study and there are numerous uncertainties and parameter-variations that may have a far larger effect. A short description of some effects are however included.

In the case of this experiment, the ITS model is intended to descent orientated as it was placed on land. This presents the sharp edges of the suction anchors (SA) to the flow. Some wake effects will arise, but these are assumed non-dominating. Wake will likely be turbulent in model-scale because of the sharp edges. Geometries with sharp edges is less effected by scaling, as the point of separation is defined. The round members of the structure, and the suction anchors when the model is pitched or rolled 90°, will likely experience a somewhat higher drag that full-scale as the flow in model-scale is laminar.

Chapter 6

Results

In this chapter, trends and observations from the experiments are presented. The main results are presented in section 6.1, regarding velocity and stability of the descent. These results are presented in full-scale values. In the rest of the chapter, modelscale is used.

Then the result of the numerical simulation is presented along with a sensitivity analysis. The observed horizontal travel for different drop-series will be shown, along with observations regarding the effect of initial orientation of the structure and effect of skidded launch. Then the results of the parachuted drop-series are presented, before the coefficient of drag from the experiments are compared to values found in the literature. The chapter finishes with possible trend observed regarding how roll angle and descent speed correlate, observations regarding the tendency direction of rotation for drop-series.

To reiterate, the body coordinate system was defined as shown in Figure 4.8, going against the more conventional method of having the x-axis going in the longest dimension of the structure. This entails that what is referred to as roll in this thesis would conventionally be denoted pitch.

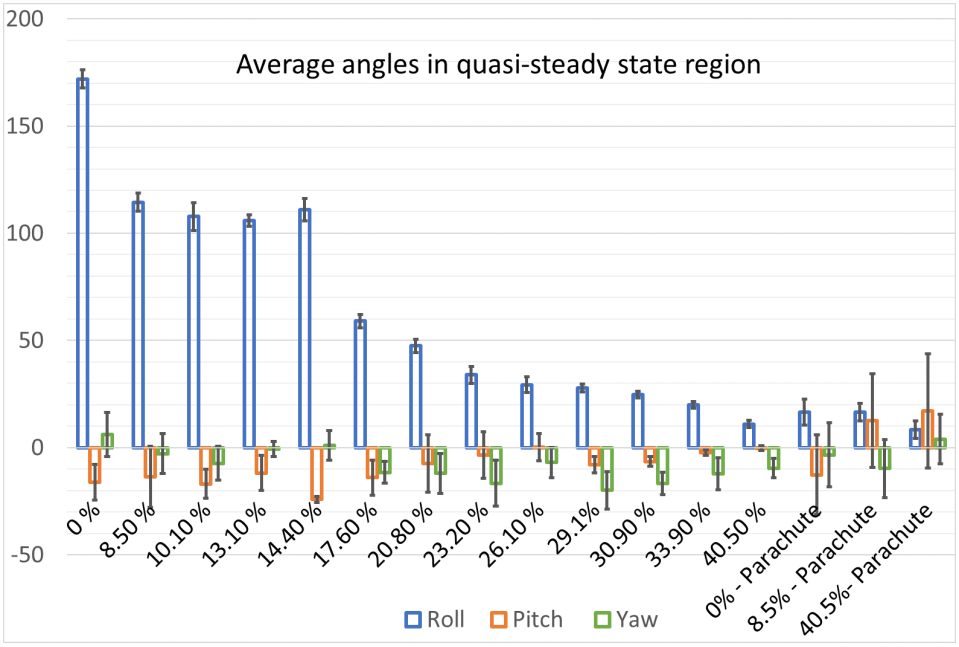

Figure 6.1: Average roll, pitch and yaw angles relative to buoyancy and with or without parachute.

Table 6.1: Buoyancy contributions from the different Buoyancy-blocks used.

Buoyancy-block	% added buoyancy
B_1	8.5
B_{1-2}	10.1
B_{1-3}	13.1
B_{1-4}	14.4
B_2	17.6
B_{2-2}	20.8
B_{2-3}	23.2
B_3	26.1
B_{3-2}	29.1
B_{3-3}	30.9
B_{3-4}	33.9
B_4	40.5

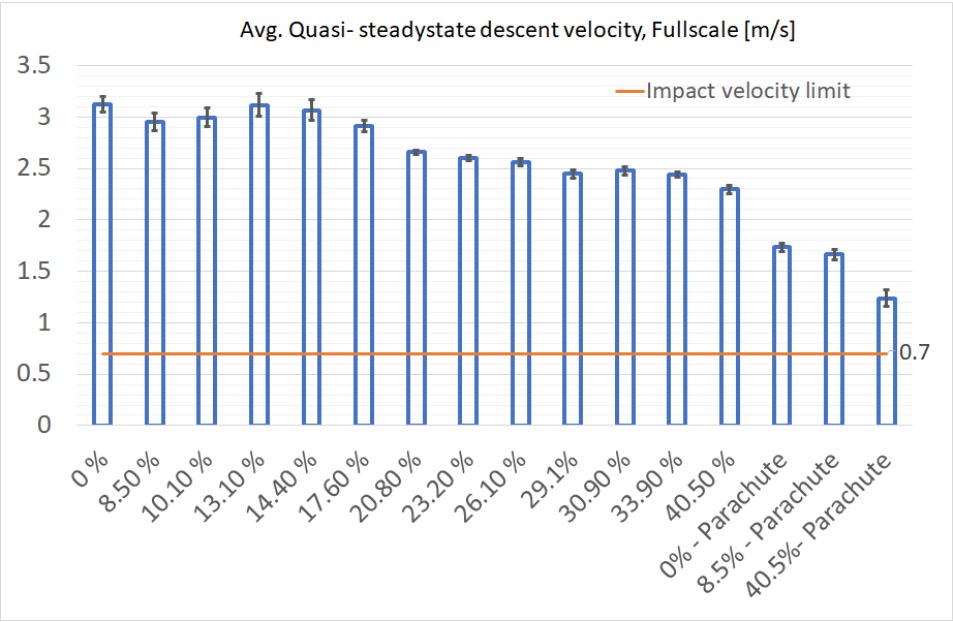

Figure 6.2: Average results of analysis of quasi-steady-state region. Error-markers show standard deviation for a drop-serieseries.

6.1 Important Trends

Figure 6.2 show the average measured descent speed of the quasi-steady-state regions observed. The full scale impact speed limit is taken as 0.7m/s ([16]).The slowest non-parachute drop is B4, with calculated full-scale velocity if 2.3m/s, or 328% of the stated limit. Thus it is clear that additional retardation of system is required, else severe upgrades to the sturdiness of the structure must be made.

The slight increase in velocity around B_{1-3} is caused by the structure hitting bottom at the top of a temporary speed increase occurring around 100° roll. This trend will be further explained and discussed in section 6.8.1.

The structure consistently rotates about its transverse axis. The source of this consistency is not known, but is possible it stems from hydrodynamic effect on the suction anchors, whose trailing edges experience a long moment arm about the roll axis of the structure.

As expected, steady-state roll angle and descent velocity decreases with larger buoyancy-blocks. Higher total buoyancy force reaches equilibrium with the drag

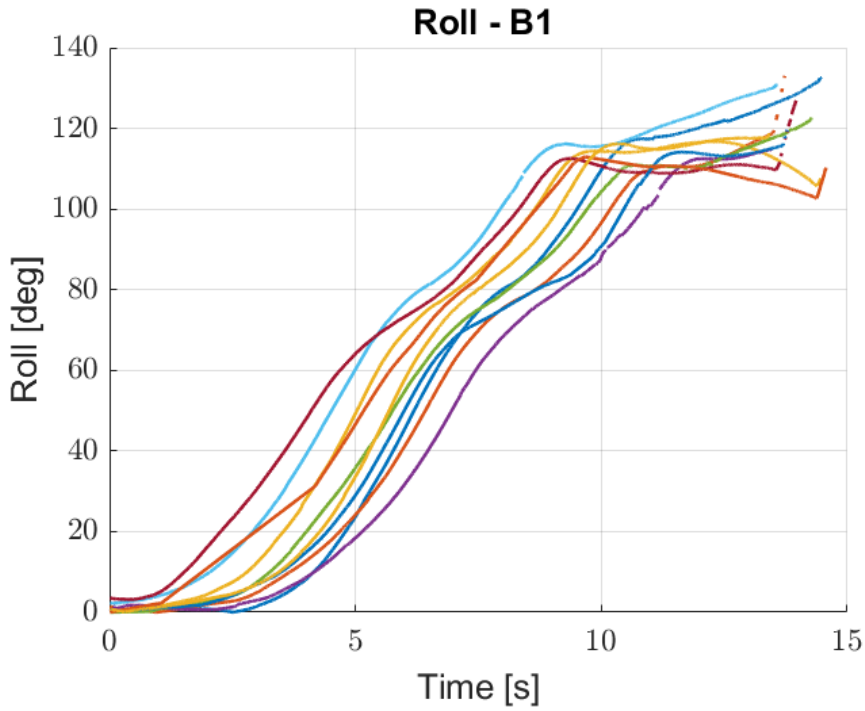

Figure 6.3: Measured Roll angle for drop-series with buoyancy-block B1. Notice the "lack" of steady state in the region past t= 10s.

induced moment faster, reducing the steady-state roll angle. In addition the blocks contribute with some added projected area, further reducing descent velocity.

Steady state regions for global descent velocity was observable for almost all drop-series. Proper steady state regions for roll angle θ was however less frequent for lower buoyancy block sizes. To showcase this, Figure 6.3 is used. All drop-series start with pronounced, near constant increase in angle. This period continues til the steady state angle is reached, where some drop-series stabilise while others slowly increase or decrease until impact. This trend is reduced with increased buoyancy.

It is important to note that the values for pitch and yaw in Figure 6.1 and 6.2 are the average of values in the time period of steady-state for descent velocity and roll angle. Yaw and pitch seldom reached any from of steady-state. Slowly varying in the beginning, yaw and pitch stay somewhat grouped until steady-state roll is reached, then diverge.

Using B1 as an example, see Figure 6.3, it is possible to divide the course of a drop

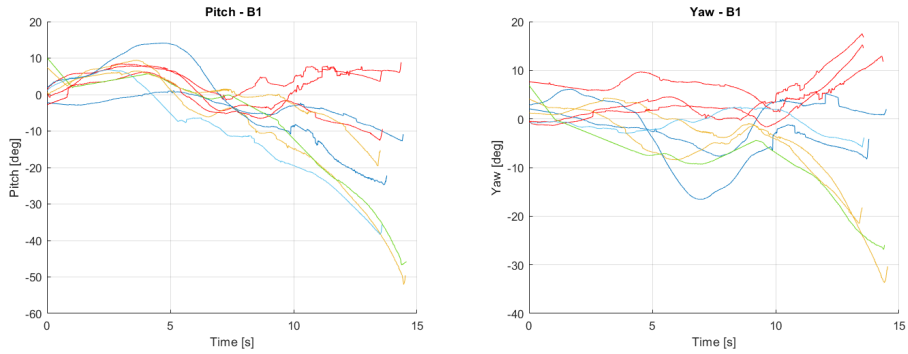

Figure 6.4: Pitch and Yaw for B1 drop-series. Notice diverging trend around t = 10sec, around same time as roll reaches quasi steady state, see Figure 6.3

into two phases. B1 is here used to showcase a trend visible for all drop-series.

The first phase is dominated by increase in descent velocity and roll angle, with less motion in pitch and yaw observed. In the second phase, roll and descent velocity reach the quasi-steady-state and around this time, a slight increase in pitch and yaw is observed. There seems to be a slight trend here of yaw and pitch diverging when roll and descent velocity reach steady state, see Figure 6.4.

The basin is too shallow to observe if pitch and yaw stabilize, therefore true steady state for the structure has likely not been observed. Larger buoyancy block means faster stabilization, but even for the largest block B4, yaw and pitch have a visible trend of slowly varying at impact.

6.1.1 Safe Descent Velocity by Extrapolation of Data

An estimation of the amount of buoyancy needed to achieve descent velocity below the stated limit is presented here. It is based on extrapolation of data, and is only meant to give an indication, not an exact value.

By assessing the weight and buoyancy of the structure itself, it can be concluded that the structure becomes neutrally buoyant at 77.5% added buoyancy. In this configuration, the structure is assumed to have no descent velocity.

By assuming a linear trend of descent velocity from observed descent velocity of B4 to the point of zero descent velocity of 77.5%, a value for the needed buoyancy to achieve the impact limit velocity can be found.By interpolation between the

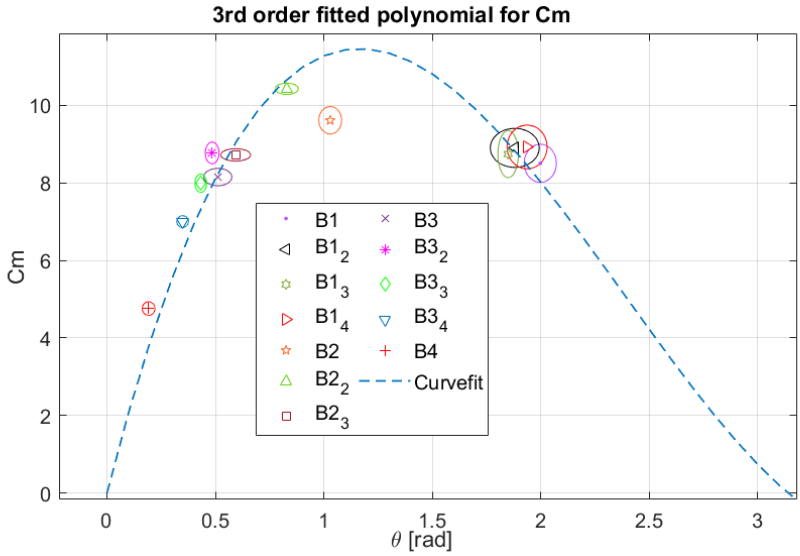

Figure 6.5: Curvefit coefficients of moment, with ellipses of standard deviation.

steady state descent values of B4 and 77.5% added buoyancy, it can be found that the structure will achieve a descent velocity within the limit for >66% added buoyancy.

6.2 Simulation Results

In this section, results from the simulation will be presented. First in this section the found values for the coefficients of drag and moment presented. Then the simulation will be compared to the experiments before a sensitivity analysis of different parameters is shown at the end of this section.

Figure 6.6 and 6.5 show the resulting polynomials from the analysis of the coefficients of moment and drag for all drop-series, estimated as shown in Section 5.1.5. No special trend was found for C_d, therefore the average was taken as the value for C_d in the simulations. The fitted polynomial for C_m was forced to be zero at roll angles of $0°$ and $180°$, which resulted in the 3rd order polynomial shown in Eq. 5.30.

Forcing the polynomial of C_m through specific points and averaging C_d increases the error relative to the measured points. The effect of this is clear in the compari-

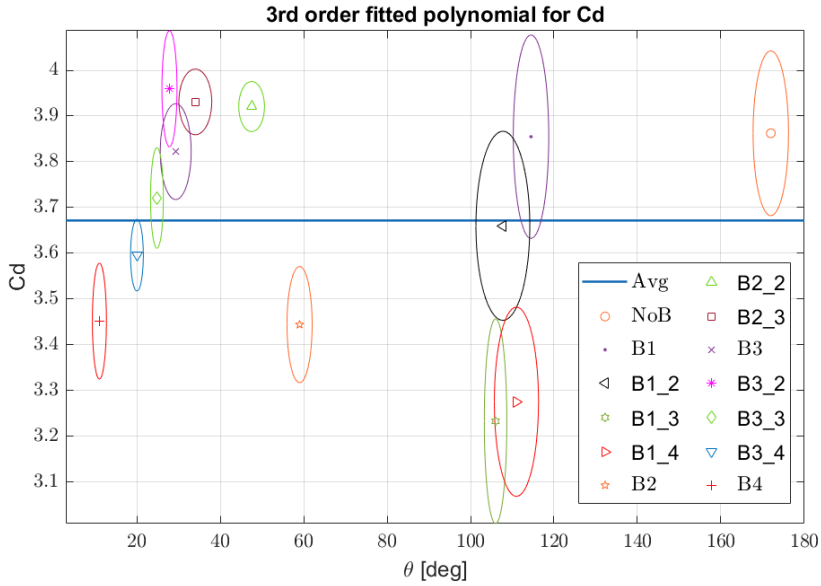

Figure 6.6: Curvefit coefficients of drag, with ellipses of standard deviation.

son between simulation and experiments.

	Measured[deg]	Simulated [deg]		Measured [mm/s]	Simulated [mm/s]
B1	114°	113.4°	B1	341	349
B2	58°	72°	B2	336	326
B3	29°	34°	B3	296	302
B4	11°	0.5°	B4	265	257

Table 6.2: Average steady state θ and $\dot{ZG}$ from drop-series and simulation

Seen in Figures 6.7 and 6.8 are measured roll and descent velocity $\dot{ZG}$, with the simulated result overlaid. The simulator does not capture the full dynamics of the drop-series, clearly seen in the case of B1 drop-series. This is to be expected as the simulator is built on a simplified model of the system, most notably excluding lift effects, but also simplified geometries. With increased size of buoyancy block,

The region of sudden velocity increase and decrease for B1 drop-series has been named *Speedbumps*, and will be discussed in section 6.8.1. The same phenomena can to some degree be seen in B2 drop-series, here the effect is more dragged out, with the drop-series ending before the velocity can begin decrease again. The

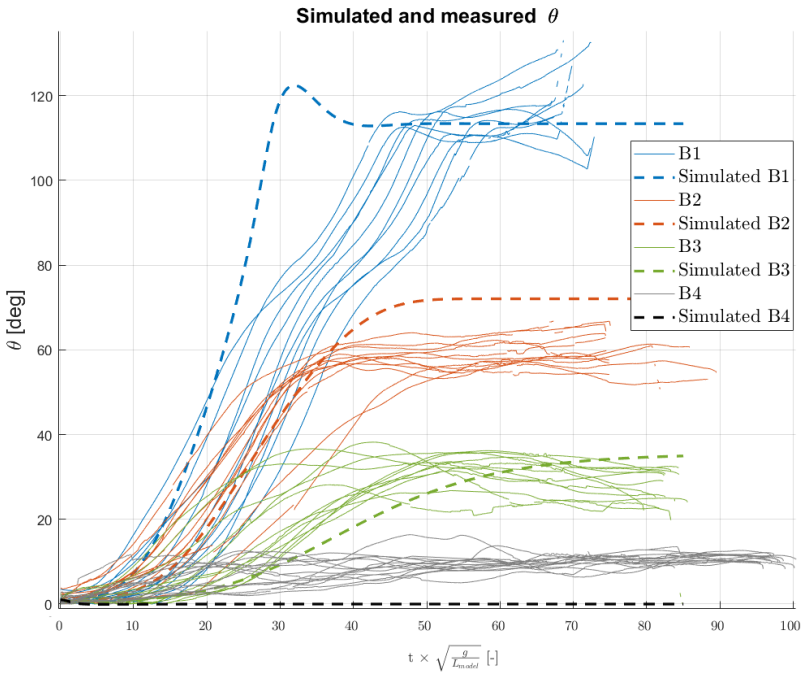

Figure 6.7: Simulated and measured roll,θ, for all main buoyancy cases

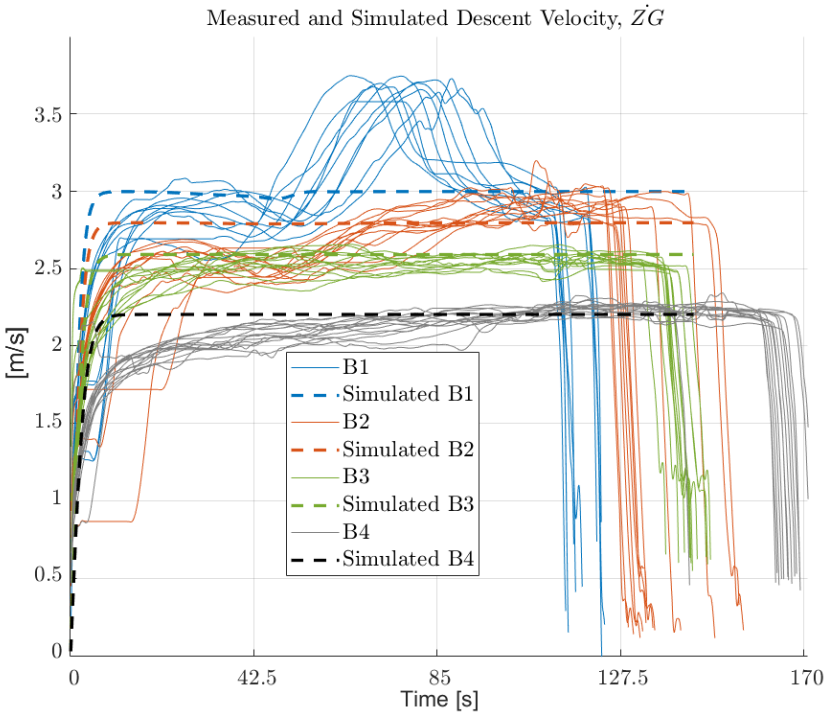

Figure 6.8: Simulated and measured descent velocity, $\dot{ZG}$, for all main buoyancy cases

effect is connected to roll angles above 50° and is therefore not visible for B3 and B4. The discrepancy of the initial increase to steady-state region is assumed connected to the stated limitations of the model.

The simulated $\dot{ZG}$ matches the measured steady state velocities with some smaller offsets. More deviations are seen in the comparison between simulated and measured roll in Figure 6.7. B2 is the most erroneous, even though the differences for B4 are most distinct.

The measured C_d of B2 is below the average and thus the simulated $\dot{ZG}$ will be too low. This error propagates into the calculations for drag-induced moment, M_d. In addition, the measured C_m of B2 is 17% lower that the curvefitted value, leading to an increase in the drag-induced moment, M_d, which again results in the offset for steady state θ observed. The large discrepancy between the measured C_m and C_d of B2 and the fitted polynomials is likely connected to an increase in $\dot{ZG}$ observed for drop-series around θ = 100°. This will be discussed more thoroughly in section 6.8.1.

The reason for the low simulated roll angle for B4 lies in the C_d and C_m used. Considering Figure 6.5, the curve-fitted polynomial for C_m gives a 16% lower value for C_m than measured for B4 drop-series. This, combined with the measured C_d of B4 being 6% lower than the taken average, leads to a significant reduction in M_d, resulting in a simulated steady state value for θ of less than 1°.

6.2.1 Sensitivity Analysis

Here the sensitivity analysis performed is presented. Initial roll angle, added mass, moment of inertia, coefficient of drag and coefficient of moment has been varied to see how sensitive the simulation model is to different parameters.

As can be seen in Figures 6.9 and 6.10, the simulation is largely insensitive to variations in initial roll angle and the moment of inertia. As the righting moment from the buoyancy block is independent of the fall velocity, the initial roll angle is corrected before the drag induced moment has time to grow.

For variations in A_{33}, the simulation becomes unstable at around 2.2 times original A_{33}. A further increase results in increased amplitude of the seemingly steady state oscillations around -34°, which is the negative of the simulated steady state roll angle, $\theta_{ss,sim}$. Why these steady state oscillations occur is not understood.

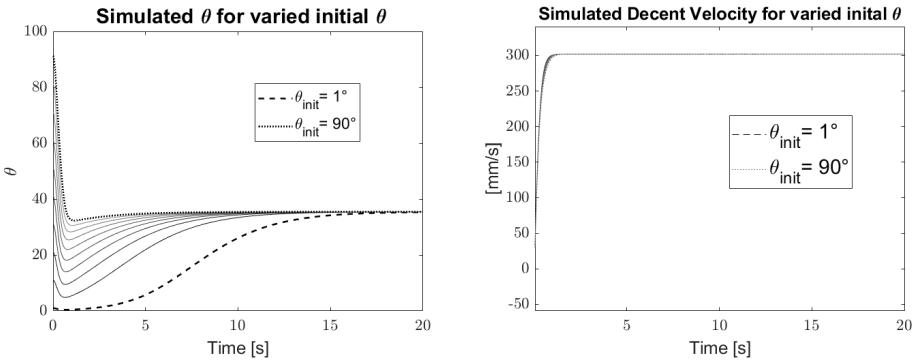

Figure 6.9: Simulation results from varying initial θ, 10° increment

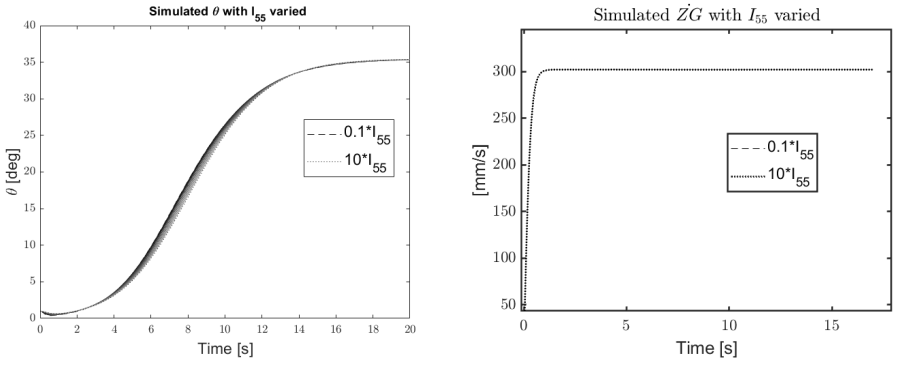

Figure 6.10: Results from varying I_{55} between 10% and 1000%, with 100% increment.

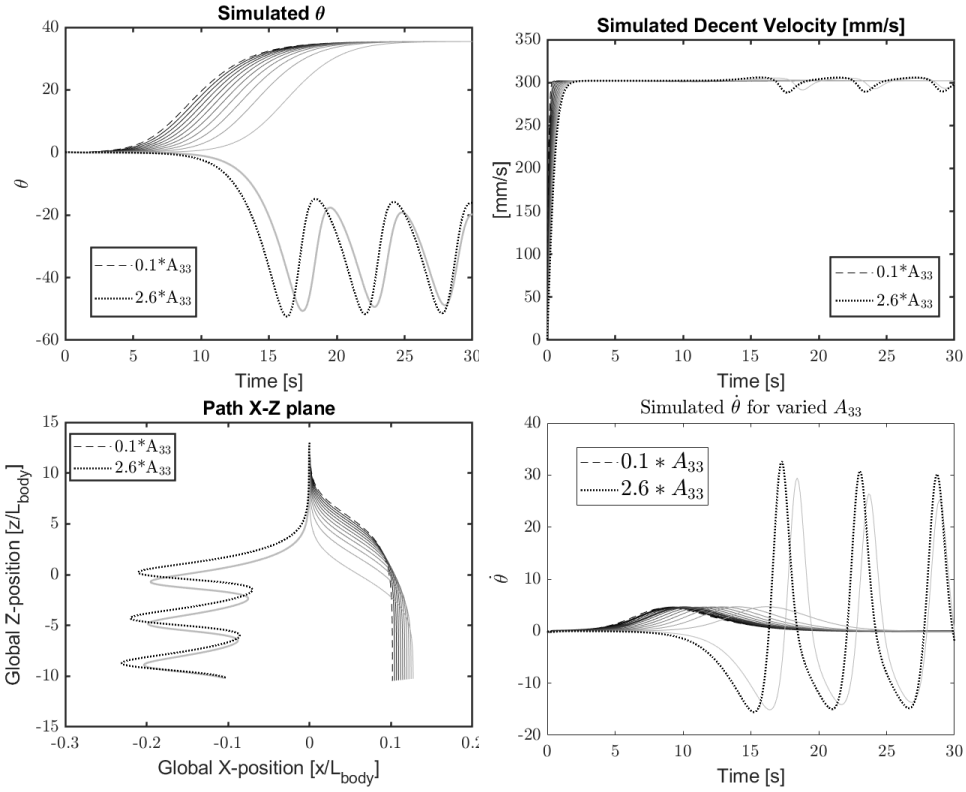

Figure 6.11: Results from varying A_{33} between 10% and 260%, 20% increment

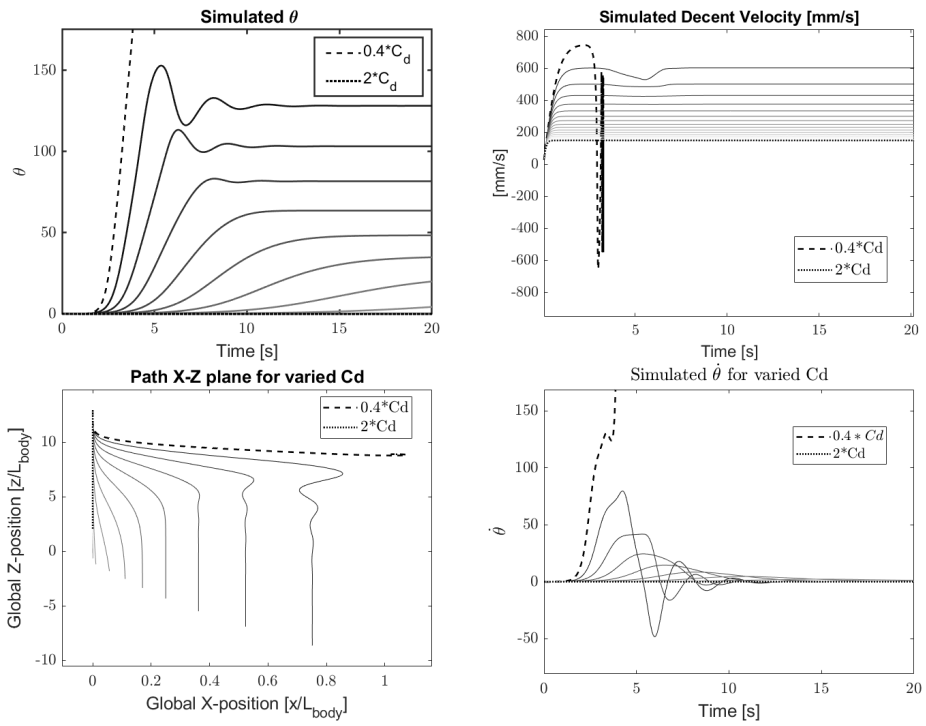

Figure 6.12: Results from varying C_d between 40% and 200%, 10% increment

Varying the projected area used, A_p, has little effect as all terms were A_p enter into also contains either C_m or C_d. These terms are inverse proportional to A_p, thus any change in A_p will be cancelled out.

Simulation turns unstable for $C_d < 1.468$, or 40% of the original value. Low C_d values lowers the simulated drag force and thus increases descent velocity, and decreases the velocity dependent moment M_v opposing the rotation. High speed and lowered resistance to rotation means free reign for the drag induced moment, turning the simulation unstable.

As seen in Figure 6.13, low values of C_m results in almost no induced roll angle, because the righting moment for the buoyant force is unaffected. At around 2.1 times the original C_m, resistance against rotation can no longer withstand the drag induced moment, turning the simulation unstable. The descent velocity is largely unaffected by variations in C_m, with the exception of when closing in on the limit of stability.

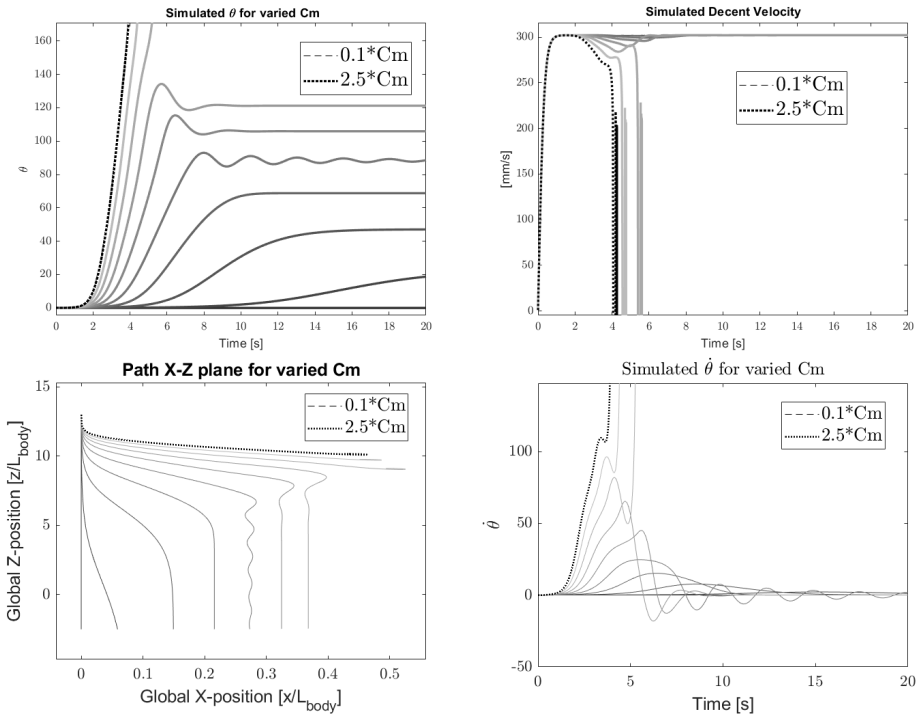

Figure 6.13: Results from varying Cm between 10% and 250%, 20% increment

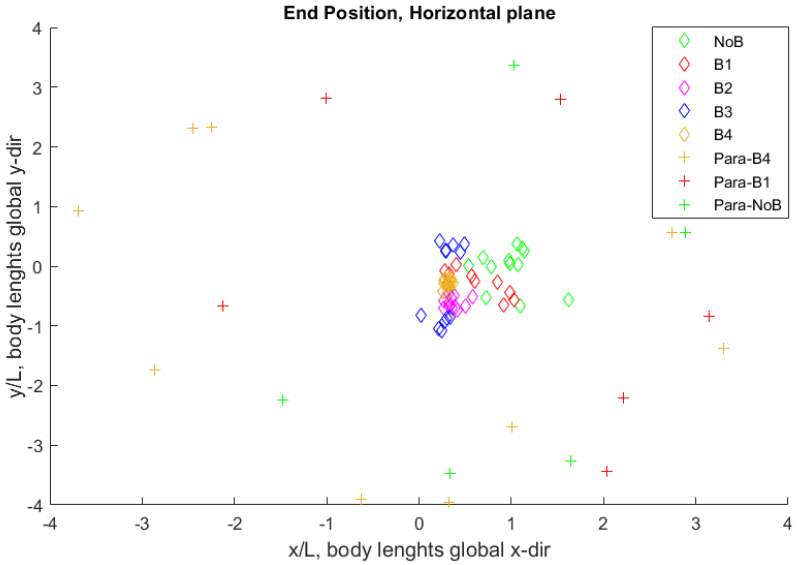

Figure 6.14: Scatter-plot showing touchdown position for different drop-series. Drops in between B1 and B4 are not shown in order to reduce clutter in figure.

6.3 Horizontal Travel During Descent

In this section, the horizontal travel of different drop-series is presented. In general it is observed that larger buoyancy blocks reduces the distance travelled.

As seen in Figure 6.14, buoyancy affects the distance travelled for normal drop-series. This effect is not large, nor is the average distance travelled for normal drop-series, seen in Table 6.3. The difference between parachuted and normal drop-series is very large, but it is important to note that the parachute used was not optimised for the structure. This will be emphasized in Section 6.6.

6.3.1 Simulated vs. Measured Travel

Here a comparison between the measured and simulated travel in the XZ plane is presented. This is of interest as it might give an indication to the importance of lift effects.

As seen in Figures 6.15, 6.16 and 6.17 the simulated trajectory does not completely

Drop	Average body-lengths travelled [mm/L_{body}]	% of fall distance travelled
NoB	1.025	7.8%
B1	0.69	5.3%
B2	0.72	5.5%
B3	0.72	5.5%
B4	0.42	3.2%
Para-NoB	3.2	25%
Para-B1	3.1	23.8%
Para-B4	3.4	26.2%

Table 6.3: Average distance travelled during descent

follow the measurements. The simulation reaches steady-state and travelled path will not increase with depth. The measured paths however, have a more or less continuous angled descent, meaning that the difference between simulated and measured travel will increase with depth. This difference is possibly caused by the un-modelled lift effects.

6.4 Effect of Drop Orientation

The result of an investigation into the descent dynamics of the B1 buoyancy block will be presented in this section. Three drop-series with varying initial orientation was performed in order to find the steady state region of B1 drop-series.

Because the structure pitches more than 90 degrees, data capture problems occur because of the singularity of Euler angles. Therefore this section is primarily discussed using screenshots from the software.

Drops performed with B1 buoyancy block were observed to to a lesser degree reach steady state than other drop-series. Several additional drop-series with this buoyancy block were therefore done in order to investigate if a more steady state could be reached for this block-size too. Initially, the drop-series were pre-rolled to 90 °, and the findings from these drop-series lead to two additional drop series. One where the structure was pre-rolled to 180 ° before release and one where the structure was pre-pitched 90 °.

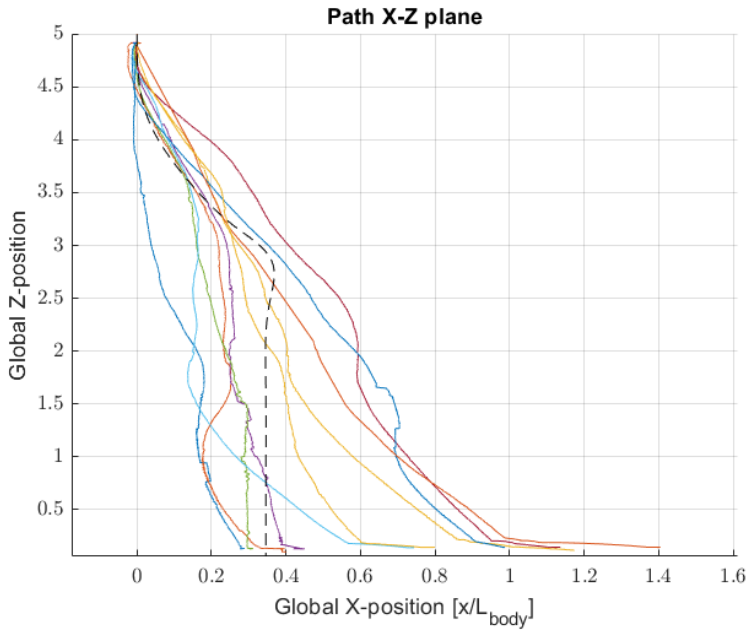

Figure 6.15: Simulated and measured path in X-Z plane for B1 buoyancy block

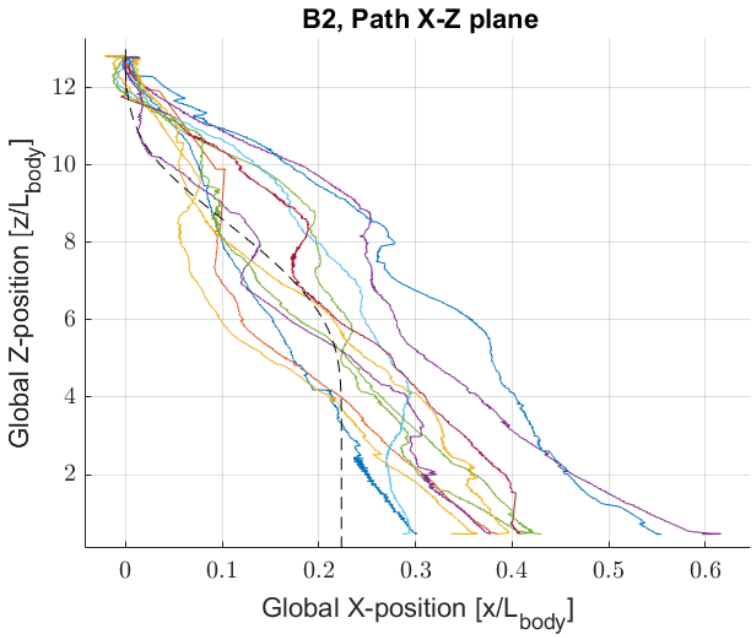

Figure 6.16: Simulated and measured path in X-Z plane for B2 buoyancy block

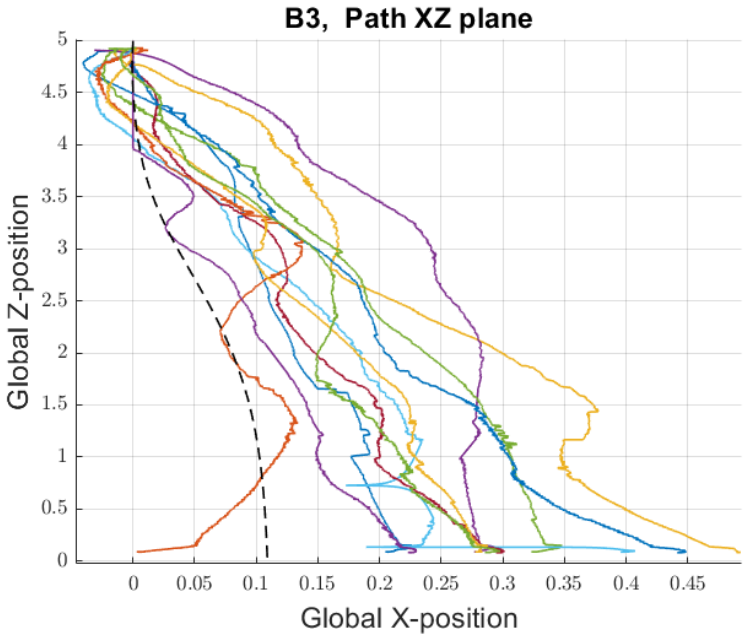

Figure 6.17: Simulated and measured path in X-Z plane for B3 buoyancy block

Overall it seems that the steady-state for for B1 drop-series is around a pitch angle of 80 °. After release, the structure seeks a roll angle around 140 ° before a burst of rotation in pitch occurs and the structure stabilizes around the pitch angle of 90 °, see Figure 6.18. Horizontal travel is significant for these unorthodoxly initial-orientated drop-series, almost comparable to that of parachuted drop-series, see Figure 6.22. This indicates substantial lift effects occurring.

Figure 6.18 shows a series of snapshots of a B1 drop where the structure was dropped with an initial roll of 90°. The structure slowly rolls to an angle of around 140° before simultaneously beginning to rapidly pitch until structure is rolled to just below 180 ° and pitched just below 90°, orientated broadside down. This phenomena, named *pitch-flip*, fully developed for about half of the drop-series, the rest only beginning to flip when encountering the basin floor. In Figure 6.23, the "speed bump" seen occurs as the same time as the pitch-flip, possibly indicating lower drag force either because of rapid rotation, or because of the region of pitch-angle experienced.

To further investigate the pitch-flip, a drop series was done where the structure was pre-rolled 180°, or upside-down, see Figure 6.19. Here the same flip occurs, and afterwards the structure seems to steadily descent downwards in this sideways,

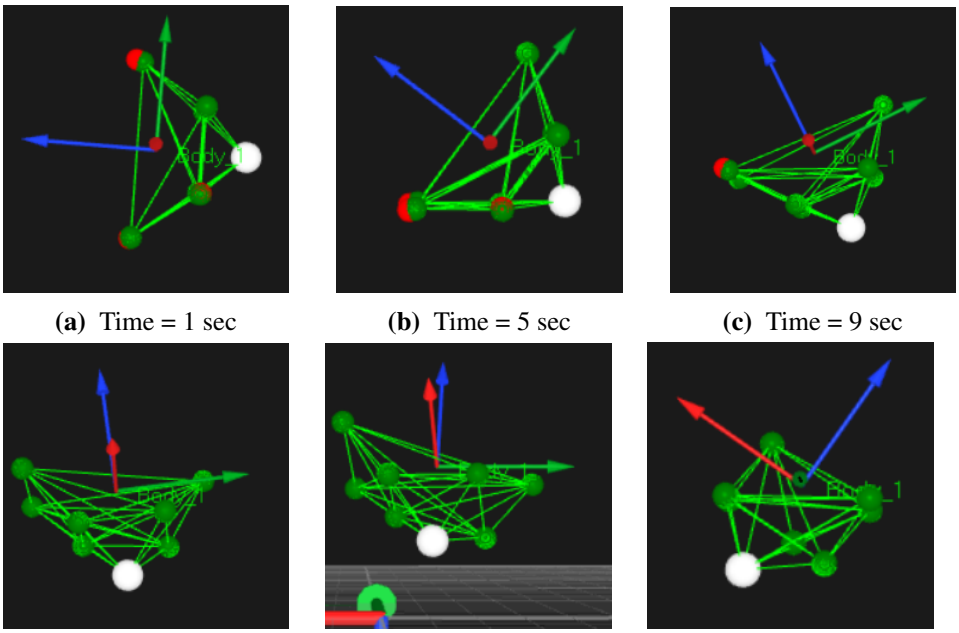

(a) Time = 1 sec

(b) Time = 5 sec

(c) Time = 9 sec

(d) Time = 12 sec

(e) Time = 14 sec

(f) Time = 14 sec, Body XZ-plane

Figure 6.18: Snapshots from QTM showing drop of B1 pre-rolled to 90° before release. All images except **f)** seen in global XZ plane, notice how structure begins to sharply pitch shortly before landing. X-direction is the red arrow, Y-direction is green and Z-direction is blue.

broadside down orientation. As mentioned, horizontal drift is substantial, for a scatter plot of landing position see Figure 6.22.

To investigate the dynamics and stability of the structure post pitch-flip, another drop-series was done where the structure was pre-pitched to 90°, see Figure 6.21 for snapshots of the motion. These drop-series are remarkably stable, rotating very little in any direction and drifting slightly "forward", in the direction the top of the model pointed. Seen in Figure 6.22, these drifted only slightly longer than the ordinary submerged B1 drop-series. The structure seems to stabilise at a pitch around 77°, see Figure 6.20.

6.5 Effect of Skidded Launch

In this section, the observed effects of skidded launch will be presented.

The model was skidded into the water by a ramp, to see how this would affected the stability of descent. This launch was only done for buoyancy block B4, as it was deemed the most stable of the tested buoyancy blocks.

The slope of the ramp was measured to 12.3°, with the edge positioned 2 cm above the surface(5,2% of length of body) or 1.5m in full-scale. This is probably in the high end of acceptable drop height, but adjustment of the ramp proved challenging. The launch velocity was estimated from video and varied between 0.8m/s and 1.1m/s. The structure was as mentioned pushed standing on the suction anchors down a sloped plate, broadside first. While sliding down, the structure often rotated in yaw, sometimes more than 90°. These drop-series are denoted "Skewed" in the figures.

In general, these drop-series were more uneventful than expected. increase in launch velocity naturally increased the maximum pitch or roll experienced as the structure hit the surface, but structure usually righted itself within one body- length of descent and proceeded to descent as a normal B4 drop with whatever yaw angle gained during the slide. In Figure 6.24 a launch is shown as a series of snapshots. It was however observed that when the structure skewed during slide, protruding members reconnected with the ramp. Because of this broadside launch advised.

Considering Figure 6.25, descent velocity for ramplaunched drop-series seems to be largely the same as for normal B4 drop-series.

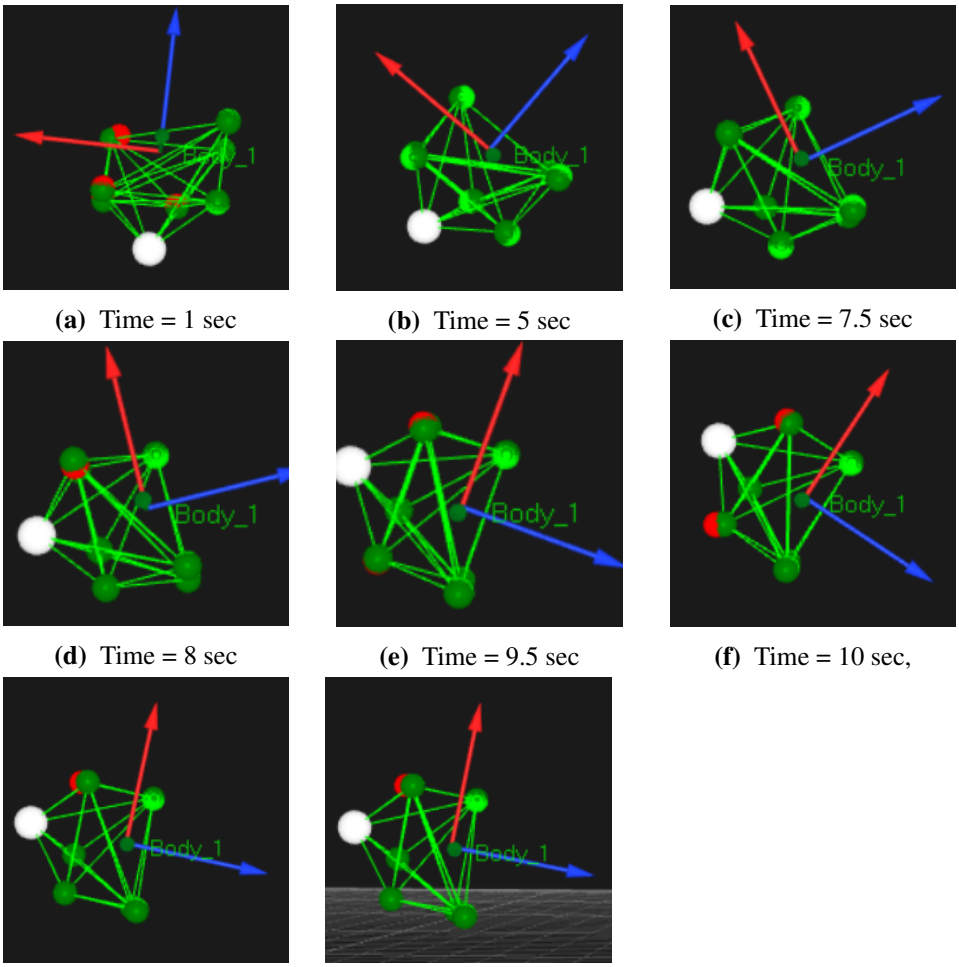

(a) Time = 1 sec **(b)** Time = 5 sec **(c)** Time = 7.5 sec

(d) Time = 8 sec **(e)** Time = 9.5 sec **(f)** Time = 10 sec,

(g) Time = 13.5 sec **(h)** Time = 15.5 sec,

Figure 6.19: Snapshots from QTM showing drop of B1 pre-rolled to 180° before release. All images Body YZ plane. Notice how structure performs the "pitchflip" around t= 10sec. X-direction is the red arrow, Y-direction is green and Z-direction is blue.

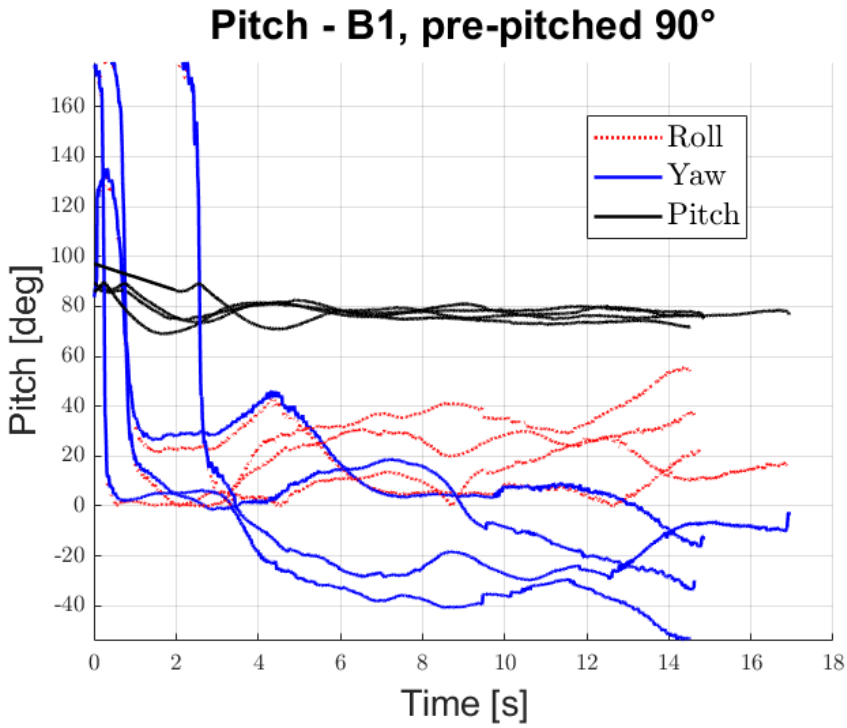

Figure 6.20: Figure showing measured roll, pitch and yaw for the drop-series pre-pitched to 90 °. As the structure has slow rotations not crossing pitch= 90°, Euler singularity issues were avoided and data regarding body angles could be extracted.

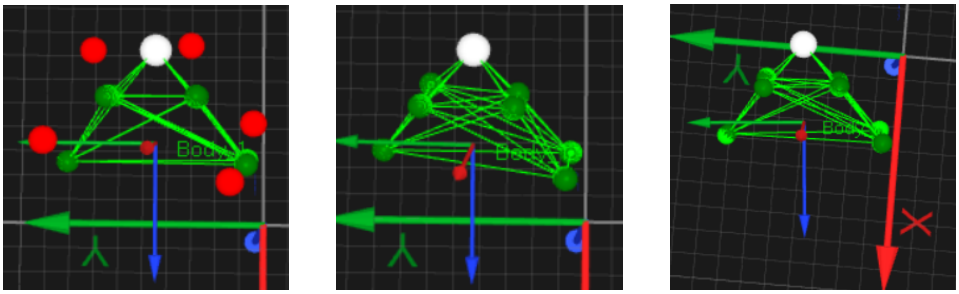

(a) Time = 1 sec **(b)** Time = 2 sec **(c)** Time = 9 sec

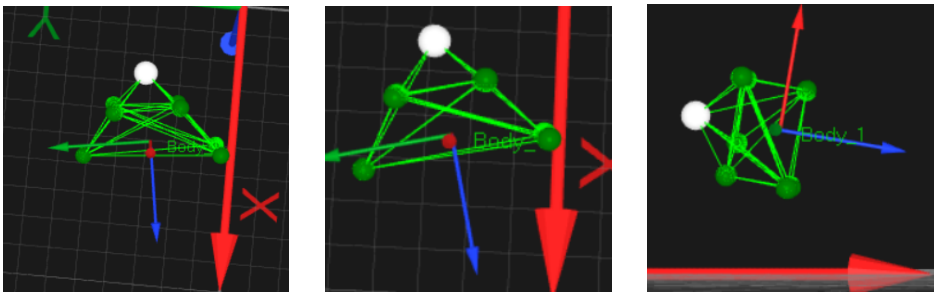

(d) Time = 12 sec **(e)** Time = 14 sec **(f)** Time = 14 sec, Body YZ-plane

Figure 6.21: Snapshots from QTM showing drop of B1 pre-pitched to 90° before release. All images except **f)** seen in global XY plane, note global coordinate system in background global X-direction is the red arrow, Y-direction is green and Z-direction is blue.

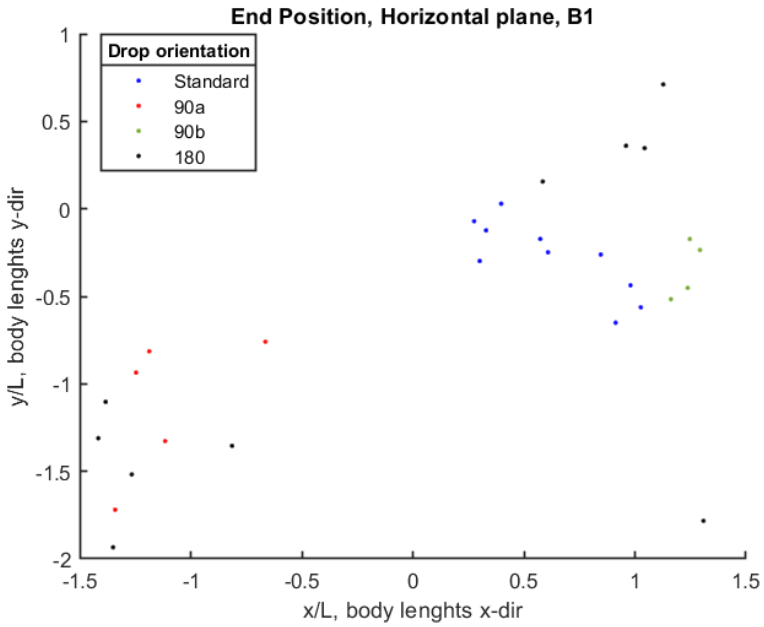

Figure 6.22: Scatter-plot of endposition in the XY-plane for drop-series with B1 buoyancy-block. *"90a"* denote drop-series dropped 90 ° rolled relative to normal, *"90b"* denote drop-series dropped 90 ° pitched and *"180"* denote drop-series dropped upside down, or pitched/rolled 180 ° from standard orientation

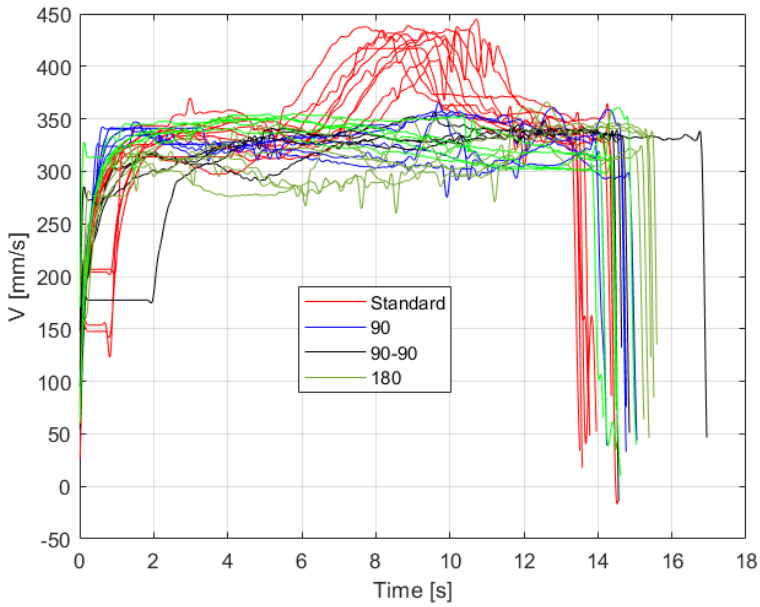

Figure 6.23: Plot showing differences in descent velocity for different drop orientations

As seen in Figure 6.27, the dynamic entrance of the descent seems to somewhat affect the path of the structure, giving a slightly larger spread for the *Broadside*-category.

Most of the interesting dynamics take place just as or immediately after the structure connects with the surface. This is a problematic period for the Qualisys software as, near the surface, reflections from the surface confuse the cameras and software. As seen in Figure 6.25, the data quality is poor early in the drop-series.

6.6 Descent Velocity Retardation- Parachuted Drops

In this section the results of parachuted drop-series are presented. As impact velocity is a key issue regarding feasibility of the L&F method, methods for reducing descent velocity below the impact-velocity limit should be explored.

Parachuted drop-series with buoyancy-blocks B1, B4 and no buoyancy were performed. It is important to note that the parachute used was not made or optimised for the experiments of this thesis. The parachute is hand made of fabrics not nor-

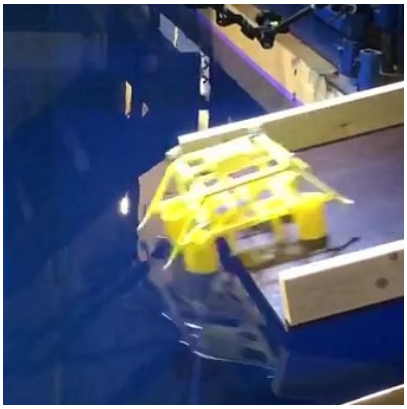

(a) Water-entry

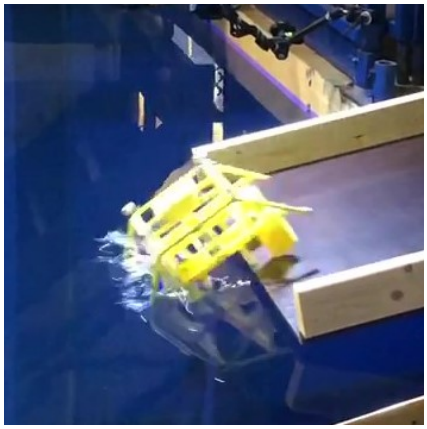

(b) 0.15 sec after Water-entry

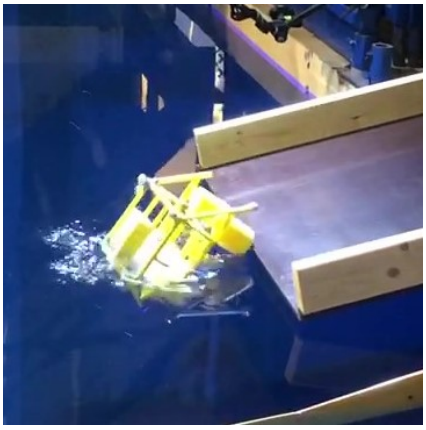

(c) 0.40 sec after Water-entry

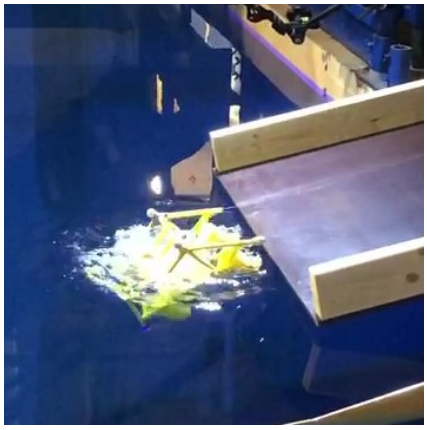

(d) 0.70 sec after Water-entry

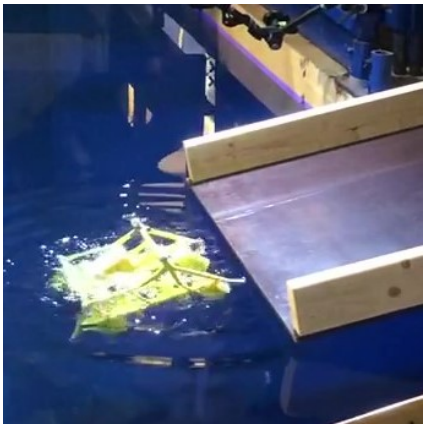

(e) 1.40 sec after Water-entry

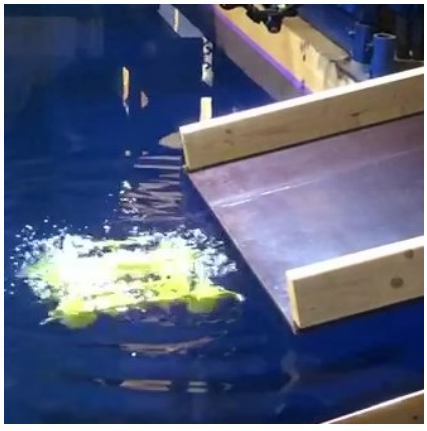

(f) 2 sec after Water-entry

Figure 6.24: Snapshots of launching. The timespan between the first and last picture is 2 seconds.

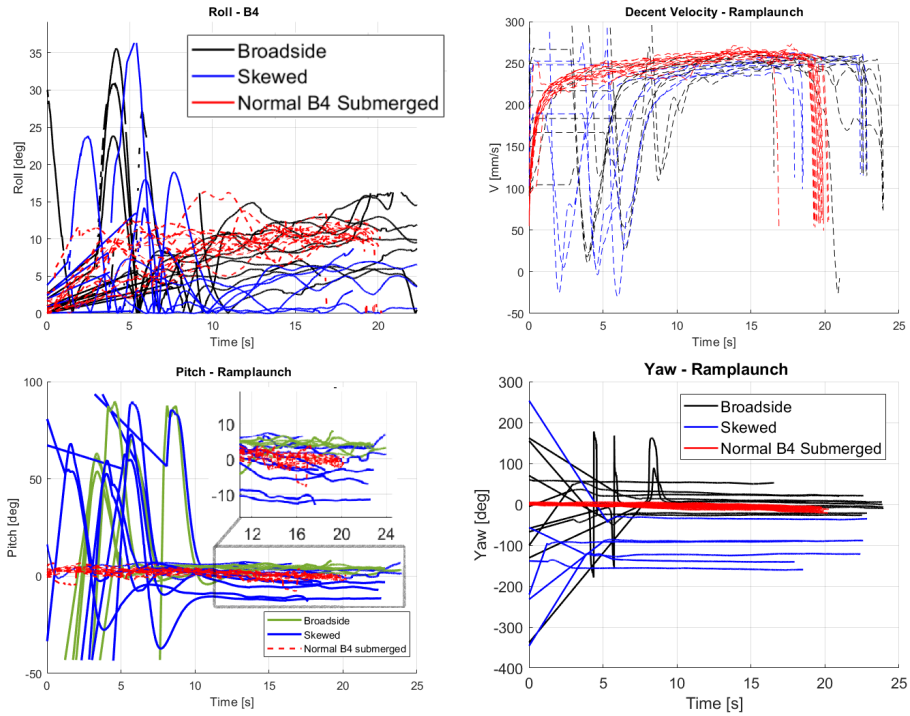

Figure 6.25: Attitude and descent velocity for normal and ramp-launched B4 drop-series

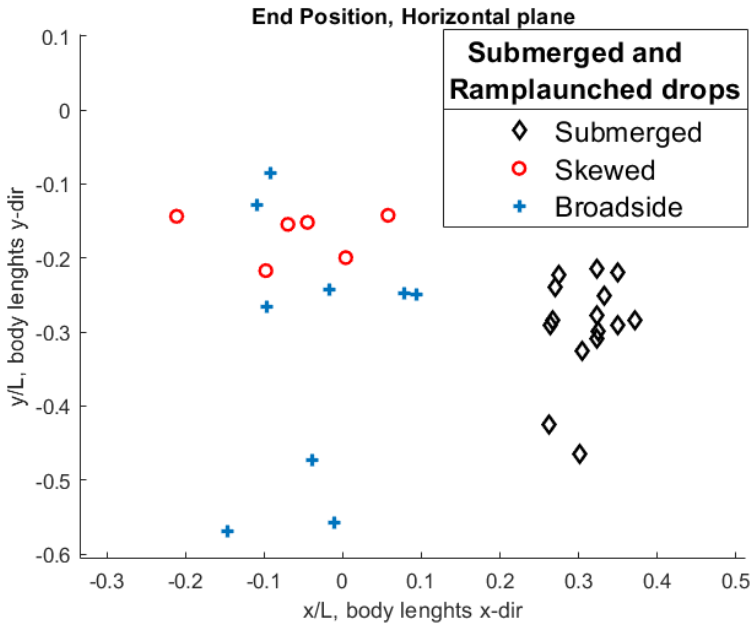

Figure 6.27: Scatterplot of touchdown position for Ramp-launched and normal submerged B4 drop-series. *"Skewed"* denotes module yawed up to 90° while skidding

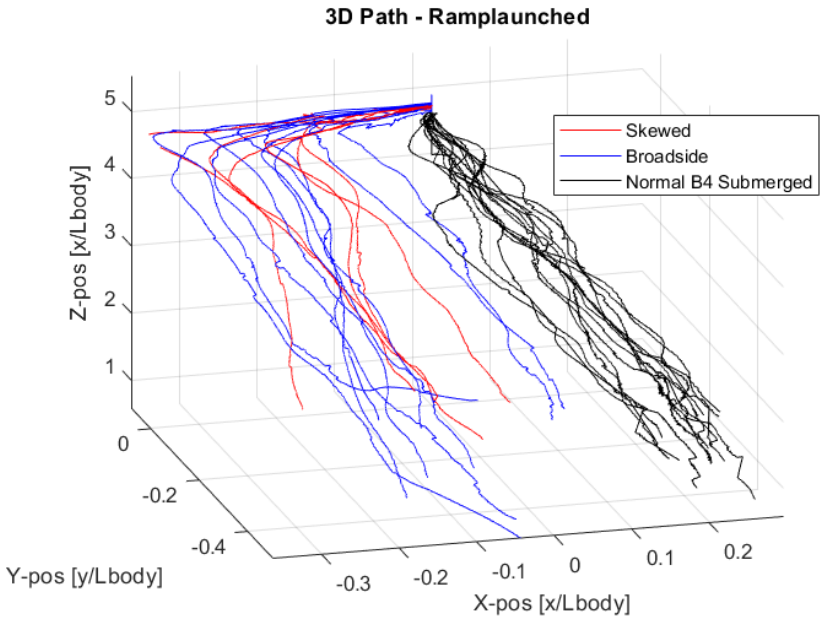

Figure 6.28: 3D path ramplaunched. Note that launch velocity only seems to affect distance travelled in launch direction, descent occurs like normal B4 drop-series

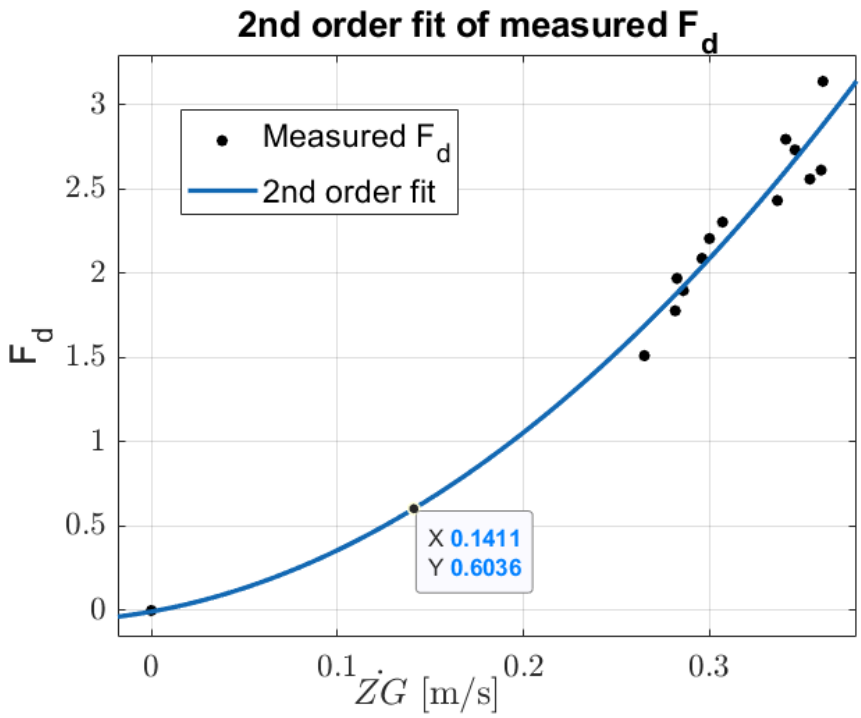

Figure 6.29: Curve-fit of measured drag force for drop-series B1-B4. Marked point is descent velocity of parachuted-B4 drop, indicating that the drag force of the structure is around 0.6[N] at that speed.

mally used in the fabrication of parachutes and can thus only be used to indicate a general effect of parachutes.

As seen in Figure 6.14, while the descent velocity is lowered, the horizontal drift is greatly increased, as shown in Table 6.3. The reason for this is likely that the parachute is handmade, not fabricated for these experiments and inaccuracies when connecting it to the structure. Connection between parachute and structure was made with fishline, and several challenges were discovered regarding getting the connection symmetric above the structure CoG. It is likely that attitude of the structure during parachuted drop-series was highly affected by this inaccuracy as well. With a professional and optimized parachute, it is possible descent can be utilized to postion structure. Like a parachutist controls his descent to the landing-zone by opening and closing parts of his parachute, so could a control system utilize a parachute to guide itself to site.

For the slowest falling drop, Para-B4, the descent speed is 0.14m/s, still about

twice the impact velocity limit. Figure 6.29 indicates that the drag force of the structure is around 0.6[N] at that speed. The total drag force in the system is the difference between the buoyant and gravitational force acting on the system in steady state. For Para-B4, the total drag force is 1.51 [N]. By Eq. 5.32, the estimated drag force added by the parachute is 1.035[N], which is around 66% of the experienced total drag force experienced.

Evidently, adding the drag force for structure and parachute gives a total drag force higher than the measured total. The discrepancy likely stems from both inaccuracies in both Figure 5.32 and the C_d value for the parachute. Figure6.29 is just a graphical representation of drag force vs. quasi-steady-state descent velocity, where orientation of structure is not considered. In addition, severe uncertainty connected to the C_d value for the parachute is clearly expressed in [10]. The calculations were done to give an idea of the force distribution between structure and parachute. A larger and optimised parachute will be needed to reduce the impact velocity below the stated limit.

6.7 Comparison of Estimated Drag Coefficient with Literature

In this section, the found coefficient of drag from experiments will be compared to coefficient of drag for suction anchor found in the literature. Model decay test in heave (longitudinal oscillations) of suction anchors of different D/L ratio has been performed by [11]. Model tests for the D/L ratio relevant for the model, 0.8, was not performed, but interpolation between the results of D/L 0.5 and 1.25 is assumed valid. For D/L= 1.25, the C_d value for KC between 1 and 2 was taken. For D/L=0.5, the KC number is not noted and the referenced report is confidential, therefore KC is assumed in the same region as for D/L = 1.25.

Drag in oscillatory flow is significantly higher than for steady flow, so a correction of the C_d dependent on KC-number, $C_{d,1<KC<2}$, is needed to obtain the steady flow C_d, $C_{d,SF}$. This correction is found in [5], see Figure 6.30. Assuming the same ratio between $C_{d,1<KC<2}$ and $C_{d,SF}$ found in Figure 6.30, is valid for model decay test in heave of suction anchors, $C_{d,SF}$ for the different D/L ratios are found, see Table 6.4. As previously noted, an error was made when making ventilation holes in the suction anchors of the model. As they were drilled with a diameter of 5% of suction anchor diameter, the resulting perforation is 0.025% of top area. Therefore, values for 0% perforation was used.

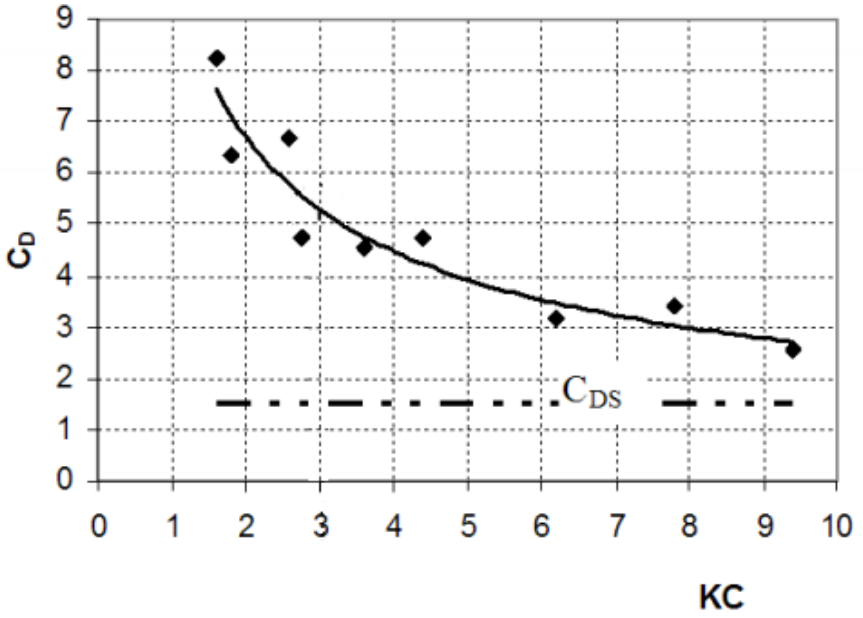

Figure 6.30: Correction from Cd_{KC} to $C_{d,SF}$, Figure 3-2 from [5]

D/L	Cd_{KC}	Cd_{SF}
0.5	2.5	0.5
1.25	2.7	0.54
0.8	-	Interpolated 0.516

Table 6.4: Coefficient of drag from model decay tests for suction anchors at 0% perforation of top-lid, beneath the wave zone, 1<KC<2. Taken from [11].

From	C_d*A_p [$*10^{-3}$]
Literature	1.61
Experiments	42.98

Table 6.5: Table for comparing C_d*A_p between literature and B4-drop-series

By interpolation, the $C_{d,SF}$ value for a single suction anchor of D/L = 0.8 is *0.516*. This is for upright heave motion of the suction anchor.

For the comparison, results from the B4 drop-series are used, as these had the closest to upright orientation experienced in this thesis, with a steady state roll-angle of 11°. Considering a single suction anchor as projected area, the C_d for B4 drop-series becomes *13.8*. Considering a better estimate of the projected area of the structure, the C_d for B4 drop-series becomes *1.02*. Here the projected area includes the buoyant block, structure members and four suction anchors.

To compare the literature with the result from the experiments, the product C_d*A_p is used.

This discrepancy is caused by the simplicity of the taken projected area of four suction anchors when calculating the C_d of the experiments. In a manifold, flow will be concentrated and accelerated between adjacent suction anchors and through the structure of the manifold. While the two values consider the same projected area, the error connected is large for the experimental results as projected area from the buoyancy-block and the structure itself is neglected for simplicity.

6.8 Other Observations

6.8.1 Roll Angle and Descent Speed Correlation

Findings regarding the "speedbump" experienced by the smaller buoyancy blocks will be presented in this section.

Shown in Figure 6.31 is the measured roll against descent velocity. Here the phenomena named *speedbump* is clearly visible, and how it is "dragged out" with increased buoyancy.The structure seem to enter into a low drag field beginning around a roll angle of 50, reaching max around 100 and then decreasing. The reason for this phenomena is not known, but is is noted that the basin is too shal-

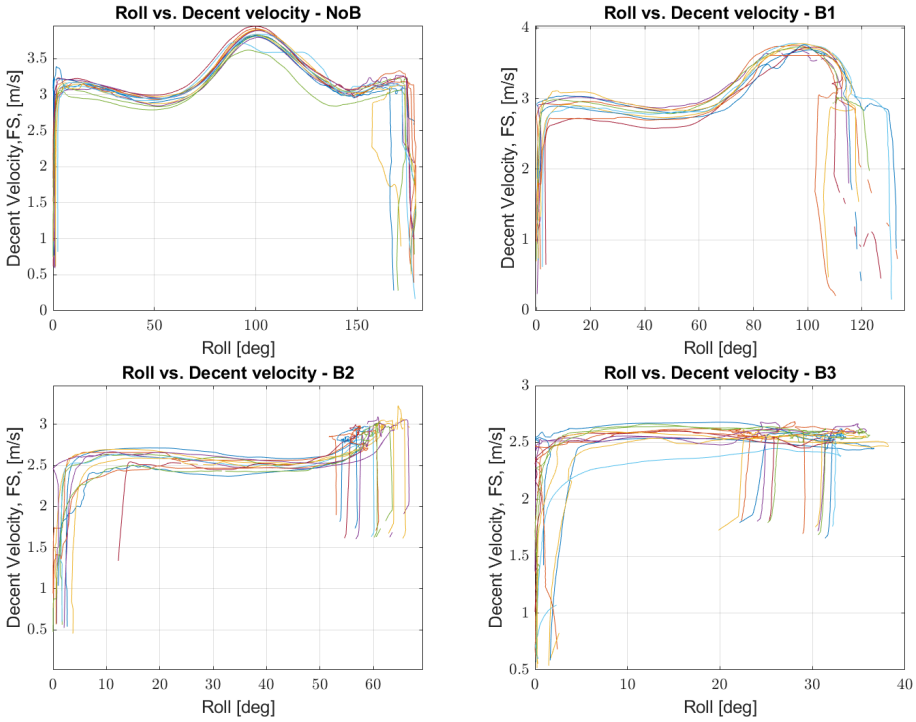

Figure 6.31: Figure showing possible trend of low drag-field in the range of $\theta \in [50,120]$.

low to allow the phenomena to play out for all buoyancy blocks. This raises the uncertainty regarding the steady state assumption for smaller buoyancy blocks.

6.8.2 Effect of Rotation Direction

As seen in Figure 6.32 B3 contains results from the structure rolling both clockwise and counter-clockwise. B3 is here used to showcase a trend that applies to all drop-series.

In general, it seems the negatively rotating drop-series reach a somewhat lower roll angle, and reach it slower, than their clockwise rolling counterparts. This in contrast to the descent velocity which is indistinguishable from the velocity of the clockwise rolling drop-series.

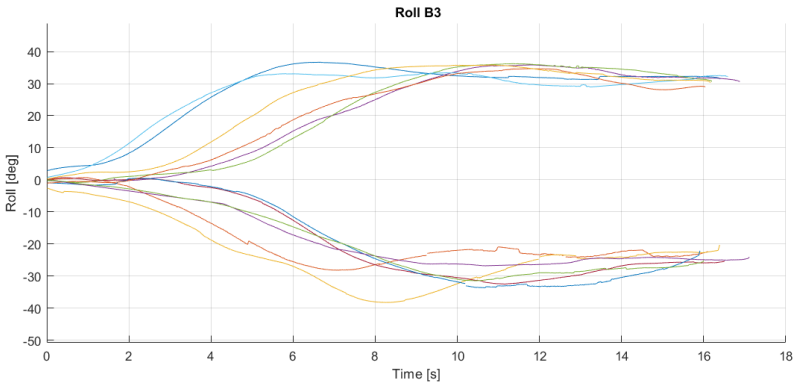

(a) Positive and negative roll, B3. Notice negative rolls stabilising at a smaller angle than positive.

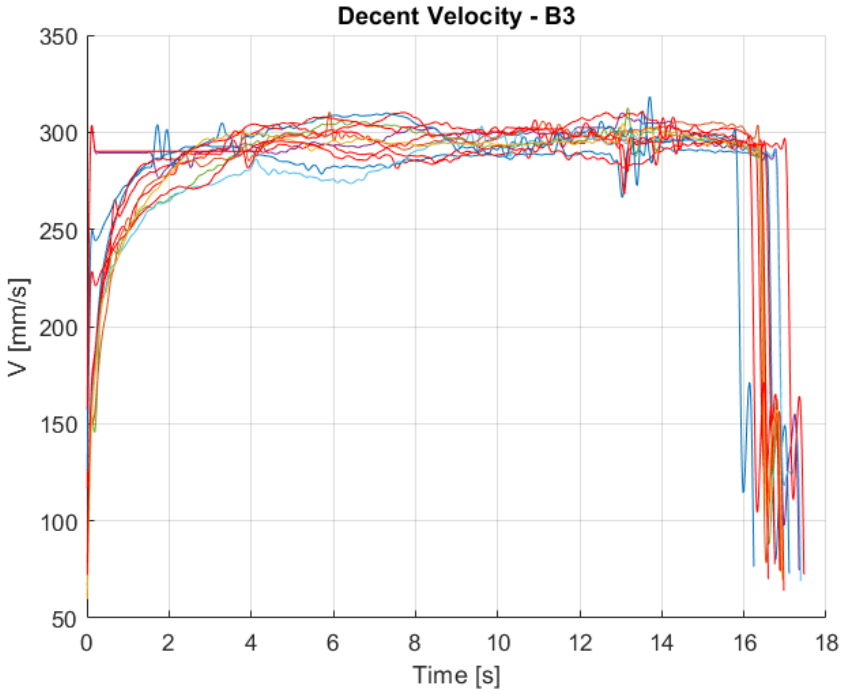

(b) Descent velocity for B3. Negatively rotating drop-series marked red.

Figure 6.32: Roll angle and descent velocity plot for buoyancy block B3

Chapter 7

Discussion

This chapter houses a discussion regarding topics presented in this thesis.There is much than can be discussed, but here the focus has been on errors and limitations connected to the model and experimental setup, validity of the simulation model and how the findings of this thesis might affect the feasibility of the L&F method.

7.1 Operability

While the case study of operability in this thesis treat the operation as finished when structure is launched, ROV operations will be needed for inspection of the landed structure and operation of suction anchors. This will add to the total length of the operation, but OP_{wf} will only be limited by launch and recovery of the ROV. Optimally, the structure does self-diagnostics after landing, and when passing external inspection by ROV, performs suction anchor installation procedure itself.

7.2 Model Inaccuracies

Model tests are inherently inaccurate because of scaling, but here the focus of the discussion will be on the modifications of the model.

As the model is 3D printed, it is safe to assume that the level of uncertainty con-

nected to the model itself is much smaller than the level of uncertainty connected to the human factor of making and installing weights and buoyancy blocks. Any error in creation or placement will disturb the symmetry, the effect of which should manifest trends in the data.

The main trends observable in the data is the consistency of rotation around the transverse axis and the slight tendency of positive rotation. It is not known what causes these consistencies, but it is theorised that hydrodynamic effect of the suction anchors and the asymmetric configuration of reflective markers may play a role. When rotated, the trailing edge of the of the lagging pair of suction anchors will have the longest arm around the transverse axis, contributing to further rotation around the transverse axis.

Because of limitations in the amount of available markers, one half of the structure lacks one marker, making the structure slightly less buoyant on one side. It is believed this is what causes the tendency of positive roll direction, though it has not been possible to prove this with the data.

Another source of uncertainty is connected to the size of the reflective markers. These were larger than expected and placed at the fringes of the structure, giving a contribution to the largest possible arm. Round in shape, they do not have the defined separation point of sharp geometries and will to an unknown degree affect the dynamics of the structure.

The buoyancy blocks will over time and drop-series absorb some water, reducing their buoyant effect. The rate of this is assumed small however, and will likely only be an issue if the same buoyancy blocks are used repeatedly in future experiments. This thesis advises to create new blocks with higher accuracy in construction and quality for future experiments. The uncertainty connected to the volume of these blocks is large, as they were created using tools that might have been to coarse for the level of detail necessary.

7.3 Limitations of the Experimental Setup

In this section a short discussion on the experimental setup is presented, focusing on limitations of the facilities, instruments and method.

The basin used may have been too shallow for drop-series with the smaller buoy-

ancy blocks to reach steady state. When post-prosessing the data, a trend emerged of drop-series seemingly reaching the bottom of the basin before reaching steady state. The slow oscillations at the end of the descent are of interest to better understand the hydrodynamics of the structure. Insights gained from the results in this thesis are how the observed oscillations seem to decrease with increased buoyancy. If a deeper basin is not available, future studies should consider performing drop-series in two parts, first part as normal and second where the structure is released with an orientation closer to the expected steady state value. The error caused by structures landing "prematurely" is discussed in Section 7.4.

Ensuring the exact same initial orientation in each drop was challenging. Attempts were made using fishing line, but it was found too challenging to symmetrically fasten it on the model. Therefore the structure was held and released by hand, conditions challenging to accurately reproduce drop-series without small variation in initial conditions. In future studies a new drop-method should be found to ensure consistency for initial conditions in the trials. A possible solution is using electromagnets, but the weight and placement must be taken into consideration when modifying the model-scale.

Despite best efforts to export high quality data from the Qualisys software, post-processing in MATLAB was challenging because of varying data quality. This is likely due to a non-optimal camera placement as well as user errors in the Qualisys software. Accurately and correctly identifying the start-time was challenging as this occurs near the surface, an area of lower data quality, giving results where different drop-series looks phase-shifted. More drop-series should have been recorded to counteract this and increase the statistical validity of the data.

The experimental setup was not optimal for observing ramp-launched drop-series. The motion capture system struggled near the surface because of the positions of the cameras and reflections in the surface. This is caused by the camera placement, as they were positioned to focus on the descent and not the entry-point. Additional motion tracking cameras should be placed near and above the waterline, giving complete tracking of the structure throughout the launch as well as descent.

With the setup used in this thesis, it will be challenging to test effect of launch velocity, angle and structure orientation in detail due to the manual initialisation. For a detailed study of launch conditions, a mechanism repeatedly initialising the launches with the same conditions should be constructed.

7.4 Validity of the Simulation Model

When comparing simulated drop-series to the measured, it is evident that the simulation model has some inaccuracies. As seen in the results, the simulated drop-series rise sharply to the steady state value and does not follow any dynamics observed. This should however be expected of a simplified model is based on steady state values.

The most important deficiency of the simulation model is the lack of modelled lift effects. However, it is important not to prescribe all differences between experiments and simulations to lift effects. Future studies should model lift effects in general and trailing edge effects on the suction anchors. For the suction anchors, slender body theory may be applied.

By simplifying motions into 2D, a large source of uncertainty is introduced. The motion of the structure during descent is dominated by roll, but yaw and pitch motions occur as well, affecting what area is affected by the flow. This changes the field of forces on the structure, and the effect of this is not covered by the simulation model proposed in this thesis.

The calculations for drag force and momentum assumes these properties solely depend on the angle and descent velocity. In reality the angular rate, or $\dot{theta}$, is important as well. It has been shown in the results (Section 6.4 and 6.8.1) that regions of rapid angle change also experiences an increase in descent velocity. This effect should be modelled in future studies.

A trend of smaller buoyancy blocks experiencing more variations in the "steady state" region was observed. This increases the uncertainty connected to the steady state values used in the simulation and decreases the accuracy of the predictions.

The derivation of the velocity dependent moment opposing the rotation M_v, in Eq. 5.13, is simplistic. The total velocity U_{tot} should have been used instead of velocity in the body z direction, U_3. Due to this, the only calculated contribution is from decomposed flow perpendicular on the suction anchor top. Including the contributions from flow perpendicular to the suction anchor axis would improve the validity of the simulation model, and should be included in future studies.

The C_d estimated from the experiments, was used to calculate the value of M_v. As M_v is dependent on angular velocity, it will not be correct to use constant C_d values from steady state, because the real value for C_d is highly dependent on both angular velocity and rotation. This should be investigated in future studies.

Noted in the experiments, and especially prominent for the B2 drop-series, is a tendency of landing before reaching steady state in descent velocity. The value of C_d observed was chosen instead of trying to "predict" the steady state. Values taken for steady state of B2 drop-series and drop-series with similar buoyancy are thus likely too high and will affect the accuracy of the simulations through the estimations for C_d and C_m.

The simulation model seems to be sensitive to the values of C_m, C_d and added mass in heave. This is believed because these terms directly affect the calculation of θ in the simulation mode. The estimates for C_m and C_d are based on steady state values and are thus theoretically not valid when the structure is rotating. More detailed studies on C_m and C_d for different orientations of the structure and should be performed in the future.

The simulation model is sensitive for parameters connected to calculation of the roll motion. The reason for this lies in the estimated C_m. C_m consists of a third order polynomial, where the third order term is positive, Eq. 5.30 in Section 5.1.5. This means that large values for θ will result in very large values for C_m, correspondingly large values for M_d and consequent feedback between M_d and θ, causing the simulation to crash.

7.5 Feasibility Status of L&F Method

In this section a short discussion is given on how the findings of this thesis may affect the question of feasibility of the L&F method.

At 40% added buoyancy, the structure is considered passively stable based on the observations of the drop-series. The effect of this is seen in the results for ramp-launched drop-series, where initial orientation inflicted by launch is mostly corrected within one body-length of descent.

This may indicate that if passive stability is ensured, the stability of the descent is largely insensitive to the initial orientation during water-entry and consequently launch angle and velocity. This would mean that the limitations surrounding launch angle and velocity would only be dependant on structural limit-loads during water-entry, and thus a launch mechanism can possibly be designed without complicated restrictions for required water-entry orientation.

None of the drop-series performed in this thesis landed with a velocity within the

stated limit for impact velocity 0.7 m/s (full-scale). This means additional measures must be taken to reduce the descent velocity, either designing the structure for more drag, use more buoyancy, utilize a parachute or similar measures.

As presented in the results, the structure becomes neutrally buoyant with 77.5% added buoyancy and theoretically achieves the descent velocity limit for >66% added buoyancy. This number is based on the assumption of a linear relation not seen when considering other drop-series drop-series in Figure 6.2.

The parachuted drop-series seem to lower the dependency on added buoyancy for achieving "correct" orientation during descent. Parachuted drop-series behaved largely identical regardless of buoyancy block used, with only a small variation in descent velocities. With a specially made parachute, it should be possible to achieve correct orientation during descent. This opens for the possibility of using parachute for some or all of the required stability during descent. This would however be connected to risk, as the stability granted by a parachute is dependant on correct opening and continuously "correct" flow. Underwater parachutes are not well understood, and studies must be performed before the risk level can be reduced to acceptable levels.

The stable descent orientation of broadside down (90° pitch) achieved for B1 might be of interest for future development of the L&F method. If unfeasible to achieve passive stability by buoyancy alone, a stable orientation for lower buoyancy amounts might be of interest in the design of the launch phase. A future plan for launch may include an optimal orientation for descending the wavezone before a parachute is deployed, righting the structure. Significant lift effects were however experienced for this orientation, which should be considered in detail in future studies.

Making the structure neutrally buoyant would greatly reduce risk in the installation operation. It may however complicate transport and launch of the structure, as a larger and heavier structure must be handled. Buoyant elements at ultra-deep waters requires internal structure to withstand the high external pressure, meaning the installed buoyancy modules will increase in both size and weight with increased installation depth. It is possible that the size of the buoyancy module needed to achieve neutral buoyancy will complicate transport and launch phase enough to render the L&F method economical or structurally unfeasible. Future studies should investigate how large a neutrally buoyant structure would be, and how this would effect transport and launch phases of the L&F method.

Chapter 8

Conclusion

The purpose of this thesis was to further the study of feasibility for the Launch & Forget installation method. This has been done by assessing passive stability and descent velocity of a structure during free-fall descent, by model-scale tests and numerical simulations.

Rotation about the transverse axis of the structure dominates the motion during free-fall. The steady state angle of this rotation is dependent on the amount of buoyancy added to the structure. An increase in 40% added buoyancy showed the most promising steady state angle of the experiments conducted.

By the results of this thesis, it seems passive stability of the structure during descent can be ensured, but the amount of buoyancy needed might affect the overall feasibility of the L&F method. Some other measures than buoyancy can possibly be used to achieve passive stability, in example a parachute, which might decrease the descent velocity and add to the stability of the structure.

Safe landing speed was not achieved in this thesis, meaning the structure will need design changes to handle a higher impact load, increase the added buoyancy above 40% or rely on additional measures for safe landing.

A simulation model has been built, for theoretical modelling of the motion during descent. The estimations for drag-effects in the model are based on steady state measurements from the experiments performed. The simulation follows the observed motion to a certain extent, and highlights importance of un-modelled

effects, the most important being lift effects.

Based on the results of this thesis it is not possible to conclude with any increase of operational limit for the proposed method, as this will wholly depend on the design and limitations of the launch system. If goals such as launch without crew on deck can be reached, it is likely that the operational limit for the L&F method can be substantially higher than for conventional crane installation methods. If transport and launch can be performed as intended, it seems likely that substantial improvements to the operation reference time, and thus operability and waiting on weather, can be achieved.

Chapter 9

Further Work

The L&F method has several aspects that has not been decided upon or studied. This thesis mostly considers Phase 3 of the method, the descent phase. Presented below are some aspects connected to the results of this thesis that should be investigated further

- The theoretical model presented in this thesis should be improved by including lift effects and additional degrees of freedom.
- A detailed investigation on effects of launch angle and velocity should be performed to further develop of a launch mechanism for the L&F method.
- More model-scale tests should be performed, varying the added buoyancy until a neutrally buoyant structure is achieved.
- More detailed investigation of drag and lift effects on the structure should be performed.
- Detailed investigation of means to reduce descent velocity of the structure.

Bibliography

[1] Axtech. 420t special handling system. Accessed 14.09.2018.

[2] Y. Bai and Q. Bai. Subsea Engineering Handbook. Elsevier Science, 2012.

[3] DNV. DNV-OS-H204 Offshore Installation Operations (VMO Standard Part 2-4). DNV-OS-H20(November):37, 2013.

[4] DNV GL. DNV RP-H103 Modelling and Analysis of Marine Operations. Modelling and Analysis of Marine Operations, (February):157, 2014.

[5] DNV GL. DNV RP-H103 Modelling and Analysis of Marine Operations. Modelling and Analysis of Marine Operations, (February):157, 2014.

[6] Equinor. Johan Castberg Metocean Design Basis. 2016.

[7] Antonio Carlos Fernandes. Scientific and Operational Consequences of Non-Conventional Model Testing in Deepwater Ocean Basins. 9(1):59–69, 2013.

[8] T.I. Fossen. Handbook of Marine Craft Hydrodynamics and Motion Control. Wiley, 2011.

[9] V Heller. Model-prototype similarity. Fluid Mechanics Section, Department of Civil and Environmental Engineering, Imperial College of London, 2018.

[10] A Helvik. Parachute tests Aamund. 2018.

[11] Norsk Hydro and Finn Gunnar Nielsen. INSTALLATION OF SUB-SEA STRUCTURES - ESTIMATION OF HYDRODYNAMIC FORCES. (930), 2002.

[12] Fridtjov Irgens. Formelsamling i mekanikk : statikk, fasthetslære, dynamikk, fluidmekanikk, 1992.

[13] Arnbjorn Joensen and David Paul. A Low Tech , Low Risk System for the Installation of Large Structures in Deep Water. SPE Offshore Europe Oil and Gas Conference and Exhibition, pages 1–8, 2011.

[14] Trygve Kristiansen. pers.comms., 2019.

[15] Kjell Larsen. TMR4225 - Lecture notes- OPERABILITY and WEATHER WINDOWS. 2015.

[16] Kjell Larsen. pers.comms., 2019.

[17] MATLAB. ode45. [Online; accessed January 12, 2019].

[18] Loic Meignan, Specialist Engineer, and Subsea Installation. [PPT]Åsgard Subsea Compression Special Handling System (SHS) ÅSC – Special Handling System (SHS). (December):1–57, 2015.

[19] Henrik Mork, Johannes Lunde, and Aker Marine Contractors. SPE 108608 A Cost-effective and Safe Method for Transportation and Installation of Subsea Structures — The Pencil Buoy Method. 2007.

[20] J. N. Newman. Marine Hydrodynamics. The MIT Press, 2018.

[21] Finn Gunnar Nielsen. Lecture notes in marine operation. 51, 2007.

[22] S Nordvik. Planning of marine operations for offshore floating wind turbines in arctic locations. 2018.

[23] T. Næss, J. Havn, and F. Solaas. On the importance of slamming during installation of structures with large suction anchors. Ocean Engineering, 89:99–112, 2014.

[24] Mario L. P. G. Ribeiro, Milton V. B. Segura, and José A. N. Fereira. Subsea Manifold Design for Pendulous Installation Method in Ultra Deep Water. 2006.

[25] S.M. Sefat and A.C. Fernandes. Stability analysis hinged vertical flat plate rotation in a uniform flow. In Proceedings of the International Conference on Offshore Mechanics and Arctic Engineering - OMAE, volume 1, pages 1–8, 2012.

[26] Sverre Steen. General Modelling and Scaling Laws. Technical Report 1, 2014.

[27] Caley Ocean Systems. Strategic alliance for fiber rope venture, 2015. [Online; accessed January 06, 2019].

[28] Kim Andre Tofteng. Efficient Installation of Subsea Equipment in Deep Water. (June), 2018.

[29] Department of Physics University of British Columbia. Understanding the coriolis force. Casar Drahtseilwerk Saar Gmbh Internal Report, Accessed 17.12.18.

[30] I. Vik and G. Kleiven. Wave statistics for offshore operations. 8th Int. Conf. on Port and Ocean Eng. under Arctic Conditions (POAC 85), Narssarssuaq, Greenland, 1985.

[31] Alan Wang, Yun Yang, Shaohua Zhu, Huailiang Li, Jingkuo Xu, and Min He. Latest Progress In Deepwater Installation Technologies. The Twenty-second (2012) International Offshore and Polar Engineering Conference, 4:1079–1090, 2012.

[32] Alan M Wang, Shaohua Zhu, Xiaohuan Zhu, Jingkuo Xu, Min He, and Changzhi Zhang. Pendulous Installation Method and its Installation Analysis for a Deepwater Manifold in South China Sea. The Twenty-third (2013) International Offshore and Polar Engineering, 9:774–784, 2013.

[33] Alan M Wang, Shaohua Zhu, Xiaohuan Zhu, Jingkuo Xu, Min He, and Changzhi Zhang. Pendulous Installation Method and its Installation Analysis for a Deepwater Manifold in South China Sea. The Twenty-third (2013) International Offshore and Polar Engineering, 9:774–784, 2013.

[34] Øystein Bunes. E-mail communication with Øystein bunes, senior principal engineer, rolls-royce, 2018. 06.09.2018-13.09.2018.

Sigurd A. Sørum

Feasibility Study of the "Launch and Forget" Installation Method for Deep Water Marine Operations

NTNU
Kunnskap for en bedre verden